CHAPTER 4

RESULTS AND DISCUSSION

A. Synthesis of α-HH

4.1 Phase analysis of α-HH

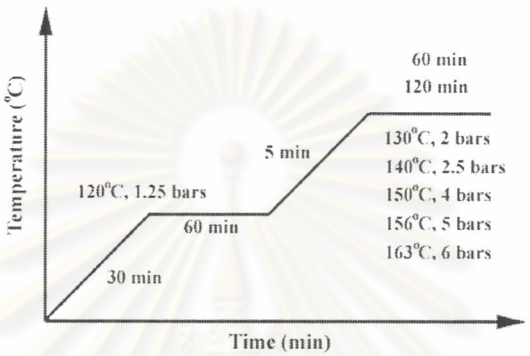

Fig. 4.1 Calcining curve and condition of autoclave treatment.

Grinding condition and phase composition of α-HH from FGD and natural gypsums calcined under various temperatures and pressures (Fig. 4.1) are tabulated in Table 4.1, Table 4.2, and Appendix : Table 1, respectively.

Table 4.1 Grinding of synthetic α-HH under various conditions (feeding size ≈ 2.0 mm).

P (bars)	T (°C)	t (min)	Feeding rate# (g/min)	Median size (μm)*		Diameter at 90% (μm)*	
				FGD	NG	FGD	NG
2	130	60	10	4.89±0.37	6.73±0.19	15.36±0.93	18.92±0.76
			20	6.18±0.26	-	19.60±0.54	-
2	130	120	10	-	6.85±0.26	-	18.21±0.80
			20	6.36±0.13	-	18.87±0.76	-
4	150	60	10	-	6.71±0.14	-	19.63±0.65
			20	6.27±0.38	-	19.17±0.63	-
4	150	120	10	-	6.90±0.32	-	18.45±0.71
			20	6.45±0.26	-	19.86±0.54	-
5	156	60	10	-	6.88±0.29	-	19.21±0.54
			20	6.38±0.28	-	18.43±0.82	-
5	156	120	10	-	6.93±0.17	-	19.43±0.62
			20	6.50±0.32	-	19.53±0.71	-
6	163	60	10	-	6.76±0.16	-	19.17±0.73
			20	6.21±0.24	-	19.75±0.59	-
6	163	120	10	-	6.51±0.24	-	18.94±0.78
			20	6.42±0.19	-	18.63±0.52	-
α-BSP				6.87±0.25		20.92±0.83	

P = pressure, T = temperature, and t = time

FGD = FGD gypsum briquettes, NG = Natural gypsum, α-BSP = Lafarge 's product

Lab grinding machine (FRITSCH Rotor Speed Mill Pulverisette 14)

* Laser granulometer CILAS 920L, diameter at 90% = cumulative 90% finer than

Table 4.2 Content of hemihydrate analyzed from both Infrared Moisture Determination Balance (IMDB) and calculation.

P (bars)	T (°C)	t (min)	%HH (IMDB)*		%HH (Calculation)	
			FGD	NG	FGD	NG
2	130	60	86.60±3.26	87.40±2.49	90.73±4.76	91.24±4.02
2	130	120	88.70±3.75	89.90±2.95	91.55±3.91	90.98±4.32
4	150	60	89.20±3.83	90.20±2.87	93.20±3.83	93.04±3.77
4	150	120	91.50±4.32	91.60±3.60	93.56±4.32	92.67±4.14
5	156	60	92.60±2.77	93.10±2.53	91.90±3.98	93.66±3.75
5	156	120	94.30±3.60	95.40±3.59	92.14±4.16	92.97±3.46
6	163	60	95.50±2.42	97.00±2.54	94.25±3.49	93.57±3.06
6	163	120	93.00±2.51	97.50±3.63	90.22±3.11	94.01±4.07
α-BSP			95.40±4.12		89.65±4.12	

P = pressure, T = temperature, and t = time
FGD = FGD gypsum briquettes, NG = Natural gypsum
α-BSP = Lafarge 's product
* Infrared Moisture Determination Balance (A&D Company Limited AD-4713, AD-4712)

The results from Table 4.1 show that, using a laboratory scale-grinding machine, a feeding rate of 20 g/min is suitable for α-HH from FGD gypsum and 10 g/min is for that from natural gypsum to produce approximately the same size of particle as commercial α-HH (α-BSP). This means that the α-HH from NG is harder than that from FGD gypsum. The results of %HH from gravimetric analysis and calculation (Table 4.2) are approximately in good agreement and close to that of the commercial. From the results of phase calculation (Appendix : Table 1), a small amount of dihydrate (DH) is still present in α-HHs produced from both FGD and natural gypsums and it disappears after heat treatment at 5 bars, 1 h. The HH content increases with the pressure, optimum at 6 bars. When calcining at 1 hour for FGD gypsum and 2 hours for natural gypsum, maximum amount of HH is obtained and the reproducibility was also better. As it has been known that morphology of α-HH is modified by the additives[10]. The effect of additives on the morphology and mechanical property of α-HH was studied and presented in 4.2.

4.2 Effect of additives on the physical and mechanical properties of α-HH

In this experiment, the optimized calcinations of FGD and natural gypsum from previous experiment are selected to produce α-HH, calcining at 6 bars, 1 h for FGD gypsum and 2 h for natural gypsum..

4.2.1 Grinding conditions of synthetic α-HH

The grinding results of synthetic α-HH are presented in Fig. 4.2.

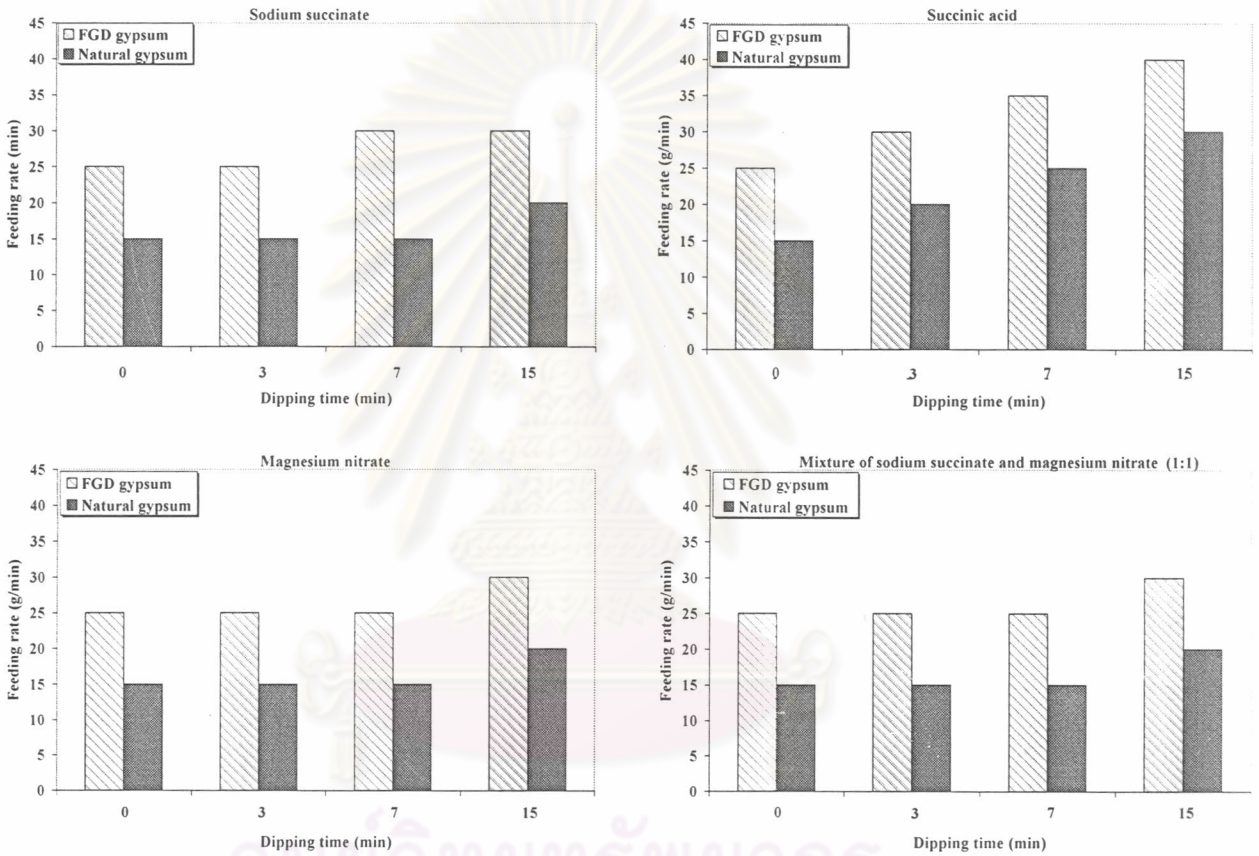

Fig. 4.2 Effect of additive and dipping time on the feeding rate of α-HH.

The results of Fig. 4.2 show that the longer the dipping time, the higher the feeding rate is needed. α-HHs calcined with some additives are easy to grind than those without additive. The suitable grinding conditions of α-HH synthesized with additives are the feeding rate 25-40 g/min for FGD gypsum and 15-30 g/min for natural gypsum and also presented in detail in Appendix : Table 2.

4.2.2 Phase analysis of α-HH synthesized with various additives and dipping times

The phase composition of synthetic α-HHs are shown in Table 4.3, Appendix : Table 3 and Fig. 4.3

Table 4.3 Content of hemihydrate analyzed from both Infrared Moisture Determination Balance (IMDB) and calculation.

Additive	Dipping time (min)	%HH (IMDB)*		%HH (Calculation)	
		FGD	NG	FGD	NG
α-HTGS		92.75±3.93		86.87±4.35	
-	-	95.50±4.59	96.50±3.76	93.03±3.40	93.21±3.76
Sodium succinate	3	96.60±3.80	96.00±2.87	94.49±3.86	93.52±3.20
	7	97.20±2.95	97.50±3.64	95.16±3.32	94.51±3.42
	15	98.30±3.01	98.40±3.83	95.20±3.93	95.37±3.93
Succinic acid	3	96.40±4.21	95.90±3.76	94.87±3.55	93.37±4.20
	7	98.60±3.28	96.20±3.98	96.02±3.84	94.80±3.24
	15	99.50±2.73	99.70±3.41	96.22±3.70	96.04±3.46
Magnesium nitrate	3	96.90±3.77	95.80±2.83	94.53±4.06	93.48±3.21
	7	97.80±3.65	97.10±4.16	95.02±3.51	94.23±3.96
	15	99.00±2.63	98.50±3.80	95.23±3.78	95.44±3.36
Mixture of sodium succinate and magnesium nitrate	3	96.80±3.13	95.60±3.45	94.76±4.11	93.64±3.50
	7	98.10±2.93	97.30±3.02	95.52±3.21	94.62±3.17
	15	99.00±3.11	98.30±3.15	95.87±3.60	95.70±3.47

* Infrared Moisture Determination Balance (A&D Company Limited AD-4713, AD-4712)

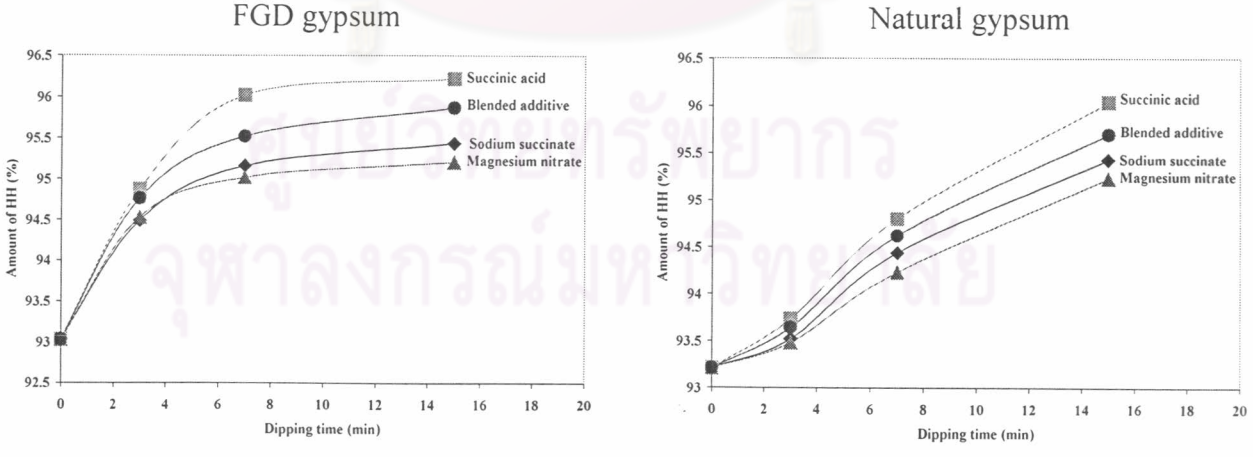

Fig. 4.3 Effect of types of additive and dipping time on the content of hemihydrate (α-HH), blended additive : sodium succinate : magnesium nitrate = 1:1 by wt.

The results from Table 4.3 and Fig. 4.3 show that the amount of α-HH synthesized from FGD gypsums greatly increases in the range of short dipping time upto 7 min, and slightly increases after this. A dipping time of 7 min seems to be the optimum point of all the curves. Of all the additives employed, succinic acid is the most effective and the order is : succinic acid > blended additive > sodium succinate > magnesium nitrate. For natural gypsum, the curves show the same trend but at the beginning, the content of α-HH slower increases with increasing dipping time and no optimum point is shown..

4.2.3 Physical and mechanical properties of α-HH produced, using various additives and dipping times

As a hydraulic cement, the physical and mechanical properties of synthetic α-HHs directly depend on its content and indirectly on modifiers are shown in Fig. 4.4 and Appendix : Table 4.

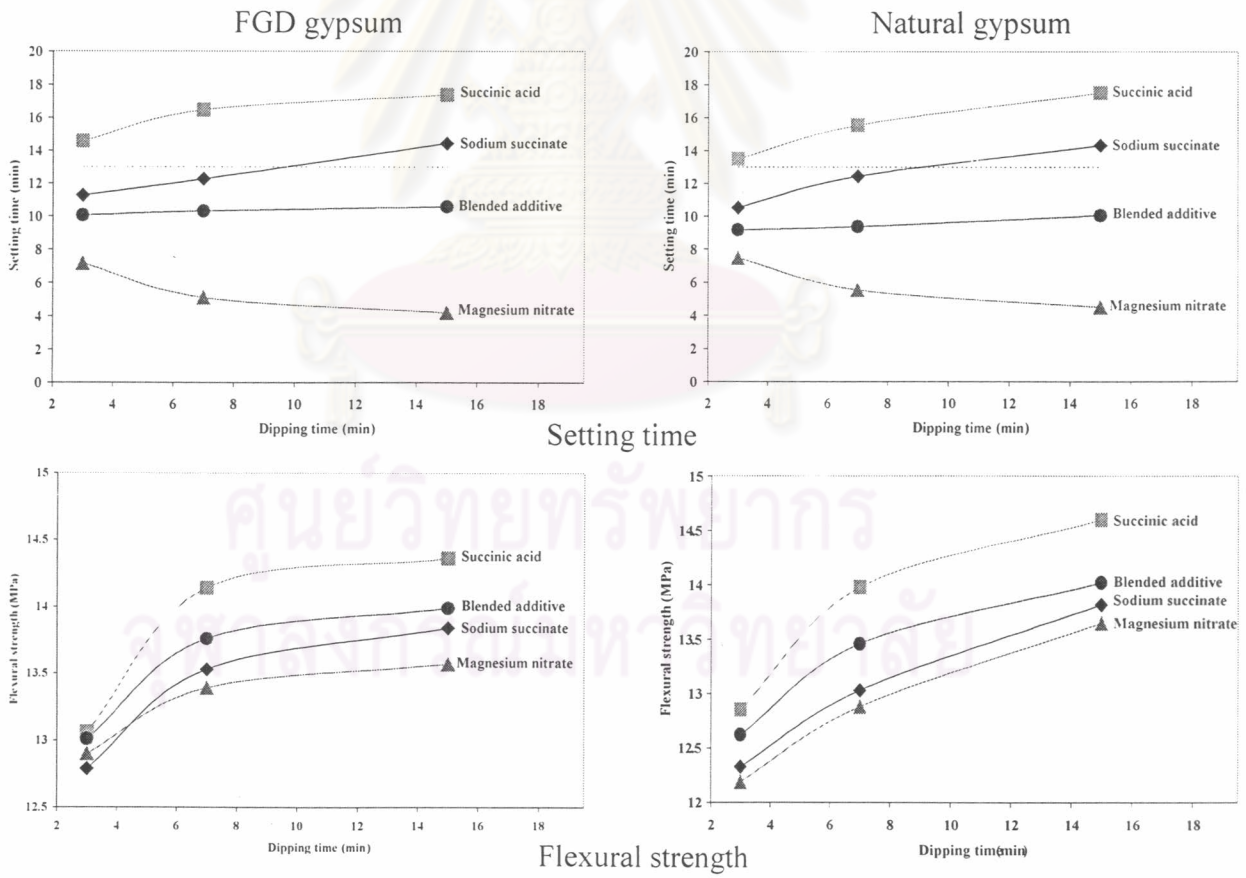

Fig. 4.4 Effect of additives and dipping time on the physical and mechanical properties of synthesized α-HHs.

From Fig. 4.4, the setting time of α-HHs produced with succinic acid and sodium succinate increases with dipping time, but clearly decreases in the case of magnesium nitrate because of its accelerating effect. It is noticed that succinic acid is a stronger retarder than sodium succinate. The flexural strengths of α-HHs produced with all types of additive, increase which are in agreement with the results of Fig. 4.3. Succinic acid is the most effective additive in this case because it produces the highest early strength. When using the combination of sodium succinate and magnesium nitrate (1:1 by wt), It is interesting that all the properties are in between those of succinic acid and sodium succinate. It is also noticed that the setting time in this case is not sensitive to the dipping time.

The results from Appendix : Table 4 also show that generally, α-HH, produced from the FGD gypsum, has comparable properties to those of the natural product with the exception of the flowability. This might be mainly caused by the narrow particle size distribution (PSD) of the FGD gypsum[2].

4.2.4 Morphology of dihydrate obtained after hydration of α-HHs

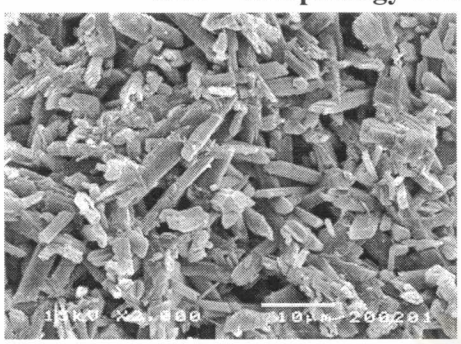

α-HH (Mae Moh FGD gypsum)

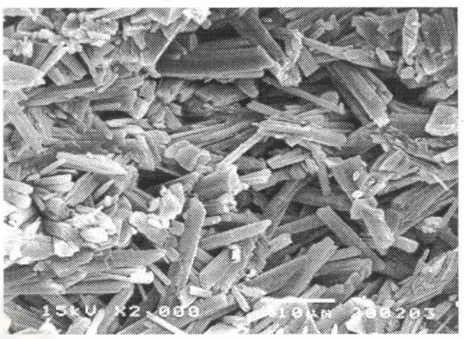

α-HH (Natural gypsum)

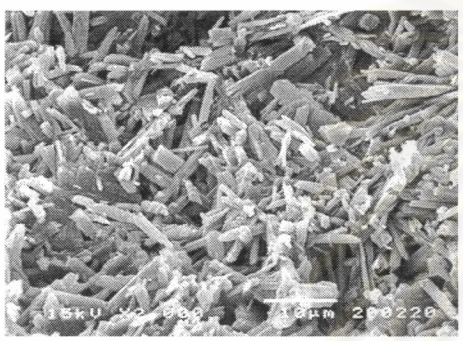

α-HH (Lippendorf FGD gypsum)

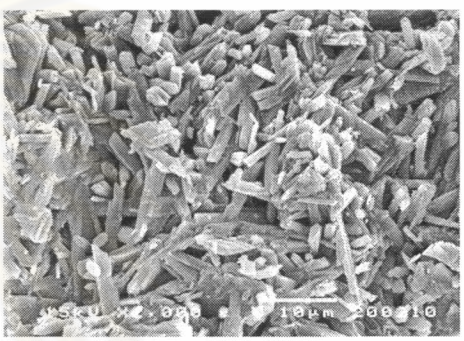

α-BSP (commercial product, without additive)

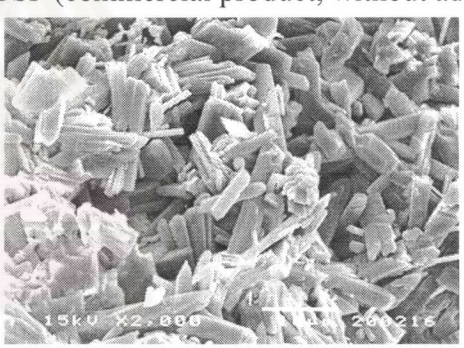

α-HTGS (commercial product, with additive)

Fig. 4.5 SEM micrographs of synthetic DH from the hydration of α-HHs synthesized without additive and commercial.

Fig. 4.5 showed the fracture microstructure of hydrated α-HHs (produced without additive) of Mae Moh and Lippendorf FGD gypsums, and local natural gypsum in comparison with the commercial product (α-BSP). It can be concluded that the hydrated products of α-HHs synthesized without additive products are composed of high aspect ratio than those of the commercial product (with additive, α-HTGS). The average DH crystals from the Lippendorf FGD gypsum is the smallest.

Mae Moh FGD gypsum

Natural gypsum

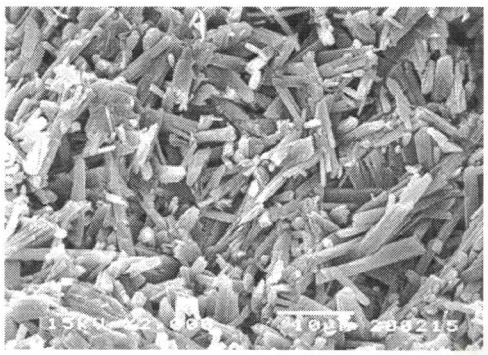

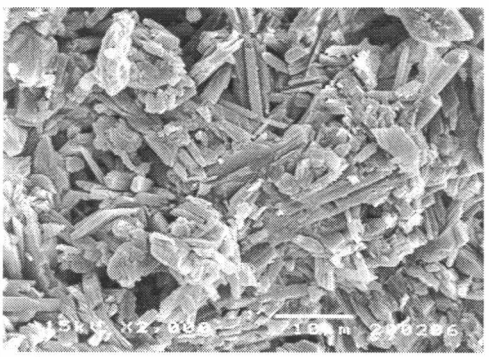

Succinic acid (7 min)

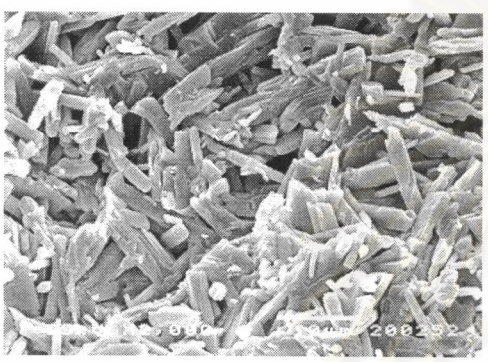

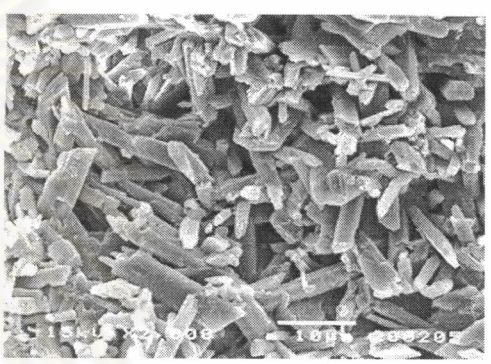

Sodium succinate(7 min)

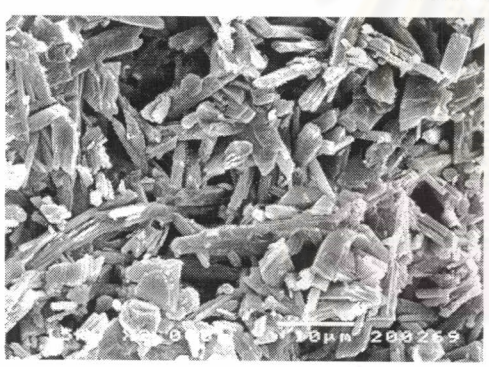

Magnesium nitrate (7 min)

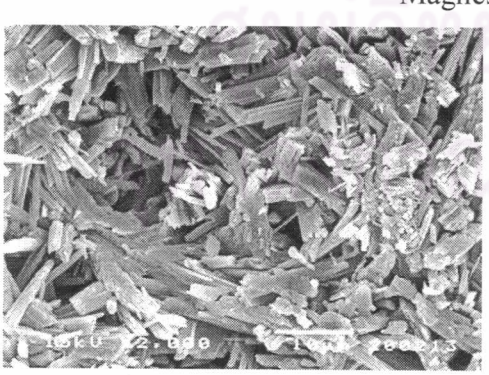

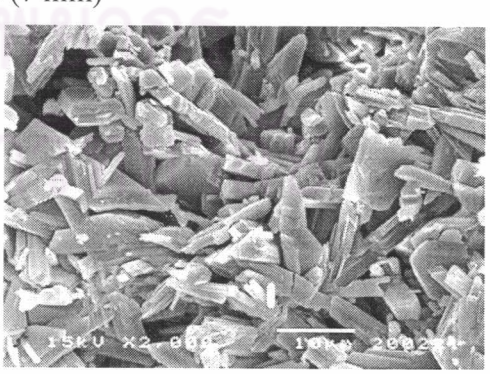

Mixtures of sodium succinate and magnesium nitrate (1:1 by wt) (7 min)

Fig. 4.6 SEM micrographs of hydrated products with various types of additives.

Fig. 4.6 revealed the microstructure of hydrated α-HHs of Mae Moh FGD gypsum and natural gypsum under the influence of various additives. It is found that additives tend to reduce both the size and aspect ratio of DH crystals and cause grain cementation. The microstructure of dihydrate from the mixed additive shows the mixed morphologies—long and small crystals with high-aspect-ratio characteristic of sodium succinate and large and thick plate crystals with low-aspect-ratio characteristic of magnesium nitrate.

4.2.5 Improvement of flowability of α-HH products

α-HHs synthesized from FGD gypsum with dipping time of 15 min and 7 min in sodium succinate and isuccinic acid, respectively are selected to be the samples for this experiment. The PSDs of selected α-HHs (under the grinding conditions of Appendix : Table 2, feeding rate 30 and 35 g/min, respectively) are shown in Fig. 4.7.

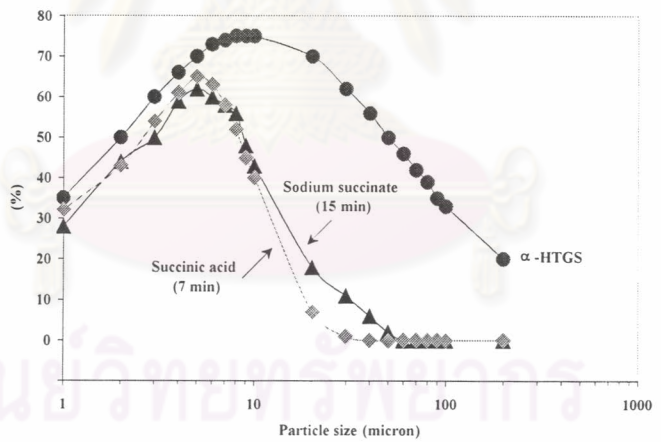

Fig. 4.7 PSD of synthesized α-HH from FGD gypsum compared with commercial product.

Fig. 4.7 show that the synthetic α-HH has a much finer and narrow PSD than the commercial product (α-HTGS). This result affects their flowability as shown in Appendix : Table 4. To improve this property, various amounts of coarse size α-HH, 10-200 μm, is added in the synthetic product. This coarse size FGD α-HH was made by crushing the α-HH from FGD gypsum and sieving through 70 mesh screen (210 μm) and mixing in the products of Fig. 4.7 in the ratios of 10, 20, and 30 wt%, respectively. The PSD results of the improved products are shown in Fig. 4.8, Table 4.4, and Fig. 4.9.

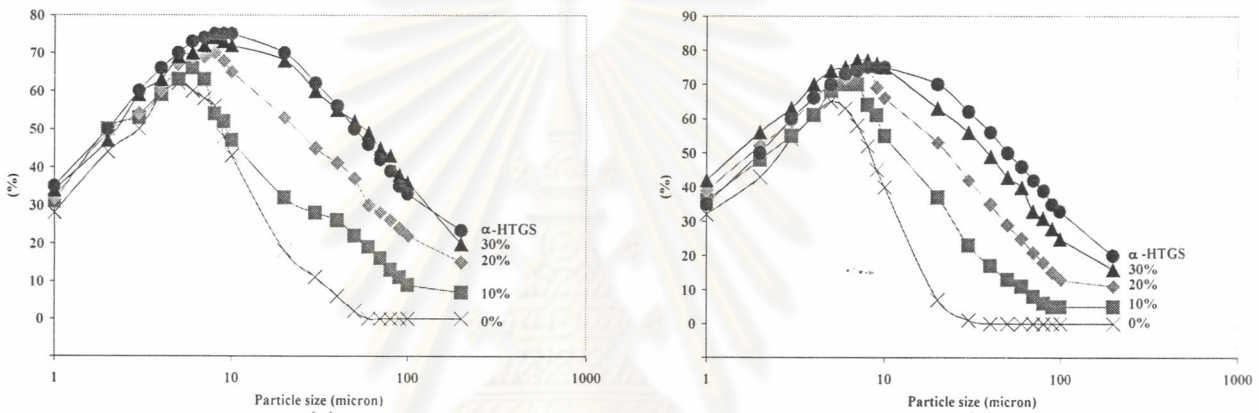

Fig. 4.8 Effect of coarse particle size addition on the PSDs of α-HH synthesized from FGD gypsum with (a) sodium succinate and (b) succinic acid.

Table 4.4 Flowability and mechanical properties of α-HHs synthesized from FGD gypsum with additive and improved PSD.

Sample	Coarse size (wt%)	Flowability+ (cm)	Flexural strength* (MPa)
α-HTGS	-	23.50±0.05	12.67±0.89
FGD gypsum + Sodium succinate 15 min	0	17.50±0.05	13.84±1.18
	10	19.90±0.09	13.98±1.29
	20	21.50±0.06	14.27±1.36
	30	23.30±0.10	14.55±1.10
FGD gypsum + Succinic acid 7 min	0	16.00±0.04	14.14±0.72
	10	19.50±0.07	14.25±1.27
	20	21.75±0.08	14.63±1.08
	30	23.00±0.05	14.80±1.25

+ Lafarge method, * DIN 1168

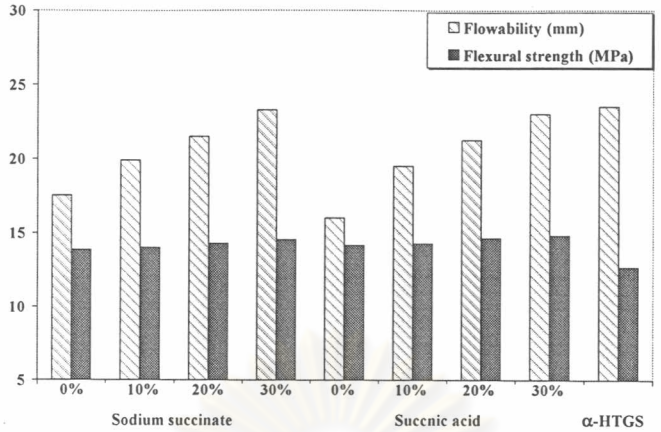

Fig. 4.9 Flowability and flexural strength of α-HH (from FGD gypsum) with improved PSD.

The results obtained from Table 4.4 and Fig. 4.4 show that the flowability increased with increasing amount of coarse size added. The flowability of the chosen α-HHs is comparable with that of the α-HTGS when the addition of the coarse size is about 30%.

4.2.5.1 Grinding condition of α-HHs synthesized with additive

The grinding results of the synthetic α-HHs are tabulated in Table 4.5 and illustrated in Fig. 4.10.

Table 4.5 Suitable grinding conditions of synthetic α-HH (feeding size ≈ 2.0 mm, -10#).

Additive	Dipping time (min)	Feeding rate (g/min)#	Median size (μm)		
			FGD-T	FGD-G	NG
□-HTGS			7.79±2.65		
Sodium succinate	10	15	-	-	7.74±0.38
		30	7.75±0.56	7.83±0.29	-
	14	20	-	-	7.85±0.27
		30	7.84±0.49	7.79±0.82	-
Succinic acid	3	20	-	-	7.56±0.19
		30	7.55±0.77	7.61±0.63	-
	7	25	-	-	7.77±0.20
		35	7.69±0.38	7.71±0.51	-

Lab grinding machine (FRITSCH Rotor Speed Mill Pulverisette 14), 15,000 rpm, 12 teeth, sieve = 1 mm.
FGD-T = Mae Moh FGD gypsum briquettes
FGD-G = Lippendorf FGD gypsum briquettes
NG = Natural gypsum

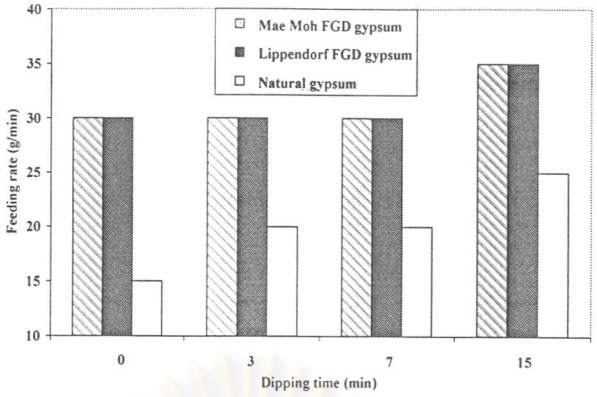

Fig. 4.10 Effect of additives and dipping time on the feeding rate of α-HH.

According to Table 4.5 and Fig. 4.10, it shows the same results as the previous experiment (Fig. 4.2) that α-HHs calcined with some additives were easy to grind and the longer the dipping time, the higher the feeding rate is needed. At the same dipping time, the feeding rate of natural gypsum is about half of the FGD gypsums.

4.2.6 Recycling of dipping solution

4.2.6.1 Phase analysis, physical, and mechanical properties of α-HHs synthesized with recycling solution

To simulate the actual practice in the factory, each dipping solution was used several times without readjusting the concentration. The effect of the recycling was monitored interms of α-HH content, setting time, and flexural strength. It is thought that the increase in pH of the dipping solution (≈7 for sodium succinate and ≈2 for succinic acid) after each dipping due to the increasing dissolved Ca^{2+} ion concentration which later hydrolyze to $Ca(OH)_2$ and act as set accelerator which explains the results of Fig. 4.12. The growth of DH crystals in the basic environment might respond for the large crystals of low aspect ratio shown in all the hydrated specimens of the 8^{th} dipping, Fig. 4.14 - 4.17.

The phase composition of synthetic α-HHs obtained at different dipping cycles is tabulated in Appendix : Table 5 and Table 6 and presented in Fig. 4.11. Physical and mechanical properties of α-HHs products are also showed in Appendix : Table 7 and illustrated in Fig. 4.12 and Fig. 4.13.

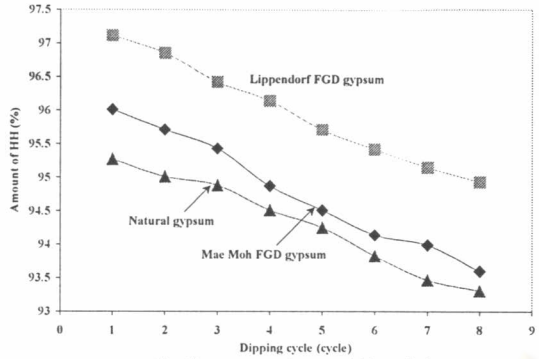

Sodium succinate (10 min)

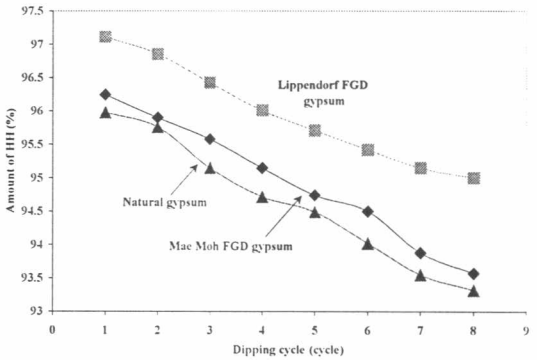

Sodium succinate (14 min)

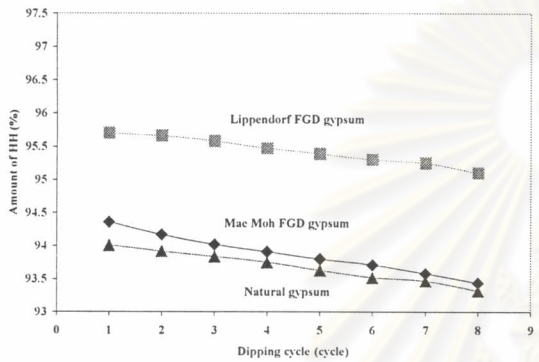

Succinic acid (3 min)

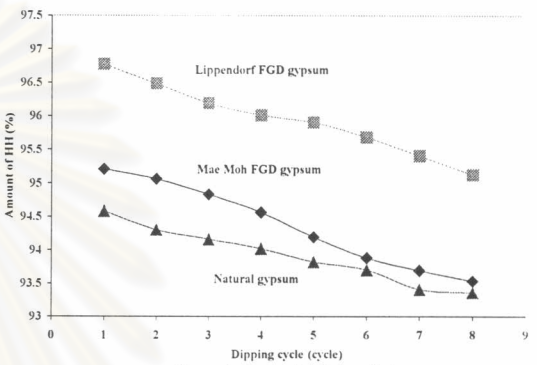

Succinic acid (7 min)

Fig. 4.11 Effect of dipping cycle on the content of α-HHs.

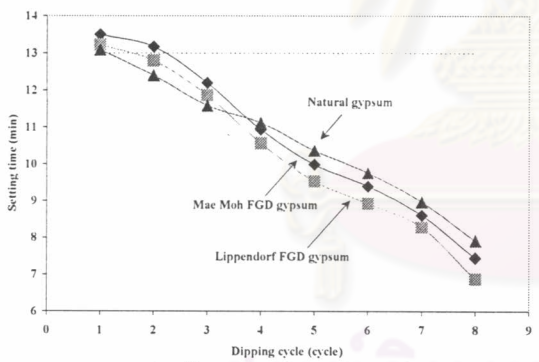

Sodium succinate (10 min)

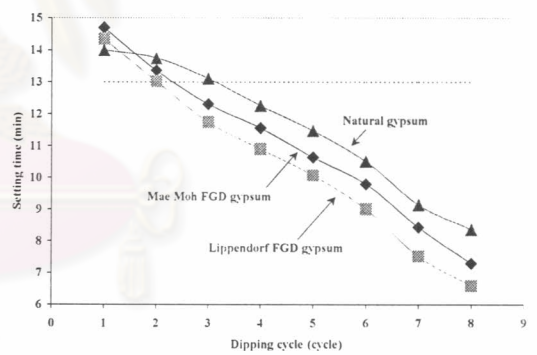

Sodium succinate (14 min)

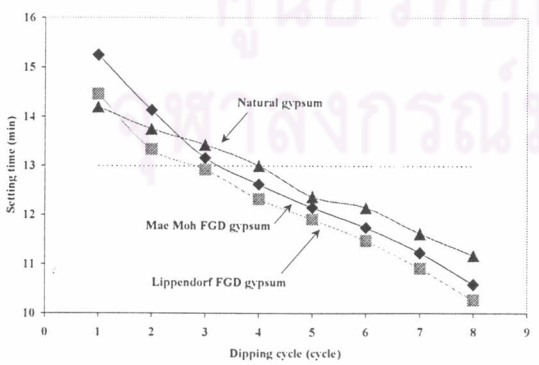

Succinic acid (3 min)

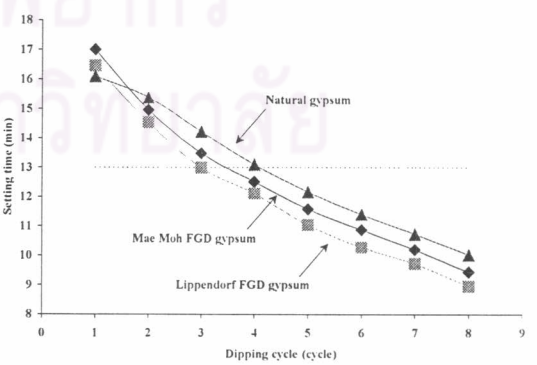

Succinic acid (7 min)

Fig. 4.12 Effect of dipping cycle on the setting time of α-HHs.

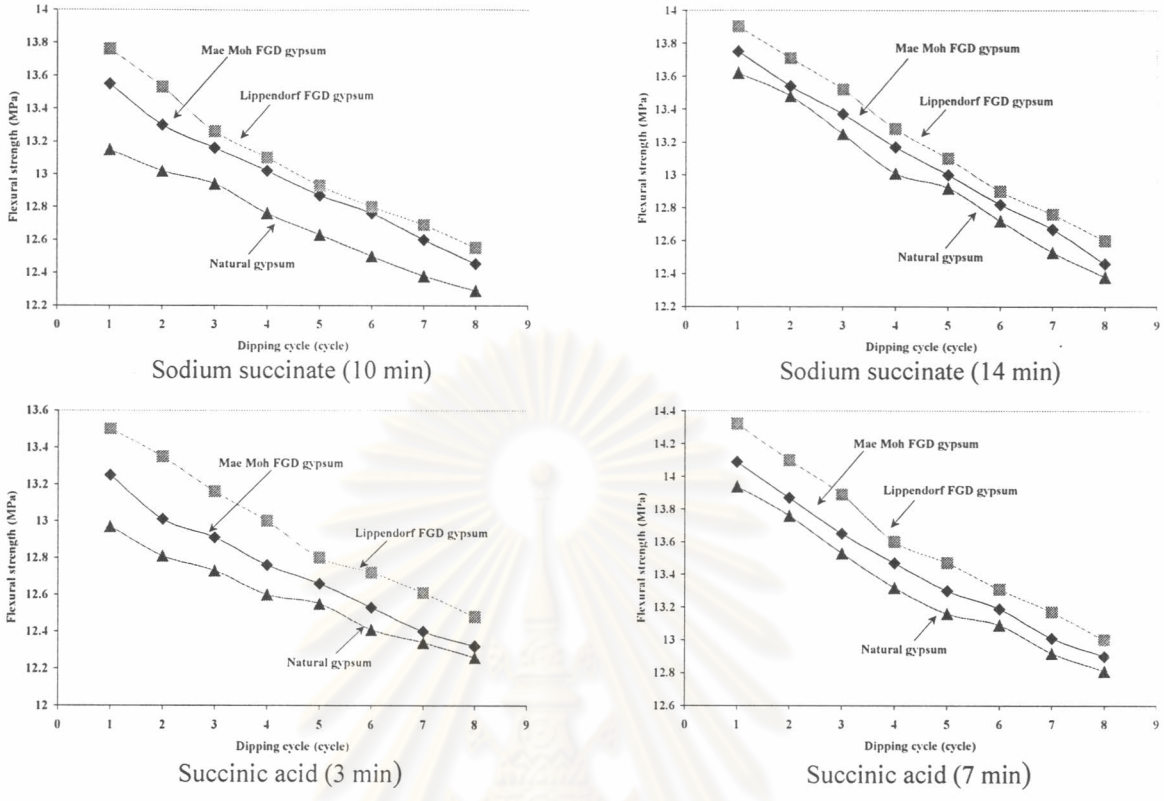

Fig. 4.13 Effect of dipping cycle on the flexural strength of α-HHs.

It was found from the results in Fig, 4.11 and Appendix : Table 5 and that there is a gradually small decrease in %HH with increasing dipping time and reused cycle which supports the result of the flexural strength (Fig. 4.13). The results of the physical and mechanical properties in Appendix : Table 7 and Table 8 are clearly shown that the setting time and grindability of all samples are significantly and positively affected by the increase in dipping time and reuse cycle while the flowability and flexural strength are less affected.

4.2.6.2 Morphology of DH obtained after hydration of α-HHs synthesized with recycling solution

1 cycle 8 cycles

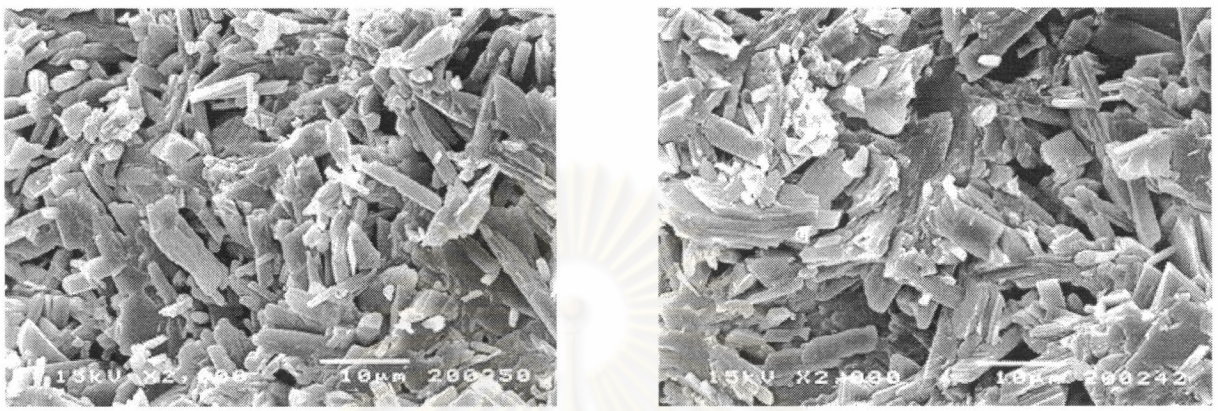

Mae Moh FGD gypsum

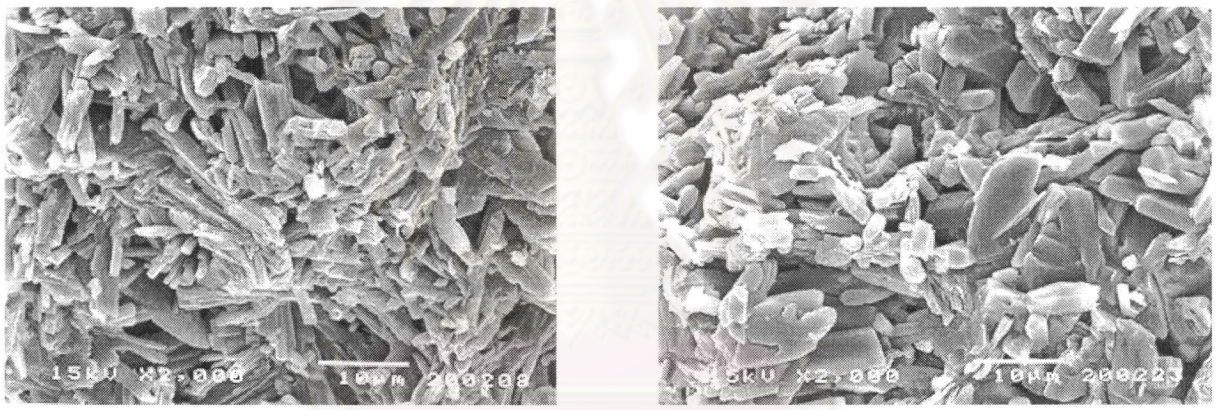

Lippendorf FGD gypsum

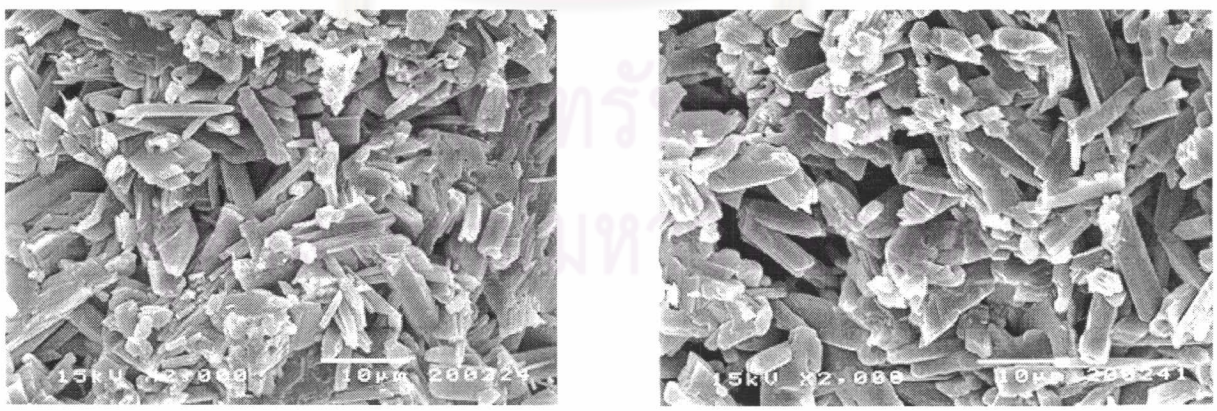

Natural gypsum

Fig. 4.14 SEM micrographs of hydrated products of α-HH synthesized with recycling sodium succinate solution (10 min).

1 cycle

8 cycles

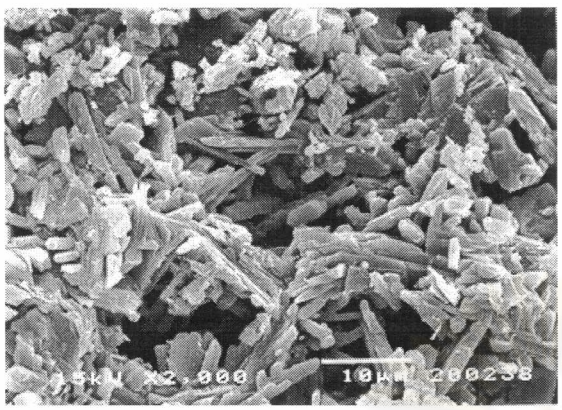

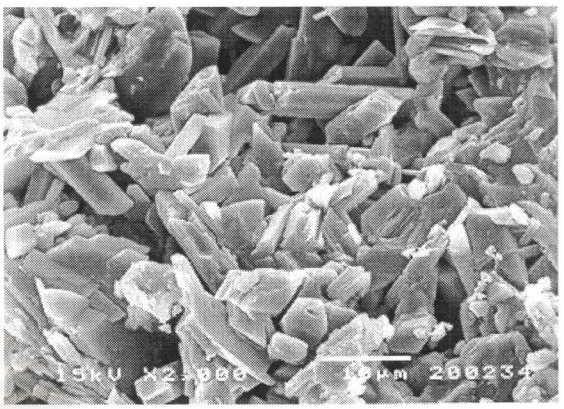

Mae Moh FGD gypsum

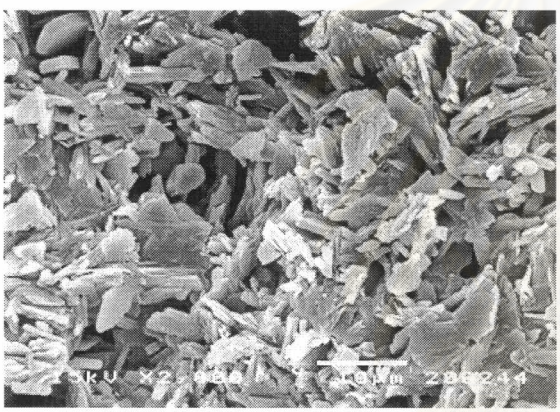

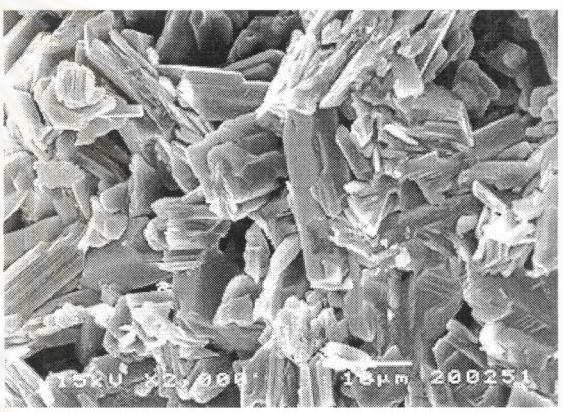

Lippendorf FGD gypsum

Natural gypsum

Fig. 4.15 SEM micrographs of hydrated products of α-HH synthesized with recycling sodium succinate solution (14 min).

1 cycle

8 cycles

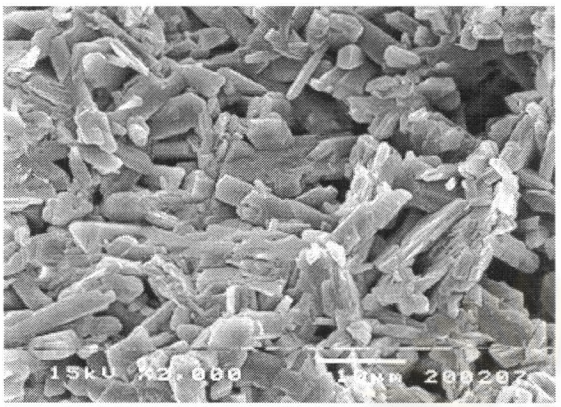

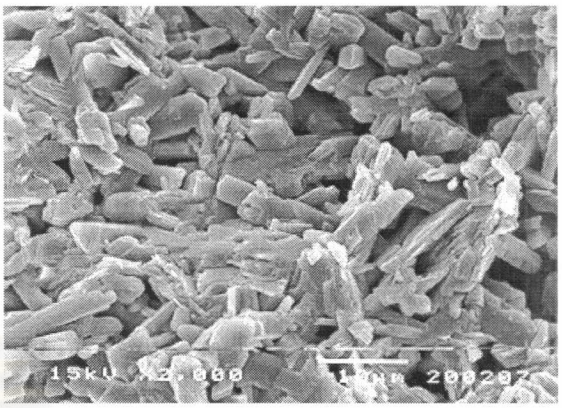

Mae Moh FGD gypsum

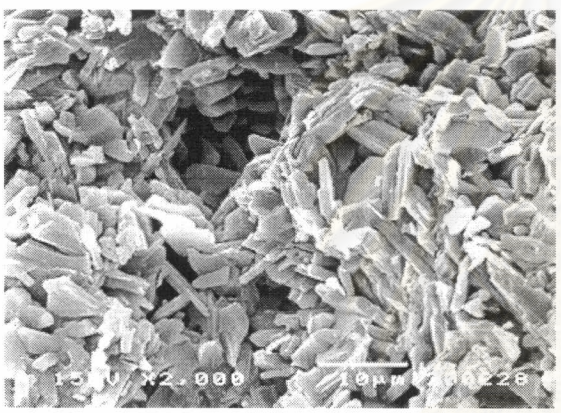

Lippendorf FGD gypsum

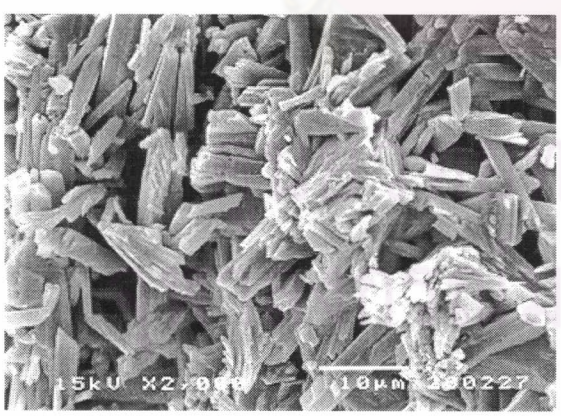

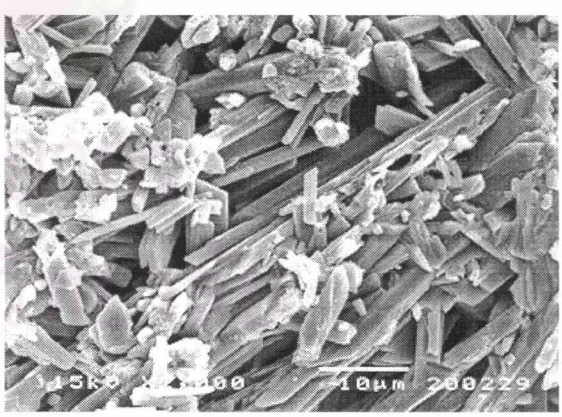

Natural gypsum

Fig. 4.16 SEM micrographs of hydrated products of α-HH synthesized with recycling succinic acid solution (3 min).

1 cycle 8 cycles

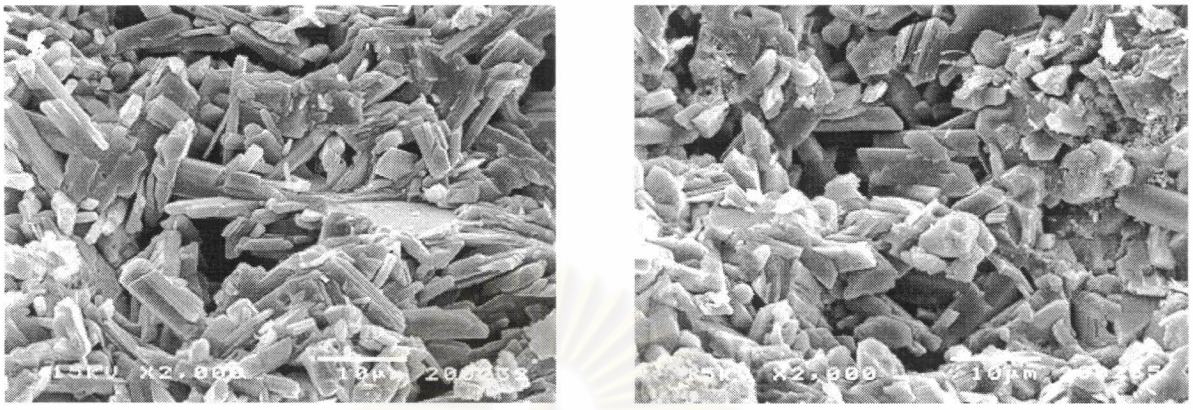

Mae Moh FGD gypsum

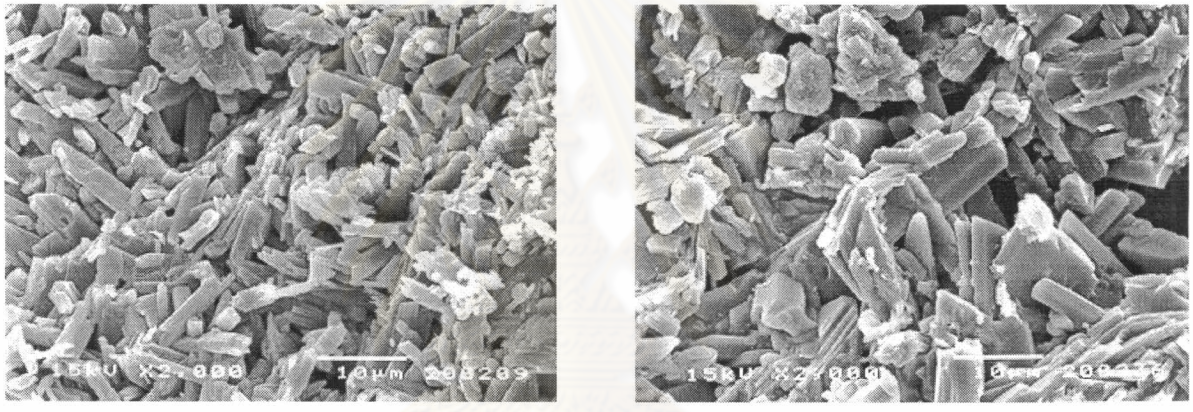

Lippendorf FGD gypsum

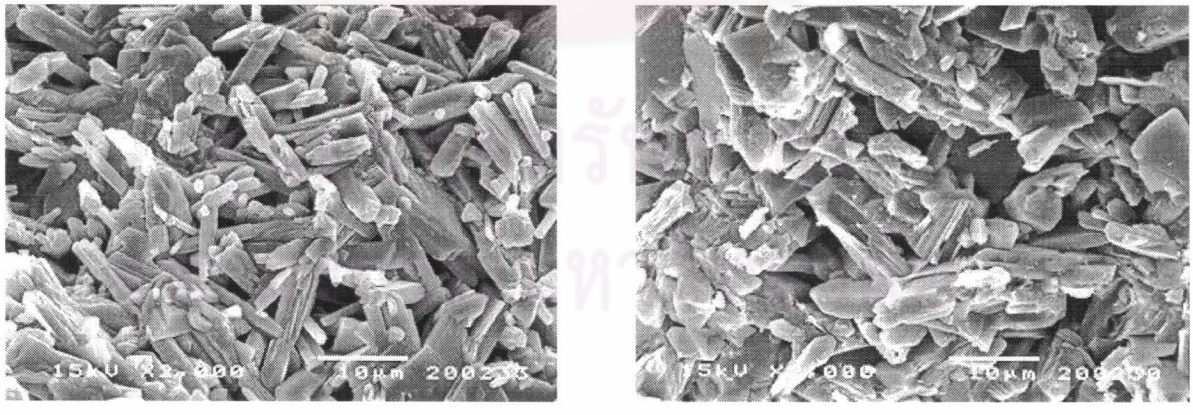

Natural gypsum

Fig. 4.17 SEM micrographs of hydrated products of α-HH synthesized with recycling succinic acid solution (7 min).

The SEM results (Fig. 4.14 - 4.17) of the hydration products of α-HHs, synthesized by calcining FGD and natural gypsums with reused solutions of additive, show different morphology of DH crystals. The DH crystals of the 1st dipping are small, prismatic and have a high aspect ratio but those of the later dippings tend to have a decreasing aspects ratio, hence leading to plate-like or laminated structure and less interlocking. Moreover, the morphology of the DH crystals of a short dipping time are quite similar to that of the 1st dipping but with a longer dipping time, the DH crystals of the last cycle (8th) appear as a stack of plates cemented into a big grain of all the additives (Fig. 4.6) employed, succinic acid yields the smallest DH crystal with high aspect ratio which explains its high flexural strength of Fig. 4.4.

B. Preparation of FGD gypsum-fly ash-lime composite materials

4.3 Formulation of FGD gypsum-fly ash-lime

Results of physical and mechanical properties of composite materials with various compositions were tabulated in Table 4.6 and presented in Fig. 4.18.

Table 4.6 Physical and mechanical properties of FGD gypsum-fly ash-lime specimens.

Properties	FGD gypsum (β-HH)-Fly ash-Lime								
	30-58-12	40-48-12	60-28-12	30-54-16	40-44-16	60-24-16	30-50-20	40-40-20	60-20-20
Compressive strength (MPa)									
1 day	1.8	1.9	2.0	1.8	1.9	2.1	1.8	1.9	2.1
3 days	1.9	2.0	2.1	2.0	2.0	2.1	1.9	2.1	2.2
7 days	2.4	2.5	2.3	2.6	2.3	2.4	2.3	2.3	2.4
14 days	3.3	4.2	3.7	4.6	3.0	2.9	3.9	3.0	2.7
28 days	5.6	6.0	4.3	6.8	5.1	3.6	4.7	3.8	3.0
Bulk density (g/cm^3)									
1 day	1.18	1.18	1.18	1.18	1.18	1.18	1.18	1.18	1.18
3 days	1.18	1.19	1.18	1.19	1.19	1.18	1.19	1.19	1.19
7 days	1.19	1.19	1.19	1.19	1.19	1.20	1.19	1.19	1.19
14 days	1.21	1.22	1.21	1.23	1.21	1.21	1.21	1.20	1.20
28 days	1.26	1.27	1.24	1.28	1.25	1.23	1.24	1.23	1.22
Porosity (%)									
1 day	27.73	28.12	28.69	27.93	28.22	28.69	27.64	28.56	28.66
3 days	27.38	27.65	27.53	27.74	27.61	28.03	27.23	28.26	28.35
7 days	26.82	27.22	27.04	27.32	26.92	27.90	26.51	27.75	27.88
14 days	26.41	26.89	26.75	26.82	26.51	27.54	26.24	27.30	27.53
28 days	25.31	25.20	25.86	24.98	25.68	26.21	25.82	26.18	26.49

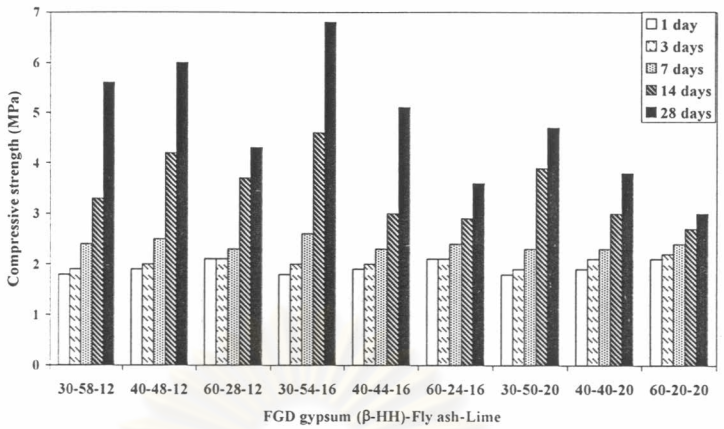

Compressive strength

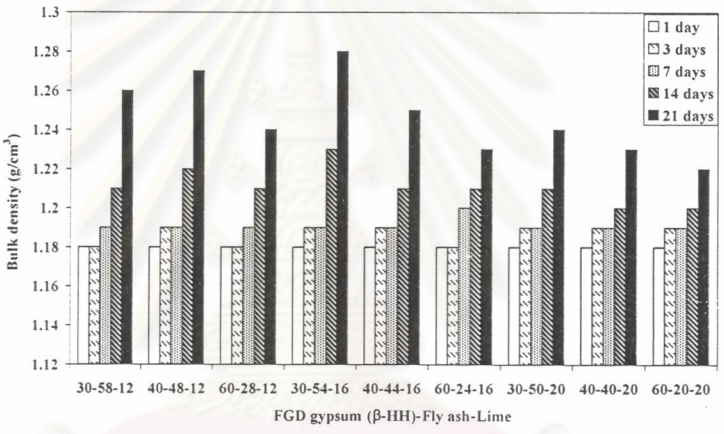

Bulk density

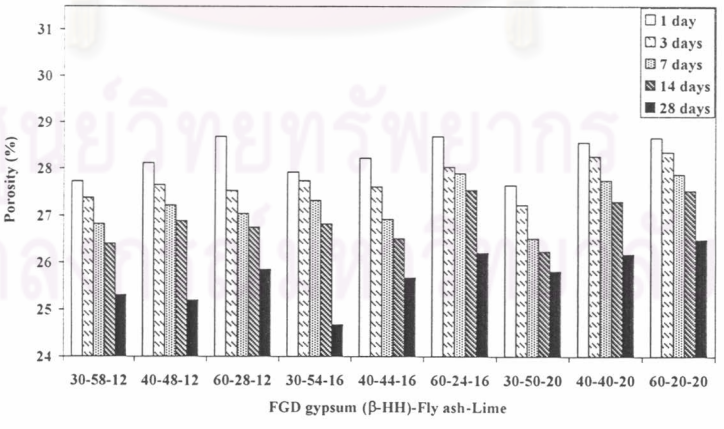

Porosity

Fig. 4.18 Physical and mechanical properties of FGD gypsum-fly ash-lime specimens with different mixing proportions.

The physical and mechanical properties of the specimens are shown in Table 4.6 and Fig. 4.18. The strength gained of these pastes are due to the hydration of β-HH (eq. 1), the pozzolanic reaction of fly ash (eq. 2 and 3). These two reactions progress slowly but continuously when there is an adequate water supply.

$$CaSO_4.1/2H_2O + 1.5H_2O \longrightarrow CaSO_4.2H_2O \quad (1)$$

$$Y[SiO(OH)_3]^- + XCa^{2+} + (Z\text{-}X\text{-}Y)H_2O + (2\text{-}Y)OH^- \longrightarrow C_x\text{-}S_y\text{-}H_z \quad (2)$$

$$2[Al(OH)_4]^- + 3SO_4^{2-} + 6Ca^{2+} + 4OH^- + 26H_2O \longrightarrow 3CaO.Al_2O_3.3CaSO_4.32H_2O \quad (3)$$

Along with the decreasing proportion of lime/fly ash ratio, the strength of paste increases obviously and reaches maximum at lime/fly ash ratio of 0.29 which corresponds to composition, 30%FGD gypsum (β-HH)-54% fly ash-16% lime, but beyond this value, the strength sharply decreases (Fig. 4.19). The XRD patterns illustrated in Fig. 4.20 also show the same results. The strong ettringite peaks are detected at lime/fly ash ratio of 0.29 and decrease sharply at the others. This result conforms to the report of Fournier M., et. al.[69] and Cereseto A., et. al.[70] Chapelle J.[58] also proposed that the presence of gypsum in the lime-fly ash system did not changed this behavior.

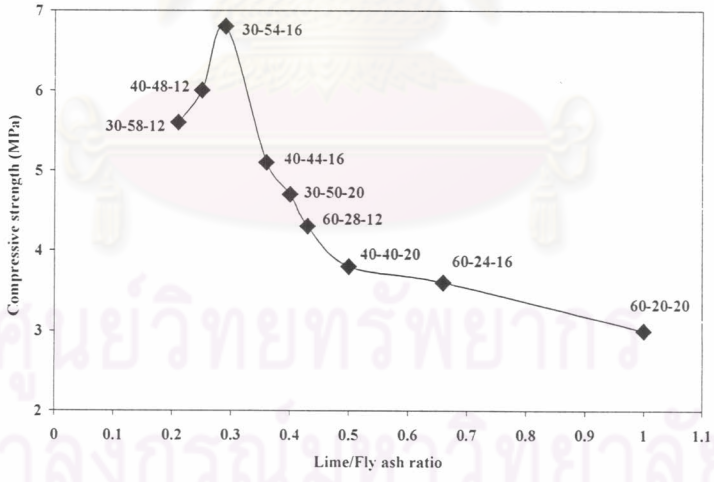

Fig. 4.19 Relation between lime/fly ash ratio and compressive strength of 28-day FGD gypsum-fly ash-lime pastes.

The results of compressive strength (Table 4.6) is in agreement with those of the bulk density and porosity. However, the strength of specimen is still low at every curing

age. Improvement of mechanical properties of the specimens was performed based on the composition containing lime/fly ash ratio 0.29.

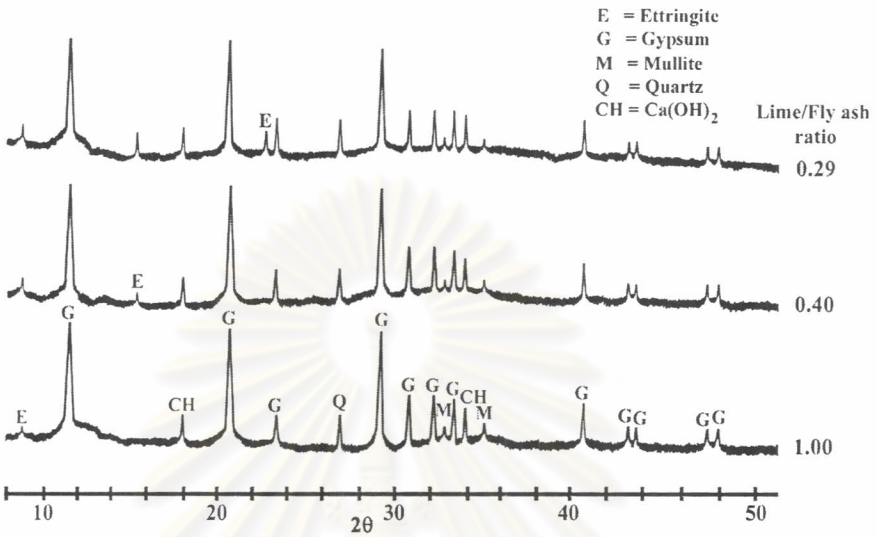

Fig. 4.20 XRD patterns of FGD gypsum-fly ash-lime pastes with various lime/ash ratio cured at 28 days in humid air (>98% RH).

4.4 Improvement of the physical and mechanical properties of FGD gypsum-fly ash-lime composite materials

4.4.1 Thermally accelerating method

a.) Phase analysis of FGD gypsum (β-HH)-fly ash-lime

XRD results of the phase composition of composite materials cured at different temperatures and scheduled ages are presented in Fig. 4.21.

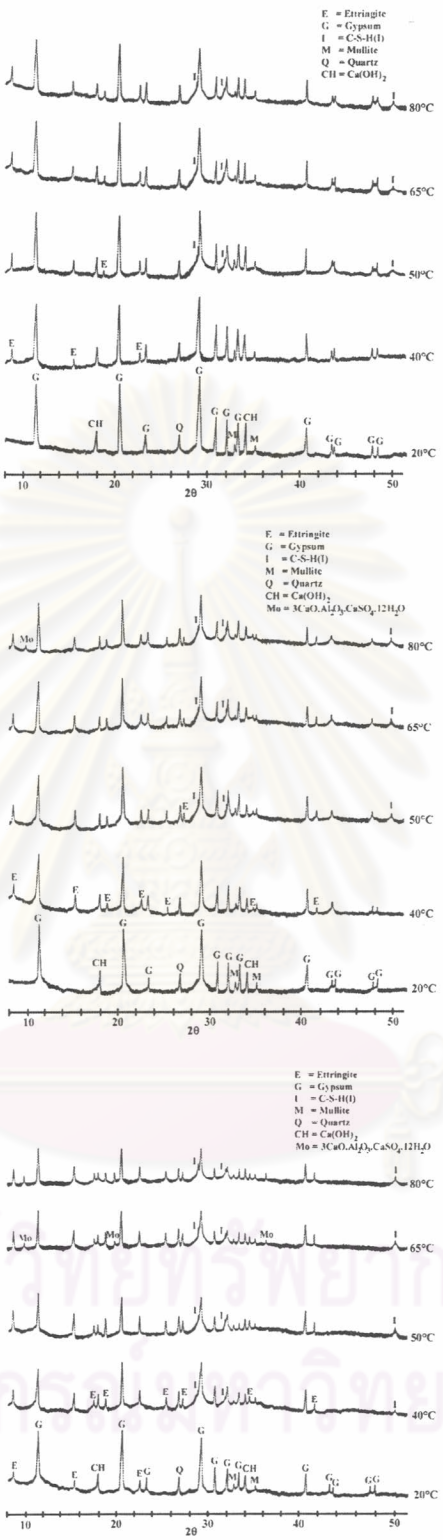

Curing for 3 days

Curing for 7 days

Curing for 28 days

Fig. 4.21 XRD patterns of FGD gypsum-fly ash-lime pastes cured at various temperatures and differents ages.

XRD analyses in Fig. 4.21 show that the main products from pozzolanic reaction are ettringite and poorly crystallised tobermorite, C-S-H(I). The higher content of ettringite and C-S-H(I) can be synthesized at higher curing temperature because the rate of pozzalanic reaction increases with temperature between 40 and 60°C[43,45,71]. The curing temperature at 50°C show the best result because gypsum has the maximised solubility at 50°C (Fig. 4.22) leading to higher ettringite phase produced (eq. 3). Above 60°C, the ettringite content decreasing because the pozzolanic reaction tends to stop or to lessen[43,45] and the solubility of gypsum also tends to diminish.

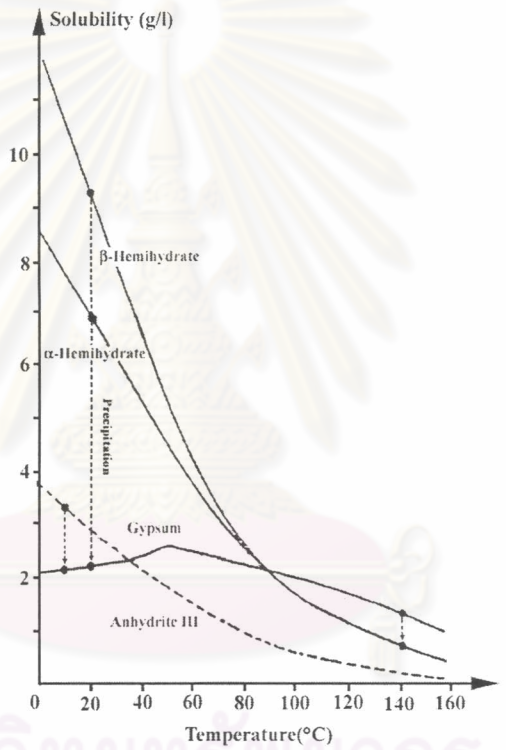

Fig. 4.22 Solubility curve for gypsum plaster[72].

b.) Physical and mechanical properties of FGD gypsum (β-HH)-fly ash-lime

Physical and mechanical properties of the composite materials cured in humid air at different temperatures at scheduled age are presented in Appendix : Table 8 and shown in Fig. 4.23.

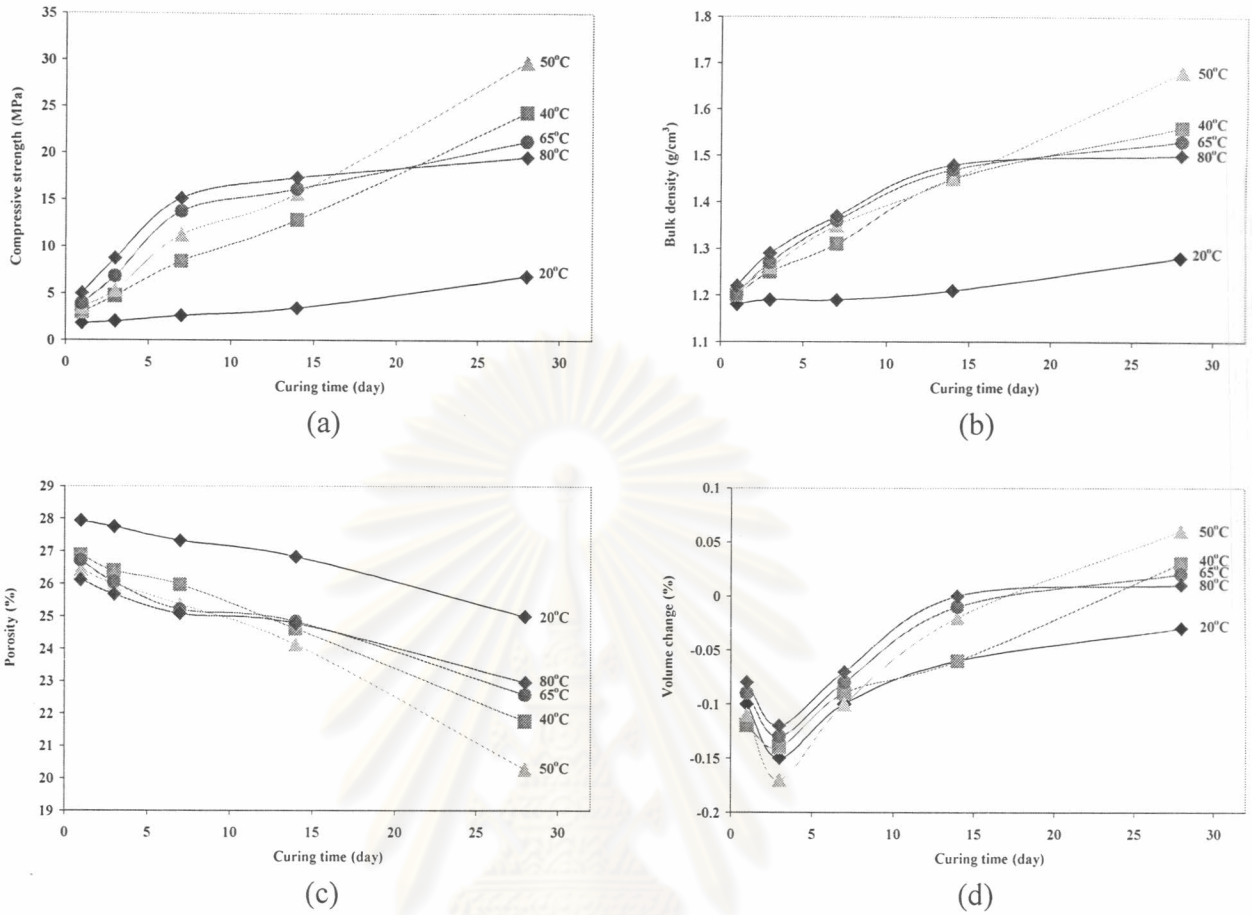

Fig. 4.23 Physical and mechanical properties of composite materials cured at various temperatures (a) compressive strength, (b) bulk density, (c) porosity, and (d) volume change.

The results from Fig. 4.23 show that compressive strength (Fig. 4.23a) increases with increasing curing temperature and content of ettringite. The formation of ettringite and C-S-H(I) in the gypsum matrix is responsible for the gain in strength of specimens. Above 50°C, compressive strength tends to reduce. The trends of bulk density (Fig. 4.23b) and total porosity (Fig. 4.23c) supports the increase in the compressive strength. These results clearly manifest that a porous structure is formed in the early period and after 3 days the matrix of gypsum is being filled by hydration products (ettringite and C-S-H(I)) and structure becomes denser, enhancing high strength. The volume stability of specimens is showed in Fig. 4.23d. All specimens show shrinkage in the first 3 days of hydration due to

the solubility of gypsum[67]. They expand significantly after 7 days due to high content of expansive hydration products.

c.) Free lime content

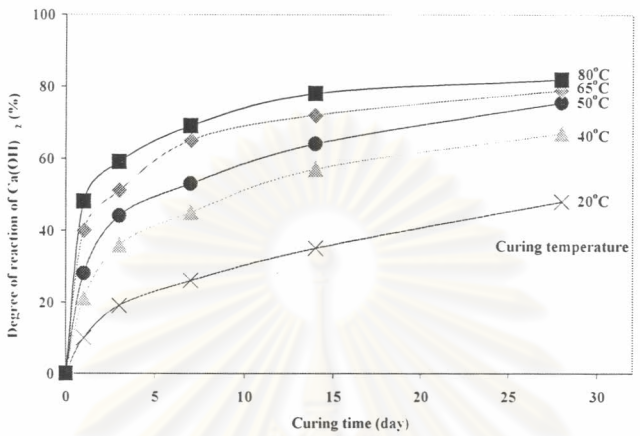

Fig. 4.24 The degree of $Ca(OH)_2$ reaction in the composite materials cured at various temperatures.

Fig. 4.24 shows the reacted percentage of $Ca(OH)_2$ in the pastes cured at different temperatures. $Ca(OH)_2$ is consumed very quickly during initial period, and then much more slowly thereafter in every curing temperature. The higher the curing temperature, the faster the pozzolanic reaction is detected. The variation in the degree of reaction of $Ca(OH)_2$ corresponding to the measurable strength and the slope of those linear relationships (Fig. 4.25) might be attributed to the formation of various hydration products with different mechanisms.

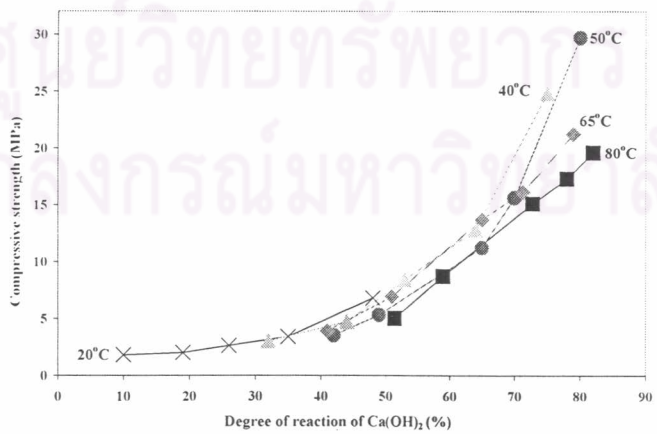

Fig. 4.25 Correlation between compressive strength and the degree of $Ca(OH)_2$ in the composite materials cured at different temperatures.

d.) Particle morphology of composite materials

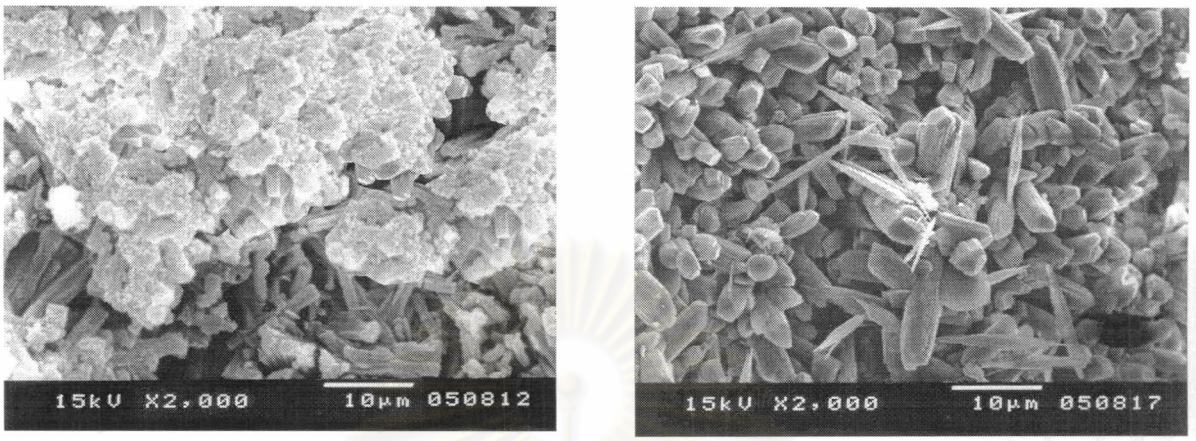

Curing 20°C for 28 days

Curing 50°C for 28 days

Fig. 4.26 SEM micrographs of FGD gypsum-fly ash-lime composite materials.

Fig. 4.26 shows that with increasing curing temperature, the hydrated products, ettringite and C-S-H(I), increase. The morphology of hydrated products changes from irregular shape to short needle like crystals.

e.) Kinetic analysis

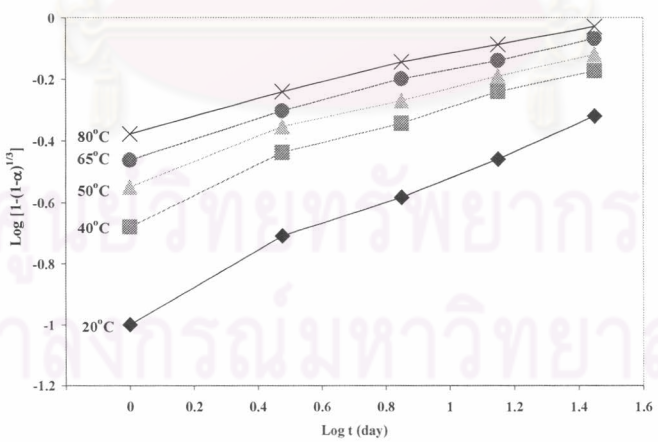

Fig. 4.27 Kinetics of pozzolanic reaction in composite materials cured at different temperatures.

Table 4.7 Reaction grade (N) and phase period of the composite materials activated with thermally accelerating method.

Curing temperature (°C)	Phase I ($N \leq 1$)		Phase II ($2 \geq N > 1$)		Phase III ($N > 2$)	
	N	Period	N	Period	N	Period
20	N/A	N/A	1.95	3 days	2.51	> 3 days
40	N/A	N/A	1.82	3 days	2.34	> 3 days
50	N/A	N/A	1.66	3 days	2.18	> 3 days
65	N/A	N/A	N/A	N/A	2.09	> 1 day
80	N/A	N/A	N/A	N/A	2.04	> 1 day

N/A = not applicable.

It is found from Fig. 4.27 and Table 4.7 that Phase I can not be detected regardless of curing temperatures. This means that Phase I has been completed before the determination of free lime. From 20 to 80°C, pozzolanic reaction behaves in the same way, i.e. Phase II ends after approximately 3 days of curing and Phase III starts thereafter. As curing temperature increase over 65°C, only phase III could be identified.

4.4.2 Physically accelerating method

a.) Phase analysis of composite materials

XRD results of composite materials containing various amount of β–HH and cured at different ages are presented in Fig. 4.28.

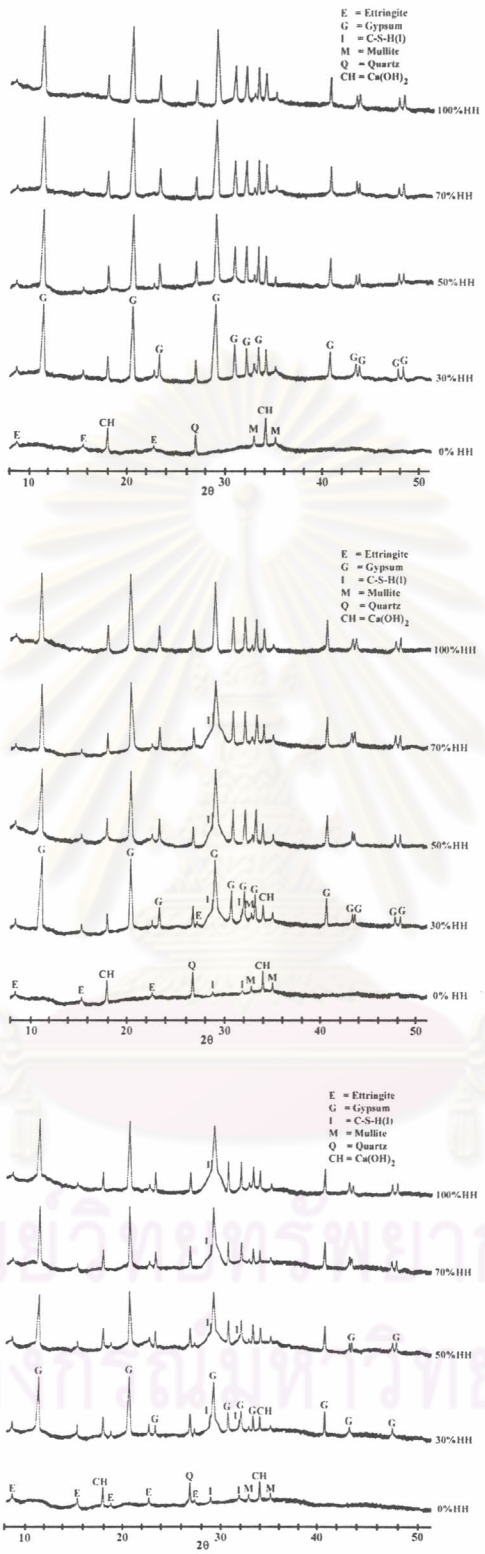

Fig. 4.28 XRD patterns of composite materials containing various contents of β-HH and cured at different ages.

Fig. 4.28 shows XRD patterns of the composite materials, improved properties by physically accelerating method. Small ettringite peaks are detected at 3 days and their intensities increased with curing time. Strong diffraction peaks of gypsum are still detected at every curing period and only slightly decrease with curing time.

b.) Physical and mechanical properties of composite materials

Physical and mechanical properties of the composite materials, improved properties by physically accelerated method at different curing ages are tabulated in Appendix : Table 9 and show in Fig. 4.29.

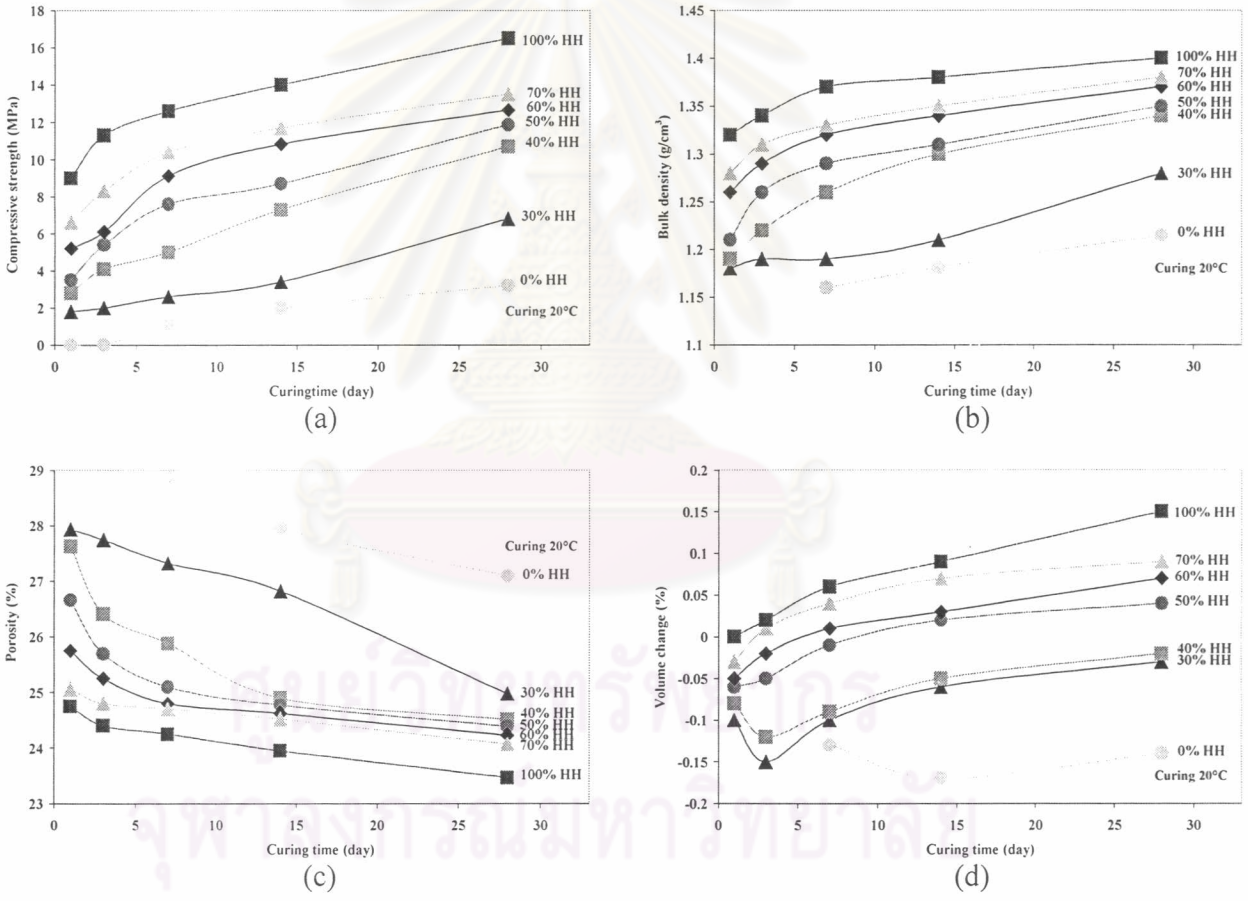

Fig. 4.29 Effect of β–HH content on the physical properties of composite materials (a) compressive strength, (b) bulk density, (c) water absorption, and (d) volume change.

It was found from Appendix : Table 9 and Fig. 4.29 that compressive strength of blended materials increases with increasing amount of β-HH in the composition. However, it shows employed reversible results in flowability (Fig. 4.30). The higher the content of β-HH is employed, the lower the flowability of the composite materials is resulted. This is occurred due to the short setting time.

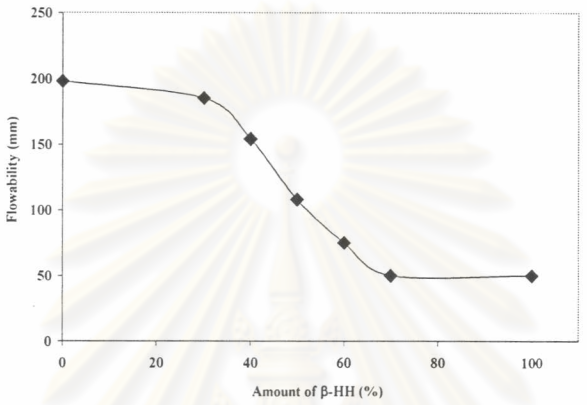

Fig. 4.30 Effect of β–HH content on the flowability of composite materials.

c.) Performance of composite materials under water

Performance under water of the 28-day composite materials improved by physically accelerating method are tabulated in Appendix : Table 10 and presented in Fig. 4.31.

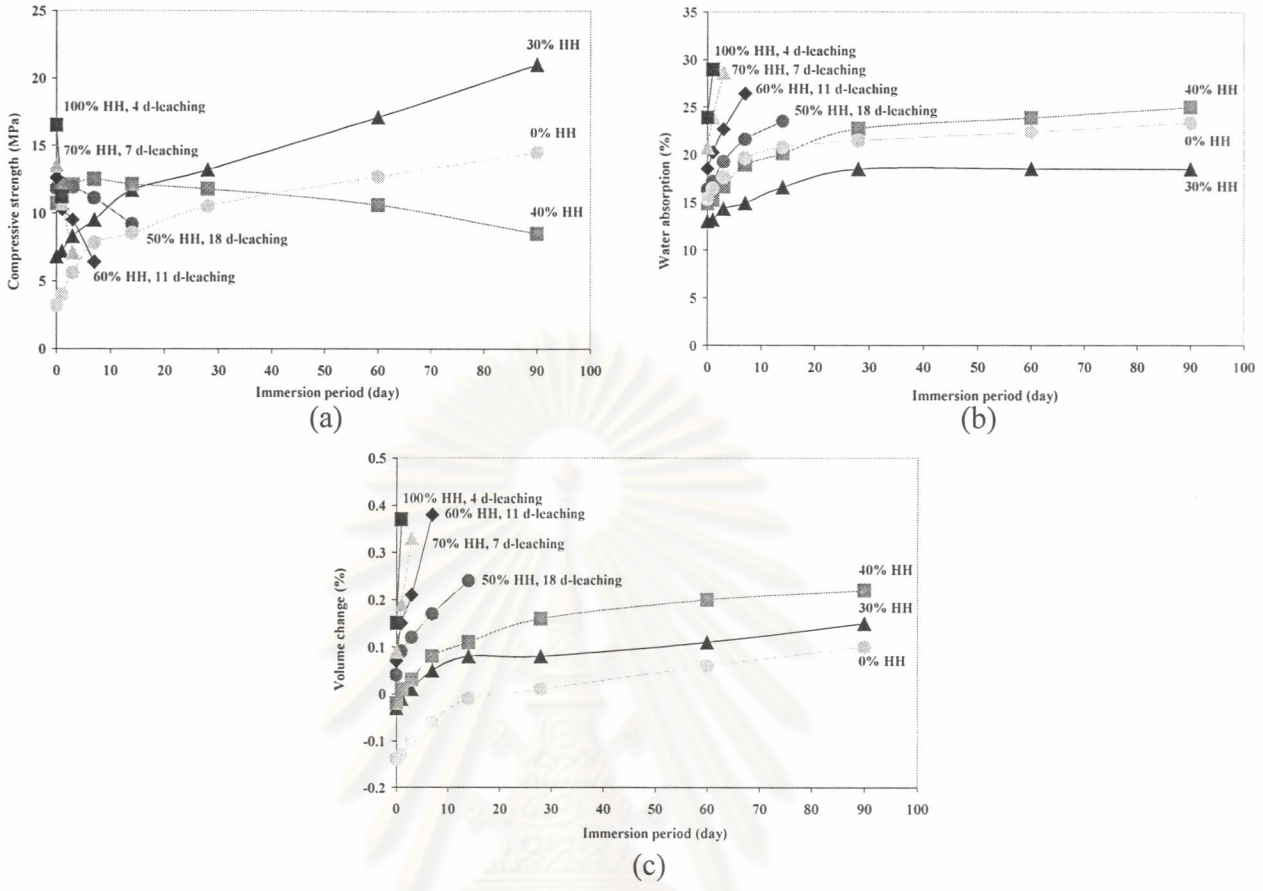

Fig. 4.31 Physical and mechanical properties of 28-day specimens under water (a) compressive strength, (b) water absorption, and (c) volume change.

Results of performance of the specimens improved by physically accelerating method cured at 20°C for 28 days are shown in Appendix : Table 10 and Fig.4.30. It is found that specimens containing β-HH higher than 40 wt% show unstability in water. This result conforms with those of P. Yan and W. Yang[73]. They reported that the content of synthetic gypsum as cementitious binder should not be higher than 40 wt% and that of fly ash must be higher.

4.4.3 Chemically accelerating method

a.) Phase analysis of composite materials activated with additive and cured ay different ages.

XRD results of composite materials activated with $CaCl_2$ and Na_2CO_3 and cured at different times are presented in Fig. 4.32 and Fig. 4.33, respectively.

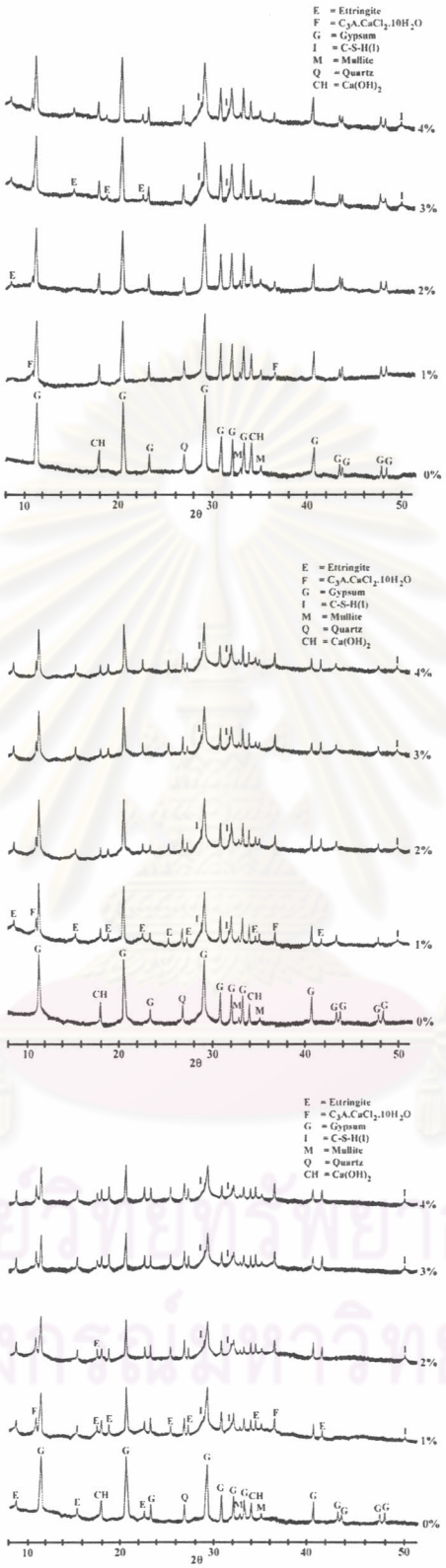

Curing 20°C for 1 day

Curing 20°C for 7 days

Curing 20°C for 28 days

Fig. 4.32 XRD patterns of composite materials activated with various contents of $CaCl_2$ and cured at different ages.

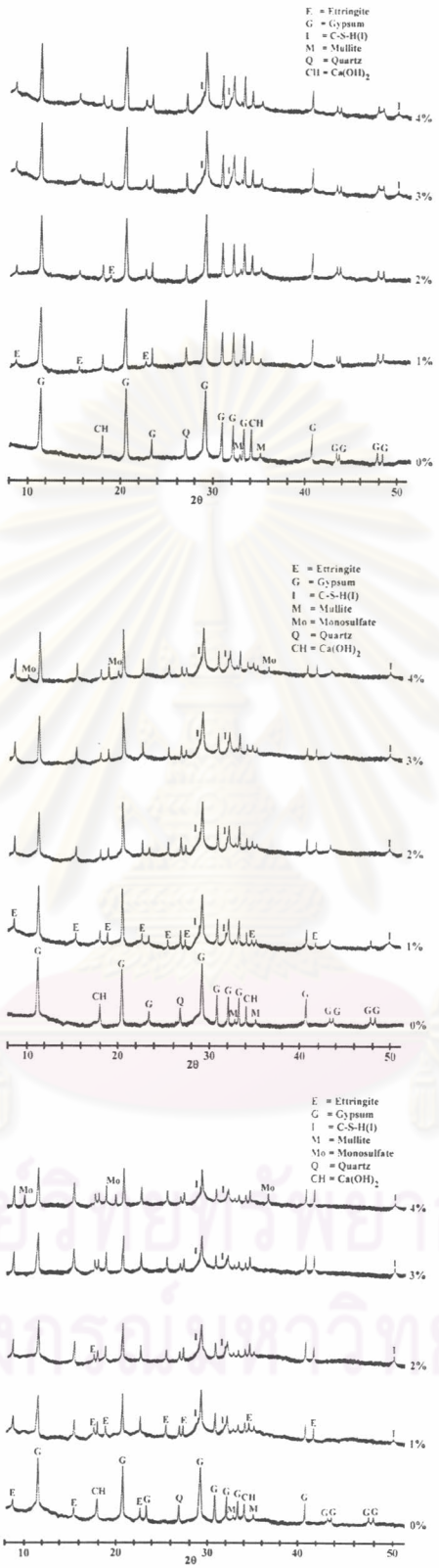

Fig. 4.33 XRD patterns of composite materials activated with various contents of Na_2CO_3 and cured at different ages.

Fig. 4.32 and Fig. 4.33 show the XRD patterns of composite materials activated with additive and cured at 20°C for 1, 7, and 28 days. In the case of $CaCl_2$ activated pastes (Fig. 4.32), The Friedel's salt ($3CaO.Al_2O_3.CaCl_2.10H_2O$), is identified and begins to form in the paste with 1% $CaCl_2$ at 1 day. The intensities of these diffraction peakes increase with curing time. The weak ettringite diffraction peaks appear with 4% $CaCl_2$ at 1 day and can be detected in every dosage of $CaCl_2$ at 7 days. The unreacted hydrated lime diffraction peaks are weaker than those in the pastes without additive.

When Na_2CO_3 (Fig. 4.33) was added, ettringite diffraction peaks were detected in every dosage of Na_2CO_3 at 1 day and increased with curing time. The diffraction peaks of monosulfate aluminate are observed in the paste with 4% Na_2CO_3 at 1 day and increase with curing time. Diffraction peaks of unreacted hydrated lime are weaker than those in the pastes without additive.

b.) Physical and mechanical properties of chemically activated composite materials

Physical and mechanical properties of composite materials activated with $CaCl_2$ and Na_2CO_3, cured in humid air at 20°C in humid air at scheduled age are presented Appendix : Table 11 and illustrated in Fig. 4.34.

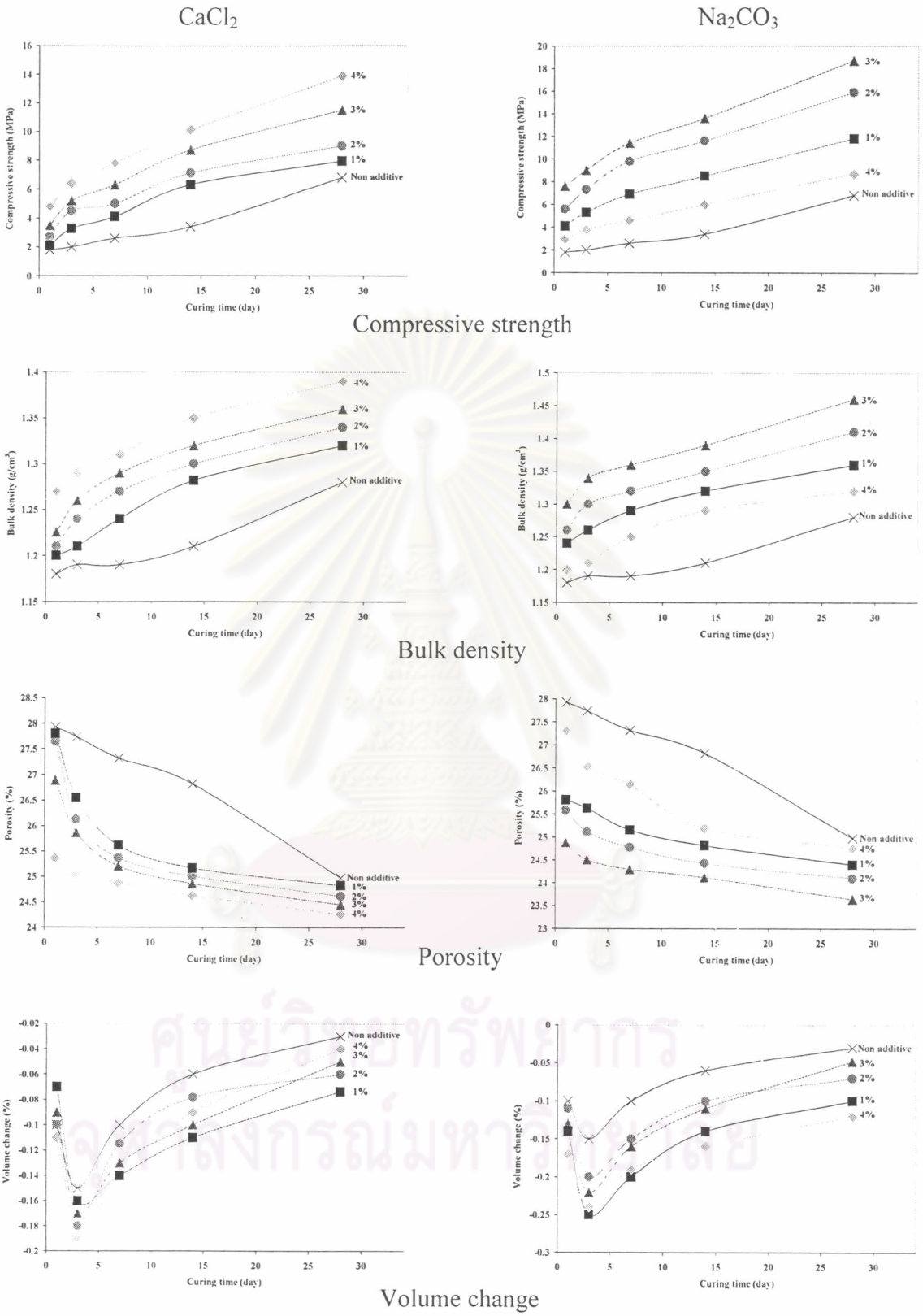

Fig. 4.34 Effect of content of additive on the physical and mechanical properties of composite materials.

Lime-Fly ash-FGD gypsum (β-HH)-$CaCl_2$ system

It was found from Fig. 4.34 that the compressive strength of specimens increases with increasing content of $CaCl_2$. This is also confirmed by the results of bulk density and porosity. It is found that the increase in additive content results in the increase of bulk density and hence porosity is reduced.

During the blending of the materials with $CaCl_2$ solution, $Ca(OH)_2$ dissolves first. The presence of $CaCl_2$ accelerates the dissolution of $Ca(OH)_2$ and gypsum ,but reduces the pH of the solution and the dissolution of fly ash, respectively. Therefore, the liquid phase of the mixture has a higher concentration of Ca^{2+} and SO_4^{2-}, but a lower concentration of dissolved monosilicate and aluminate species. This results in the formation of lower ettringite phase and tends to react chemically to form Friedel's salt[74] (Fig. 4.32) (eq. 1) ($3CaO.Al_2O_3.CaCl_2.10H_2O$)

$$2[Al(OH)_4]^- + 2Cl^- + 3Ca^{2+} + 4H_2O + 4OH^- \longrightarrow 3CaO.Al_2O_3.CaCl_2.10H_2O \qquad (1)$$

The formation of $3CaO.Al_2O_3.CaCl_2.10H_2O$ increases the solid volume (Table 11) much more than gypsum. Therefore, $CaCl_2$ activated specimens show the higher strength and denser structure than the unactivated specimens.

Lime-Fly ash-FGD gypsum (β-HH)-Na_2CO_3 system

The results from Fig. 4.34 also show the effect of the content of Na_2CO_3 on the compressive strength of specimens. It is found that the compressive strength increases with increasing content of Na_2CO_3 and the maximum strength is obtained at 3% of Na_2CO_3. The drop of compressive strength with higher contents of Na_2CO_3 is explained by Jinawath et al.[75] that Na_2CO_3 acted as the accelerator[2] and too high content of Na_2CO_3 severely shortened the setting time of β-HH and hence permitted not enough time to prepared a complete test specimens. This is confirmed by the flowability result (Fig. 4.35).

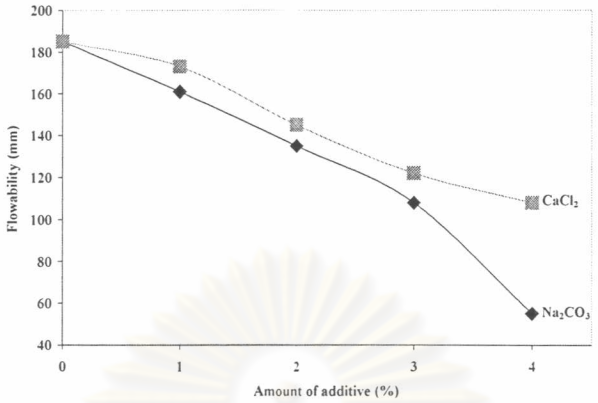

Fig. 4.35 Effect of additive on the flowability of specimens activated by chemically accelerating method.

The other reason is due to the formation of monosulfate aluminate (Fig. 4.33). Thermodynamic calculation indicated that ettringite is the stable phase below 70°C and monosulfate aluminate above 70°C[76]. Due to the higher concentration of reactants and the environmental conditions, it is possible for monosulfate aluminate to form directly or from the conversion of ettringite below 70°C in the Na_2CO_3 pastes (eq. 2, 3, and 6)[74].

$$2[Al(OH)_4]^- + SO_4^{2-} + 4Ca^{2+} + 6H_2O + 4OH^- \longrightarrow 3CaO.Al_2O_3.CaSO_4.12H_2O \quad (2)$$

$$6Ca(OH)_2+2Al_2O_3+3CaO.Al_2O_3.3CaSO_4.32H_2O \rightarrow 3[3CaO.Al_2O_3.CaSO_4.12H_2O]+2H_2O \quad (3)$$

$$Na_2CO_3\,(aq) + Ca(OH)_2\,(aq) \longrightarrow 2NaOH + CaCO_3\,(s) \quad (4)$$

$$CaSO_4.2H_2O(s) + NaOH\,(aq) \longrightarrow Ca(OH)_2\,(s) + Na_2SO_4\,(aq) \quad (5)$$

$$3CaO.Al_2O_3.3CaSO_4.32H_2O+4NaOH \longrightarrow 3CaO.Al_2O_3.CaSO_4.12H_2O+2Na_2SO_4 + Ca(OH)_2+20H_2O \quad (6)$$

The conversion of ettringite to monosulfate aluminate causes the decrease in the solid volume. This means that the Na_2CO_3 activated pastes will exhibit a lower strength at higher concentrations.

When Na_2CO_3 is added, the reaction between $Ca(OH)_2$ and Na_2CO_3 as expressed by eq.(4) happens first. The reaction increases the pH of the solution, accelerates the dissolution of fly ash and speeds up the pozzolanic reaction between $Ca(OH)_2$ and fly ash. At higher contents of Na_2CO_3, the reaction results in the increase of NaOH concentration and promotes gypsum dissolution and the formation of calcium hydroxide (eq. 5). As gypsum dissolves in NaOH, both calcium and sulfate ion concentrations increase and calcium hydroxide precipitate. The formation of calcium hydroxide therefore competes with that of ettringite. Thus the amount of calcium hydroxide formed limits ettringite formation and allows for the formation of other phase[74].

The properties of related hydration products in lime-fly ash-gypsum pastes are listed in Table 4.8. The generation of ettringite (Fig. 4.33) increases the early strength of hardened pastes very significantly and densifies the structure. These results are comfirmed by the results of bulk density and porosity (Fig. 4.34).

Table 4.8 Properties of related reaction products[12,76].

Formular	Molar mass (g/mol)	Crystal form	Density (g/cm^3)	Volume change (%)
$CaSO_4.2H_2O$	172	Needle	2.31	10.1
$CaO.SiO_2.\ 1.5H_2O$	143	Fibre bundles	2.0-2.2	17.5
$3CaO.Al_2O_3.13H_2O$	560	Hexagonal plate	2.02	58.9
$3CaO.Al_2O_3.CaCl_2.10H_2O$	561	Hexagonal plate	2.03	95.4
$3CaO.Al_2O_3.3CaSO_4.32H_2O$	1254	Needle	1.73	164.2
$3CaO.Al_2O_3.CaSO_4.12H_2O$	622	Hexagonal plate	1.99	79.2

c.) Free lime content

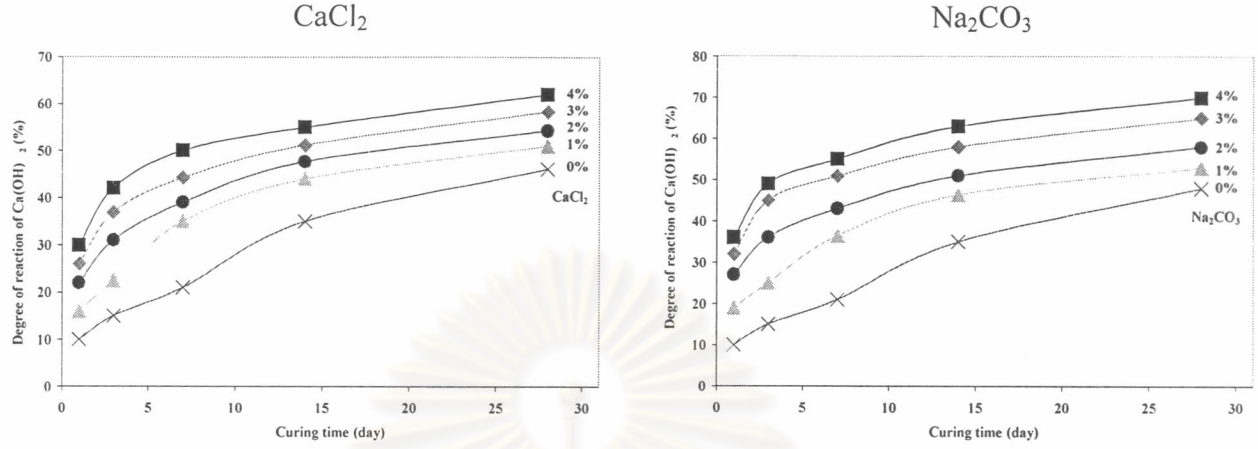

Fig. 4.36 The degree of $Ca(OH)_2$ reaction in the chemically accelerating composite materials.

Fig. 4.36 shows the reacted percentage of $Ca(OH)_2$ in the chemically activating composite materials. The consumption of $Ca(OH)_2$ in Na_2CO_3 and $CaCl_2$ activated pastes tends to be faster than that in the one without additive during the initial reaction state. The higher the content of additive is used in the composition, the higher the degree of $Ca(OH)_2$ consumption is detected. Therefore, it can be concluded that the addition of both additives accelerate the early pozzolanic reaction. The results in Fig. 4.37 show that the slopes of the linear relationships are different. This is resulted from the formation of various hydration products with different mechanisms.

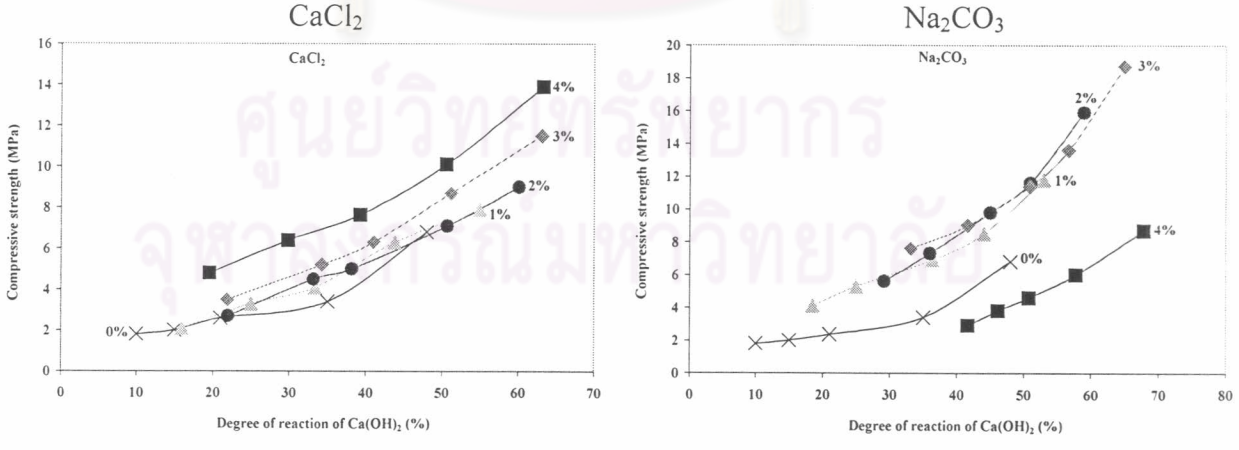

Fig. 4.37 Correlation between compressive strength and the degree of $Ca(OH)_2$ reaction in the chemically accelerating composite materials.

d.) Particle morphology of chemically accelerating composite materials

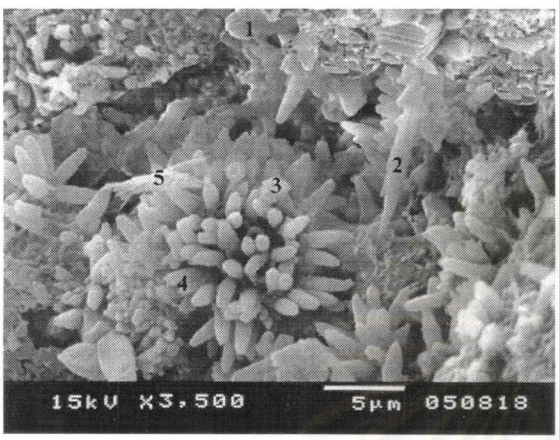

$CaCl_2$ 4 wt% activated paste

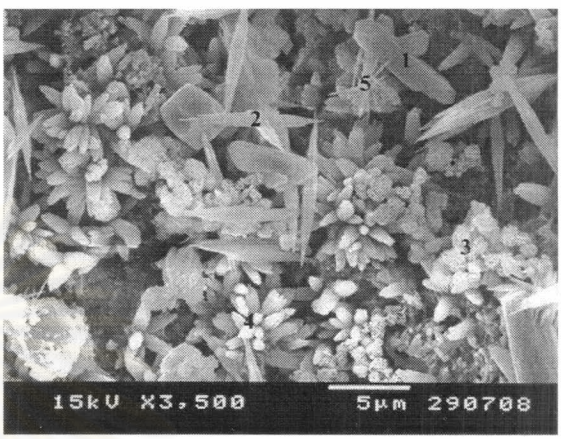

Na_2CO_3 3 wt% activated paste

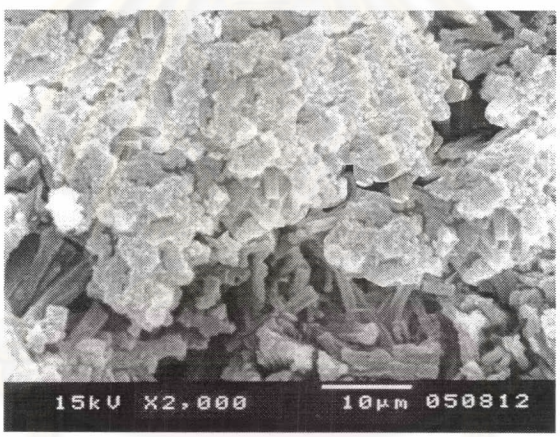

Non-additive paste

Fig. 4.38 SEM micrographs of chemically accelerating composite materials cured in humid air at 20°C for 28 days.

Fig. 4.38 shows the effect of $CaCl_2$ and Na_2CO_3 on the microstructures of the hardened composite materials at 28 days. Comparing the fracture surfaces of these samples, $CaCl_2$- and Na_2CO_3-activated pastes reveal a better developed hydration products than the non additive paste which shows only compact lath crystals of gypsum and clusters hydrated product. The various morphologies of hydration products in $CaCl_2$- and Na_2CO_3-activated pastes have been identified by the energy dispersing spectroscopy (EDS). It is found from the EDS results in Fig. 4.39 that the hydration products

can be divided in to two groups. The first one is gypsum (area 1, big crystals) and the second one is the combination products of ettringite and C-S-H(I) (area 2, 3, 4, and 5). The difference among these combination products is the Al_2O_3/SiO_2 ratio. The higher the ratio, the higher the tendency of phase separation is investigated. According to the XRD analyses in Fig. 4.32 and Fig. 4.33, Friedel's salt and C-S-H(I) are also found. However, these two hydration products with a morphology and composition are not detected by SEM. This might be due to the limitation of the instrument.

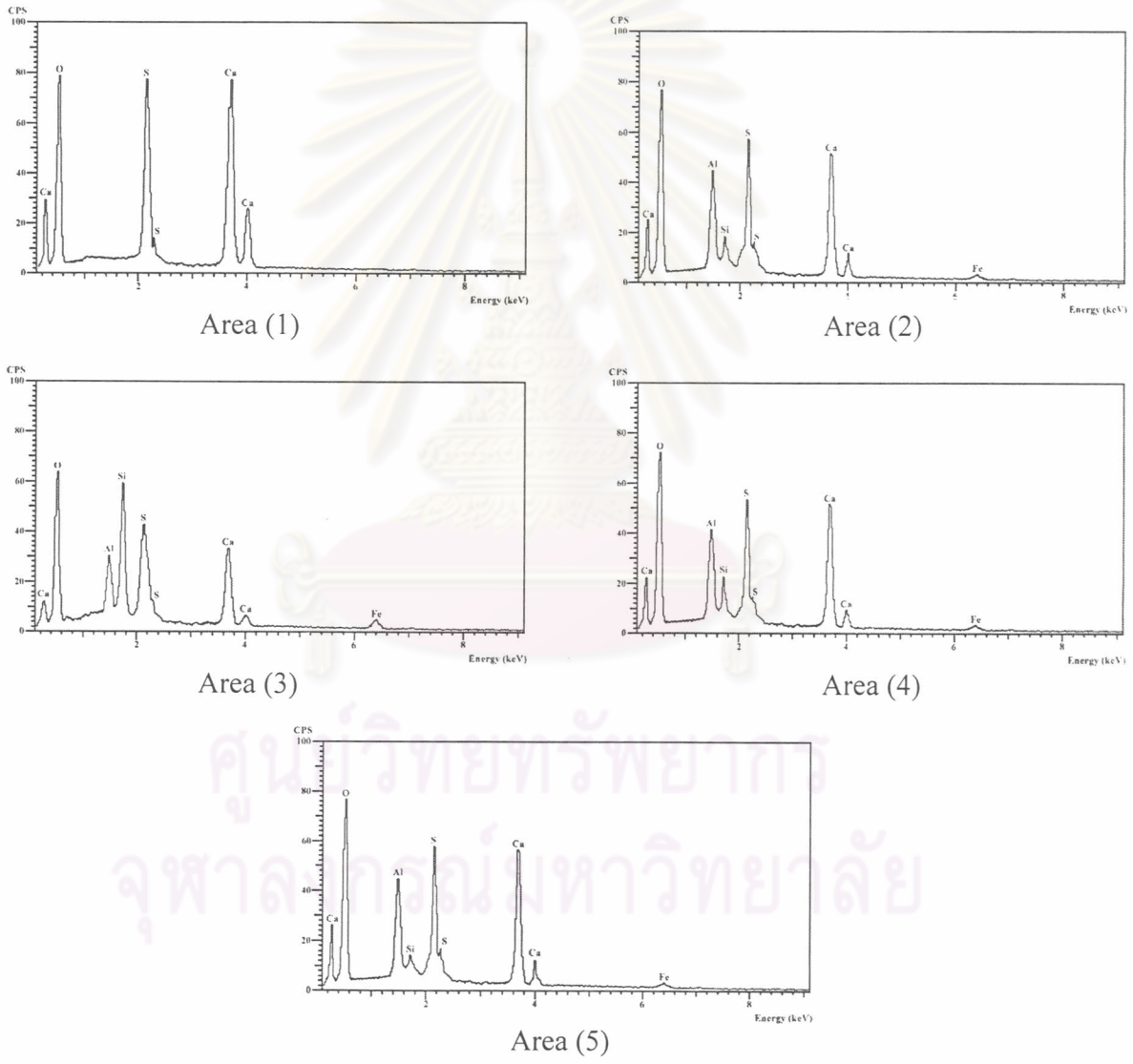

Fig. 4.39 EDS results of chemically accelerating composite materials focused at the different areas of specimens relating to the SEM micrographs, illustrated in Fig. 4.38.

e.) Kinetic analysis

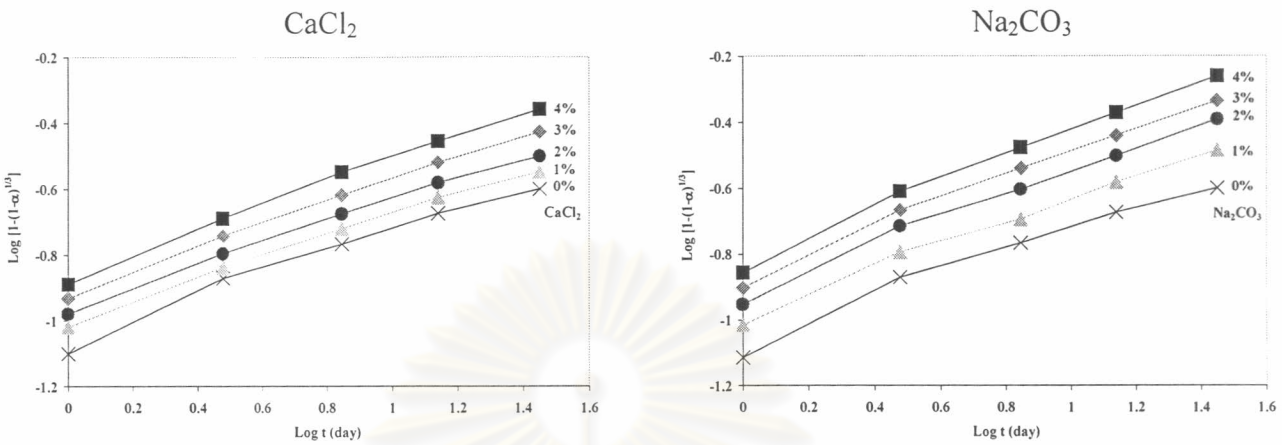

Fig. 4.40 Pozzolanic reaction kinetics in the chemically accelerating composite materials.

Table 4.9 Reaction grade (N) and phase period of the composite materials activated by chemically accelerating method.

Amount of Additive (wt%)	Type of additive	Phase I (N ≤ 1)		Phase II (2 ≥ N > 1)		Phase III (N > 2)	
		N	Period	N	Period	N	Period
-	-	N/A	N/A	1.95	3 days	2.51	> 3 days
1	$CaCl_2$	N/A	N/A	N/A	N/A	2.08	> 3 days
	Na_2CO_3	N/A	N/A	1.96	3 days	2.12	> 3 days
2	$CaCl_2$	N/A	N/A	N/A	N/A	2.14	> 3 days
	Na_2CO_3	N/A	N/A	1.84	3 days	2.16	> 3 days
3	$CaCl_2$	N/A	N/A	N/A	N/A	2.23	> 3 days
	Na_2CO_3	N/A	N/A	1.78	3 days	2.30	> 3 days
4	$CaCl_2$	N/A	N/A	N/A	N/A	2.32	> 3 days
	Na_2CO_3	N/A	N/A	1.73	3 days	2.41	> 3 days

N/A = not applicable.

Based on the measurement of reaction kinetic in Fig. 4.40 and Table 4.9, it can be seen that the introduction of $CaCl_2$ has a significant effect on the pozzolanic reaction in the composite materials. It seems that only Phase III is the reaction phase detected in all the $CaCl_2$ admixtures and the reaction grade N decreases with increasing amount of $CaCl_2$. Thus, the addition of $CaCl_2$ significantly alters the pozzolanic reaction behavior.

The trend of pozzolanic reactions in the Na_2CO_3-activated pastes is very similar to that of the non additive paste except for some offset reaction degree in the early stage. This means that the addition of Na_2CO_3 accelerates the consumption of $Ca(OH)_2$ or pozzolanic reaction rate mainly during the first period.

4.4.4 Mechanically accelerating method

a.) Phase analysis of composite materials improved by mechanically accelerating method

XRD results of the phase composition of composite materials cured at different temperatures and scheduled age are presented in Fig. 4.41.

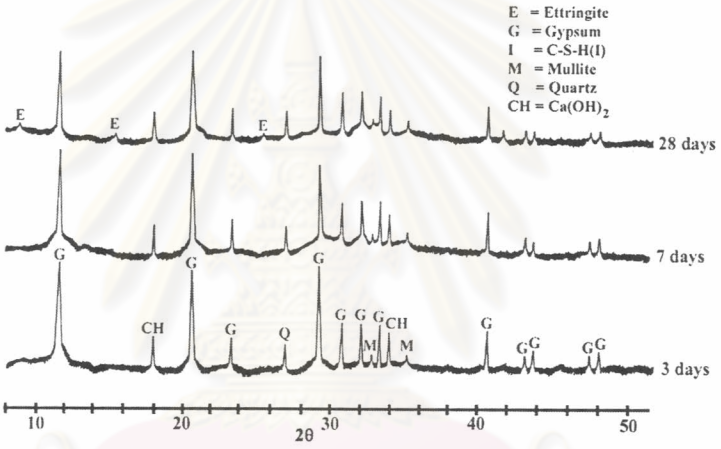

Fig. 4.41 XRD patterns of composite materials improved by mechanically accelerating method cured at different ages.

According to the XRD analyses Fig. 4.41, small ettringite peaks are investigated at 28 days but no C-S-H(I) phase detected at all the curing ages. Diffraction peaks of gypsum and unreacted hydrated lime are still remained and slightly decreased with time. Low content of hydrated phases in the mechanical accelerated specimens might relate to the high density and low porosity of the compacted specimens.

b.) Physical and mechanical properties of mechanically accelerating composite materials

Physical and mechanical properties of the composite materials improved by mechanically accelerating method at various curing ages are presented in Appendix : Table 12 and shown in Fig. 4.42.

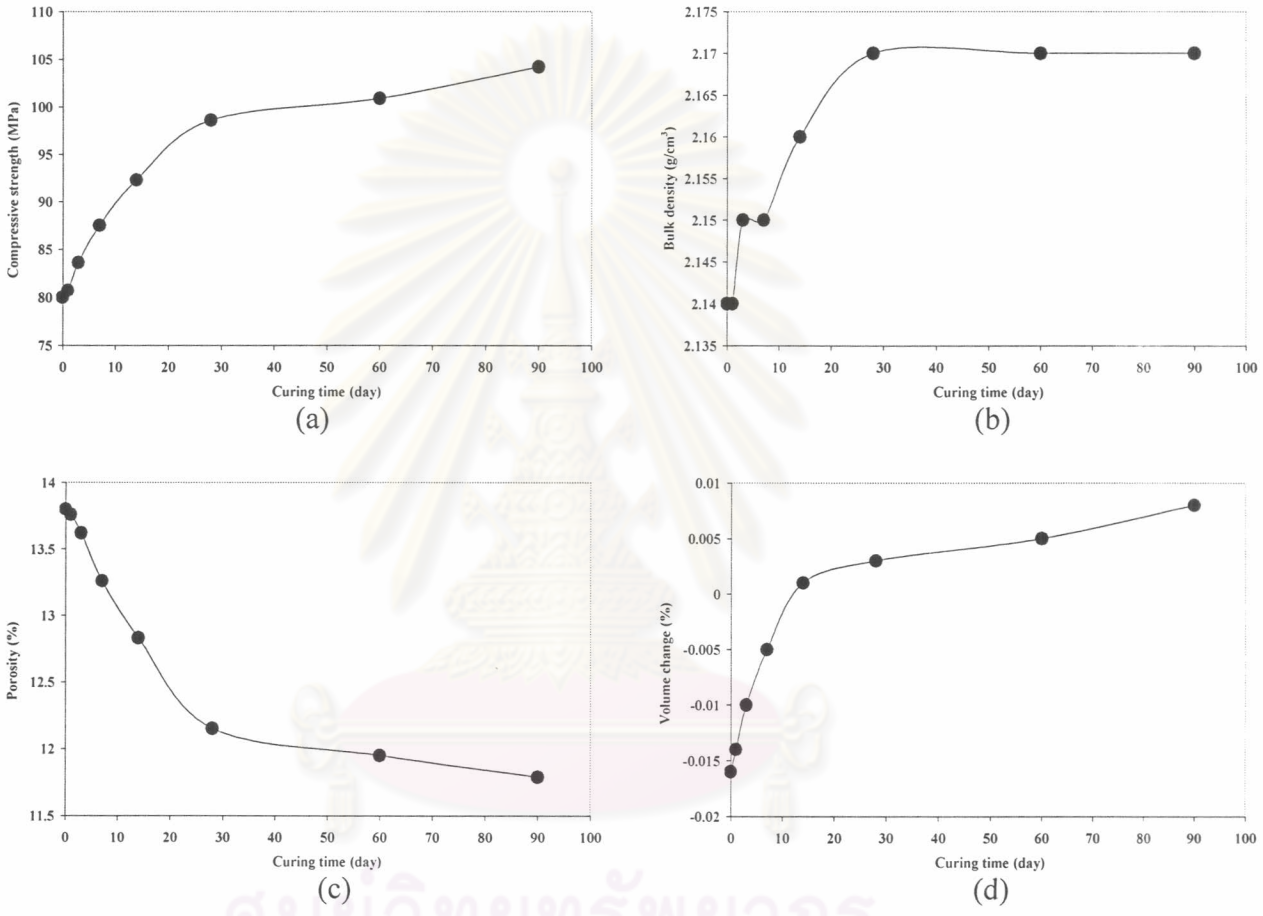

Fig. 4.42 Effect of mechanically accelerating method on the physical and mechanical properties of composite materials (a) compressive strength, (b) bulk density, (c) porosity, and (d) volume change.

It is found from the experiment that the mechanically accelerating composite materials shows high strength in the beginning of curing stage and gradually increases with time (Fig. 4.42). Moreover, the mechanically accelerating method reinforces the specimens to have higher strength than the others.

Due to high bulk density and low porosity, the humidity from the curing atmosphere is difficult to react with unreacted substances remaining inside. Therefore, the pozzolanic reaction proceeds very slow. This results conform to the results of XRD analyses. However, the most important advantage of mechanical accelerated method is based on a productivity aspect. The preliminary thermal treatment to prepared β-HH from the FGD gypsum, for use as binder in the other methods is not required in the mechanically accelerating method and the FGD gypsum can be used in the as-received form.

c.) Particle morphology of mechanically accelerating composite materials.

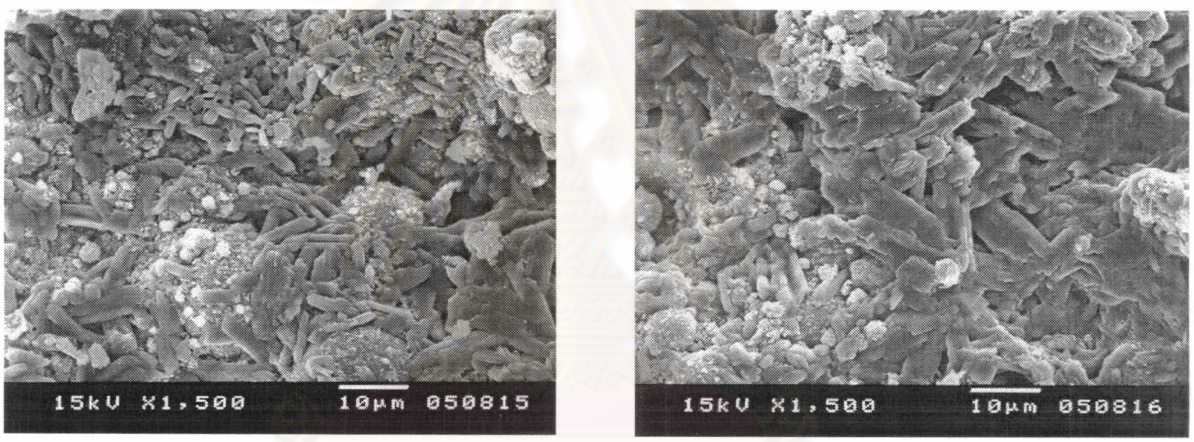

After demould Curing for 28 days

Fig. 4.43 SEM micrographs of mechanically accelerating composite materials.

It is found from the SEM micrographs (Fig. 4.43) that compaction causes the contact of raw materials after demould and hence, during curing, the hydration quickly proceeds and the hydration products fill pores. This supports the high strength of the mechanically accelerating composite materials at the early age. The hydration products from pozzolanic reaction keep on going with curing time and result in the dense cementation of the hydrated mass.

d.) Performance of mechanically accelerating composite materials under water

Performance under water of the composite materials cured in humid air at 20°C for 28 days and improved with mechanically accelerating method at different ages are shown in Appendix : Table 13 and presented graphically in Fig. 4.44.

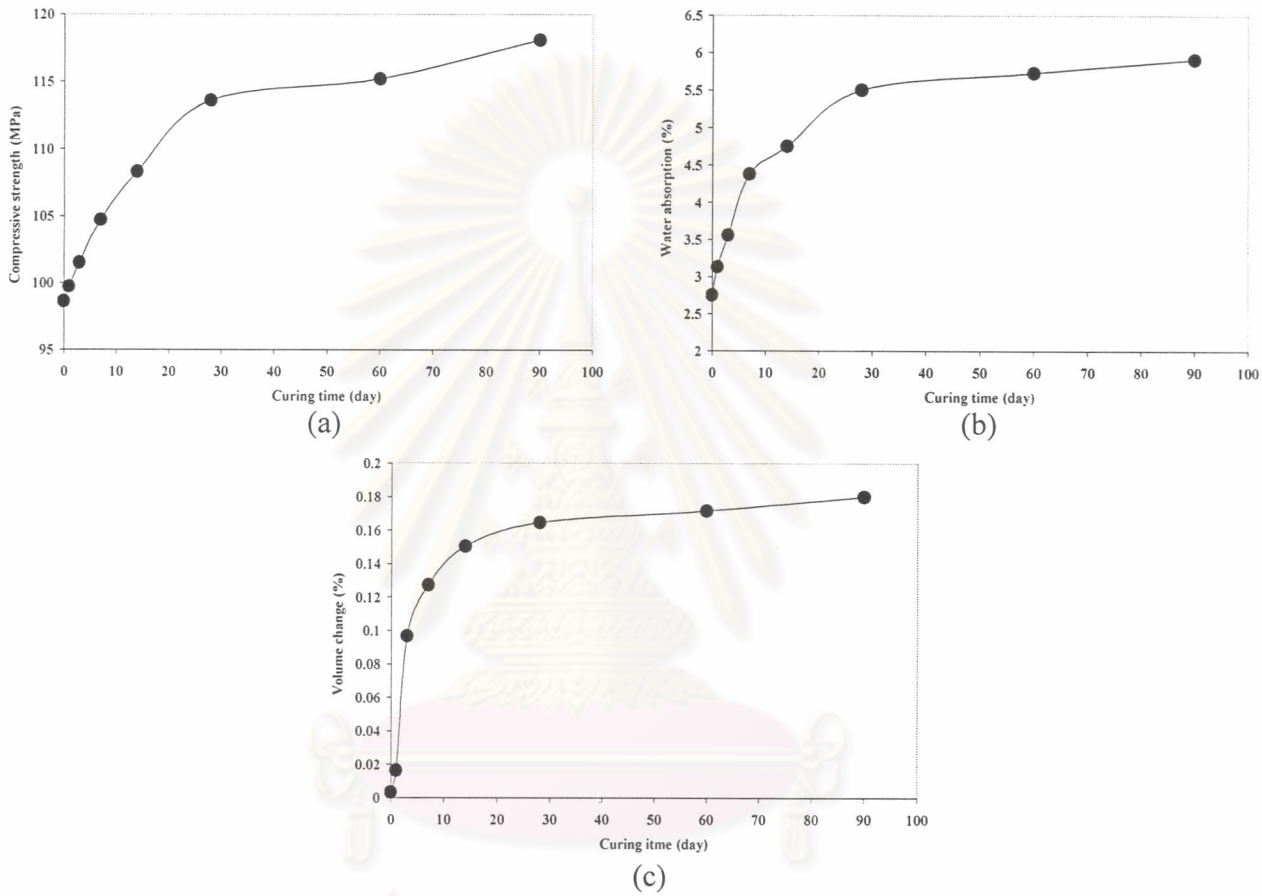

Fig. 4.44 Physical and mechanical properties of mechanically accelerating specimens under water (a) compressive strength, (b) water absorption, (c) volume change.

It is found from Fig. 4.44 that the strength increases with increasing immersion time because the excess water proceeds the pozzolanic reaction and produces more hydrated phases. The water absorption of the composite increases and no leaching away of the matrix is detected. The superior behaviour of the composite towards water may be ascribed to the filling of most of voids and pores of the gypsum matrix with hydrated products. The volume change measurements indicate that the swelling under water does not excess 0.20 Vol% at 90 days and tends to be constant at the later age.

4.4.5 Combination of accelerating methods

4.4.5.1 Thermally and chemically accelerating method

a.) Phase analysis of composite materials improved by the combination methods.

XRD results of the phase composition of composite materials cured at 50°C and scheduled age are illustrated in Fig. 4.45.

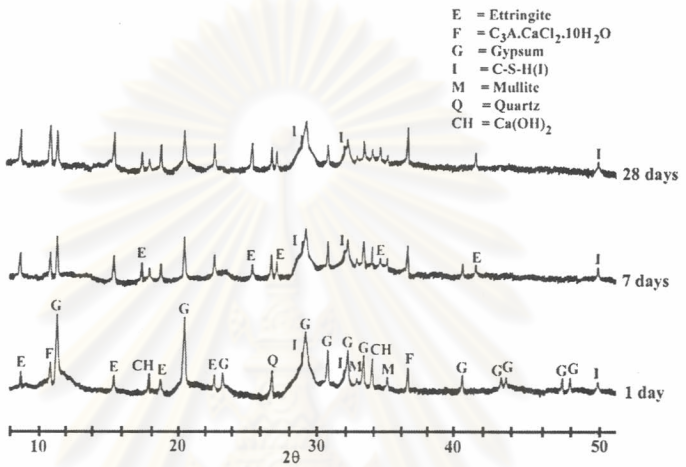

(a) Activated with $CaCl_2$ 4 wt%, cured at 50°C in humid air

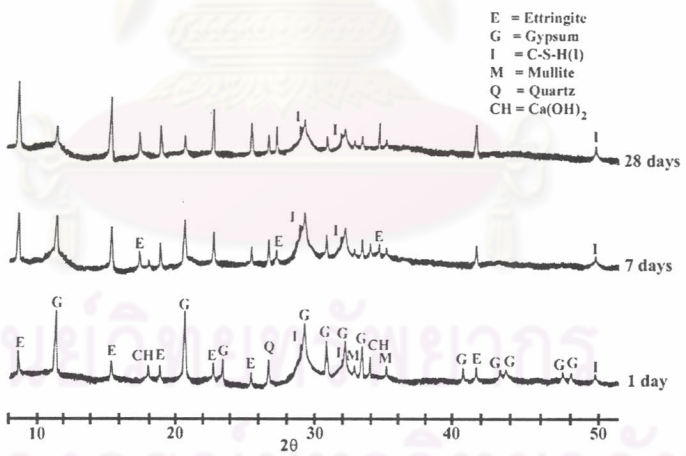

(b) Activated with Na_2CO_3 3 wt%, cured at 50°C in humid air

Fig. 4.45 XRD patterns of thermally and chemically accelerating composite materials cured at various ages.

Fig. 4.45 (a) shows the XRD patterns of 4 wt% $CaCl_2$-activated pastes. Diffraction peaks of Friedel's salt ($3CaO.Al_2O_3.CaCl_2.10H_2O$) are

identified and intensified with time. Diffraction peaks of hydrated lime slightly diminishes with time and almost disappears at 28 days.

XRD patterns of 3wt% Na_2CO_3-activated pastes cured at 50°C are presented in Fig. 4.45 (b). Strong ettringite peaks are detected at 1 day and increases sharply with time. Diffraction peaks of gypsum are weaker than those cured at 20°C and diminishes with time. Diffraction peaks of unreacted hydrated lime are detected at 1 to 7 days and disappears at 28 days.

b.) Physical and mechanical properties of composite materials improved by thermally and chemically activating method

Physical and mechanical properties of composite materials activated with $CaCl_2$ 4 wt% and Na_2CO_3 3 wt% cured at 50°C and scheduled age are presented in Appendix : Table 14 and illustrated in Fig. 4.46.

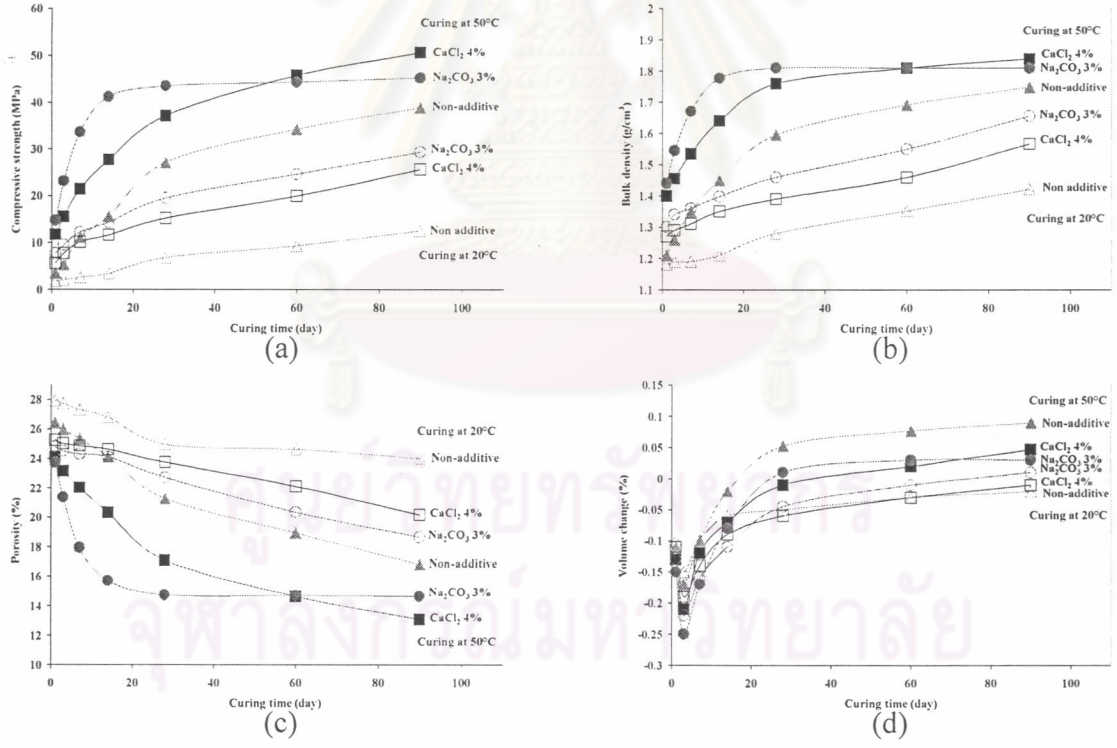

Fig. 4.46 Effect of thermally and chemically accelerating method on the physical and mechanical properties of composite materials (a) compressive strength, (b) bulk density, (c) porosity, and (d) volume change.

It is found from the previous results that activated pastes with $CaCl_2$ 4 wt% and Na_2CO_3 3 wt% showed the optimum results at curing temperature 20°C. Therefore, these contents of additive are selected to use in pastes cured at 50°C. The results from Appendix : Table 14 and Fig. 4.46 showed that the increase in curing temperature accelerates the dissolution of fly ash and the formation of reaction products in both $CaCl_2$- and Na_2CO_3-activated pastes. All these pastes cured at 50°C exhibit a more rapid initial strength gain than those of the lower curing temperature. The presence of Na_2CO_3 induces a significant increase in early strength but a slow later strength gain, while $CaCl_2$-activated pastes exhibits a slightly lower strength at early ages but tends to go for a higher strength than the Na_2CO_3-activated pastes at later ages. Moreover, it is also found that the chemical activation shows much more significant acceleration effect than the thermal activation.

c.) Free lime content

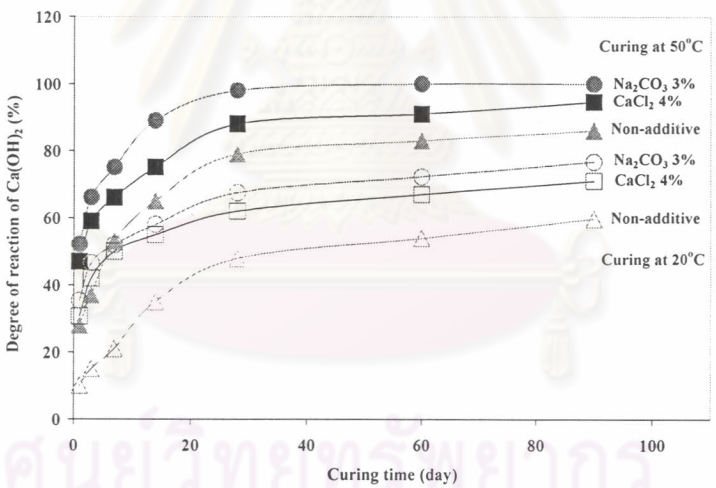

Fig. 4.47 The degree of $Ca(OH)_2$ reaction in the composite materials improved by thermally and chemically accelerating method.

Fig. 4.47 shows the reacted percentage of $Ca(OH)_2$ in the composite materials activated by the combination of temperature and chemicals. It can be concluded that the addition of Na_2CO_3 accelerates the early pozzolanic reaction since $Ca(OH)_2$ is consumed very quickly and then much more slowly thereafter and completely after 28 days. The consumption of $Ca(OH)_2$ in $CaCl_2$-activated pastes is similar to that of the

Na_2CO_3-activated pastes during the first 3 days and diminishes later. It is also found from the results that, in the early curing period, the chemically accelerating method shows more effective for accelerating pozzolanic reaction than the temperature method. The consumption of $Ca(OH)_2$ in Na_2CO_3- and $CaCl_2$-activated pastes are faster than that non-additive paste during the initial rapid reaction state. The higher the content of additive is used in the composition, the higher the degree of $Ca(OH)_2$ consumption is detected. Therefore, it can be concluded that the combination of accelerating methods is more efficient to enhance the pozzolanic reaction than using a single one.

The results in Fig. 4.48 also show that the slopes of the linear relationships are different. It resulted from the formation of various hydration products of different mechanisms.

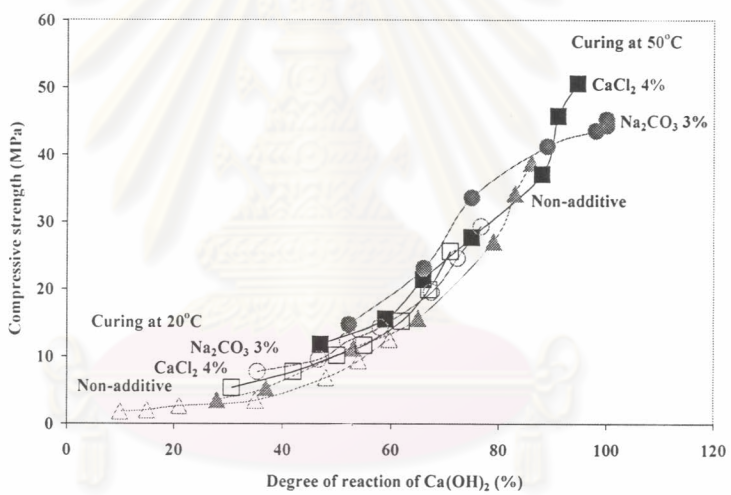

Fig. 4.48 Correlation between compressive strength and the degree of $Ca(OH)_2$ in the thermally and chemically accelerating composite materials.

d.) Particle morphology of composite materials activated by thermally and chemically accelerating method

$CaCl_2$ 4 wt% activated paste cured at 50°C

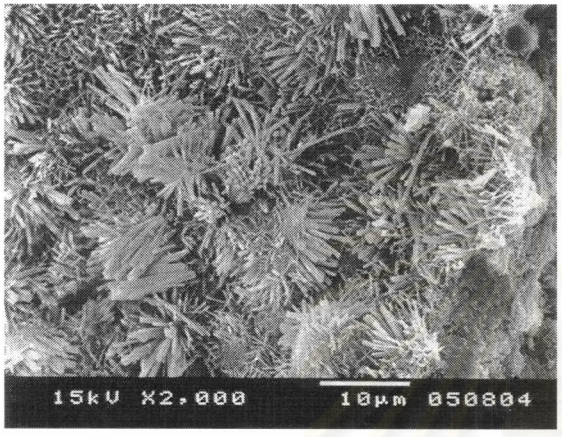

a.) Fracture surface

Na_2CO_3 3 wt % activated paste cured at 50°C

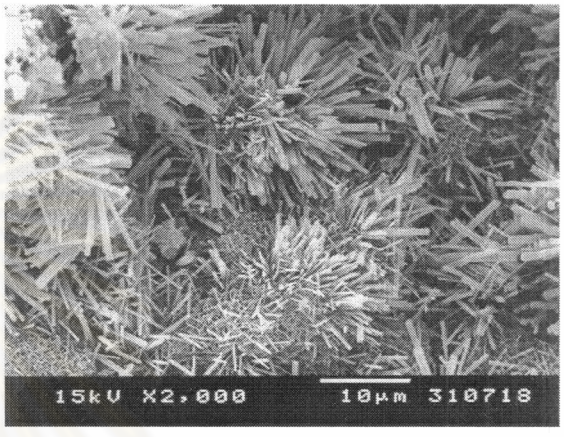

b.) Fracture surface

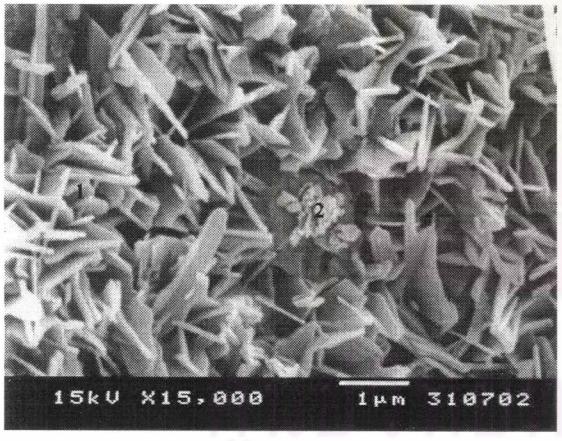

c.) Matrix enlarged

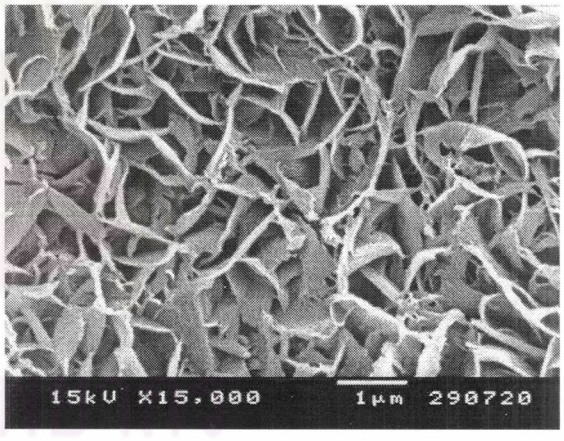

d.) Matrix enlarged

Fig. 4.49 SEM micrographs of thermally and chemically accelerating composite materials cured at 28 days.

Fig. 4.49 shows the microstructure of the hardened composite materials at 28 days. The fracture surfaces of $CaCl_2$- and Na_2CO_3-activated pastes (Fig. 4.49a and Fig. 4.49b) reveal clearly a more hydration products and a less porous structure than those in the non-additive pastes. On the fracture surface of the $CaCl_2$-activated pastes, the outline of fly ash particles can be distinguished but all of them are covered by a layer of hydration products. This means that not all the fly ash particles in the $CaCl_2$-activated pastes are completely reacted. On the other hand, the outline of fly ash particles on the surface of the Na_2CO_3-activated pastes can not be detected.

The morphology of the hydration products can be clearly observed on the fracture surface of both $CaCl_2$- and Na_2CO_3-activated pastes. They are shown as protruding clusters of big fiber on the matrix of fine mesh. According to the XRD analysis in Fig. 4.45, the clusters of big fiber showed in Fig. 4.49a and 4.49b are ettrigite. These results are confirmed by the results of EDS presented in Fig. 4.50a and 4.50b. The hexagonal plates are the main observation in the matrix of $CaCl_2$-activated pastes. These hexagonal plates are referred to Friedel's salt (Fig. 4.49c, area 1). Moreover, Non crystalline morphology of C-S-H(I) is also detected as a minor constituent (Fig. 4.49c, area 2). These results are also verified by the EDS exhibited in Fig. 4.50c and Fig. 4.50e. Honeycomb-liked structures can be observed in the matrix of the Na_2CO_3-activated pastes (Fig. 4.49d). Those structures are C-S-H(I) based on the results of XRD (Fig. 4.45) and EDS analysis (Fig. 4.50d).

$CaCl_2$ 4 wt% activated paste cured at 50°C

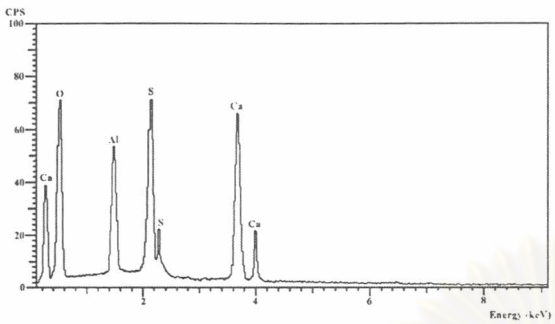

a.) Fracture surface, clusters of big fiber

Na_2CO_3 3 wt% activated paste cured at 50°C

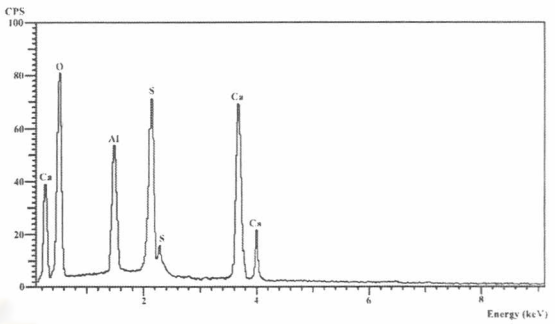

b.) Fracture surface, clusters of big fiber

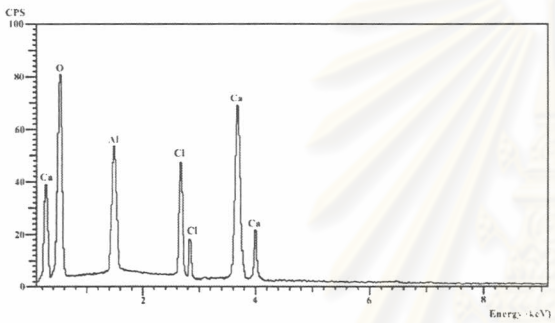

c.) Matrix (area 1)

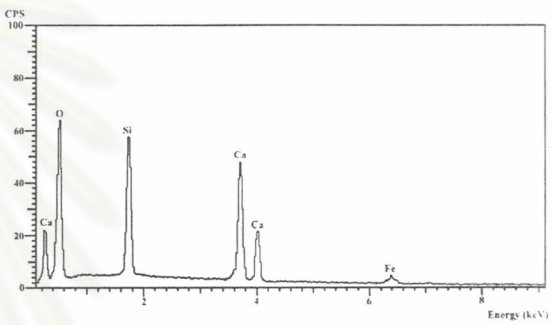

d.) Matrix

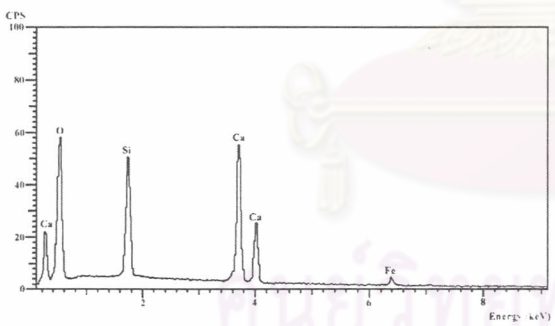

e.) Matrix (area 2)

Fig. 4.50 EDS results of thermally and chemically accelerating composite materials analyzed on the different areas of specimens relating to the SEM micrographs illustrated in Fig. 4.49.

e.) Kinetic analysis

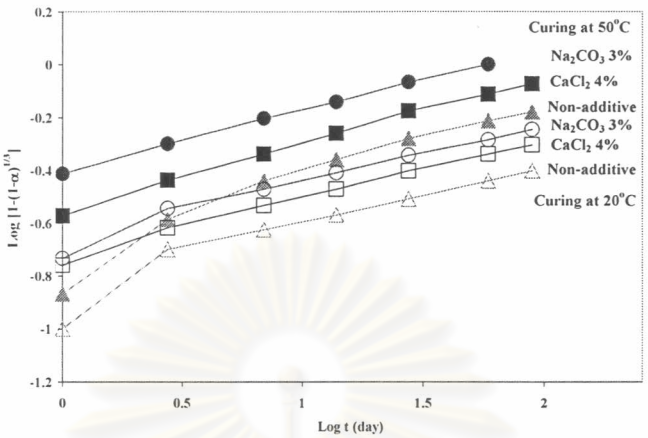

Fig. 4.51 Pozzolanic reaction kinetics in the thermally and chemically accelerating composite materials.

Table 4.10 Reaction grade (N) and phase period of the composite materials activated by thermally and chemically accelerating method cured at different temperatures.

Type of additive	Curing temperature (°C)	Phase I ($N \leq 1$)		Phase II ($2 \geq N > 1$)		Phase III ($N > 2$)	
		N	Period	N	Period	N	Period
Non additive	20	N/A	N/A	1.95	3 days	2.51	> 3 days
	50	N/A	N/A	1.66	3 days	2.18	> 3 days
$CaCl_2$ 4 wt%	20	N/A	N/A	N/A	N/A	2.32	> 3 days
	50	0.26	> 1 day	N/A	N/A	N/A	N/A
Na_2CO_3 3 wt%	20	N/A	N/A	1.78	3 days	2.30	> 3 days
	50	0.23	> 1 day	N/A	N/A	N/A	N/A

N/A = not applicable.

It is found from the reaction kinetics in Fig. 4.40 and Table 4.10 that reaction grade (N) is less than 1 in the composite materials activated by combination method, therefore, the total pozzalanic reaction is controlled by the dissolution of reactants[74]. The dissolution of $CaOH_2$ should be much faster than that of the pozzalan. Thus, the total pozzolanic reaction in the $CaCl_2$ and Na_2CO_3-activated pastes is governed by the dissolution of the pozzolan at 50°C.

f.) Performance under water of composite materials activated by thermally and chemically accelerating method.

Performance of the composite materials improved by thermally and chemically accelerating method, cured at 20°C and 50°C for 28 days at different ages are presented in Appendix : Table 15 and in Fig. 4.52.

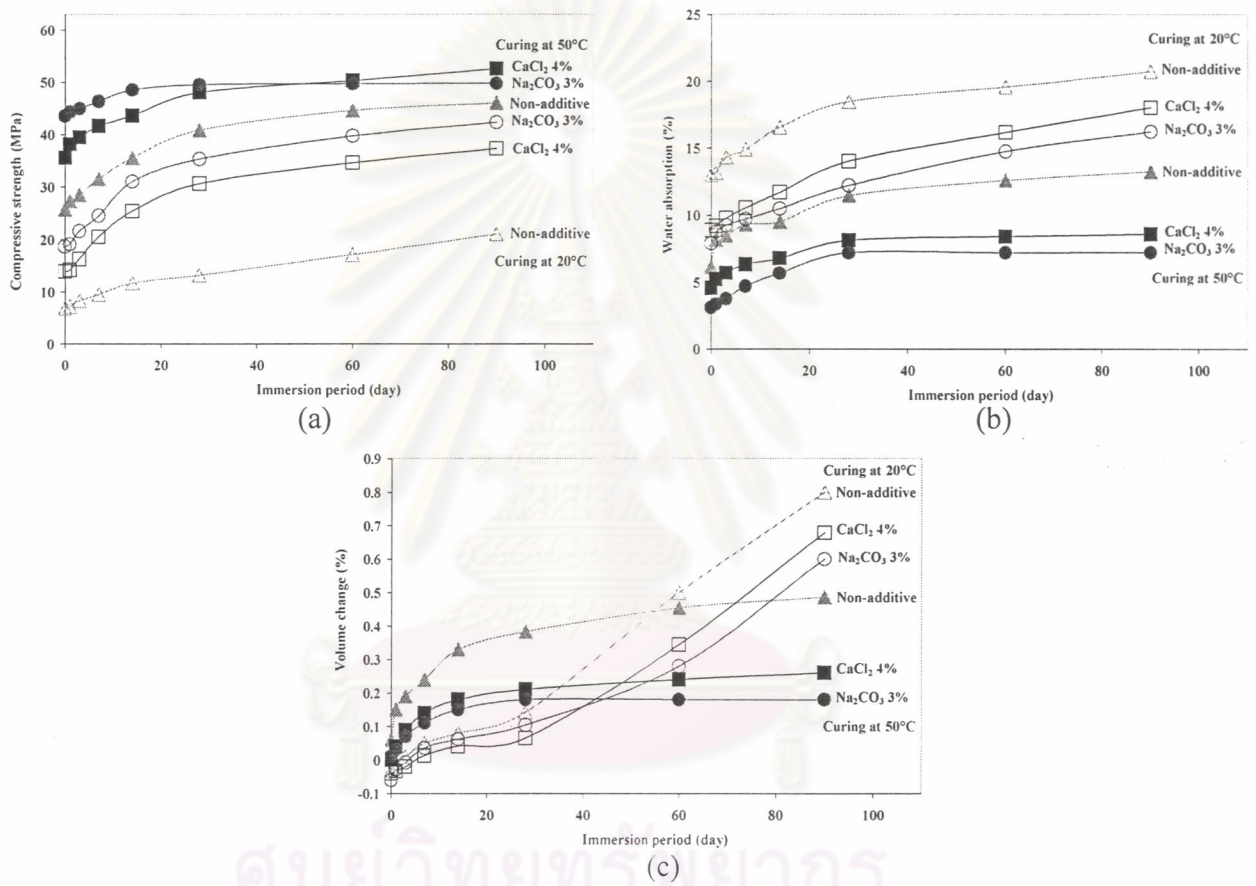

Fig. 4.52 Physical and mechanically properties of specimens improved by thermally and chemically accelerating method, cured for 28 days and followed by immersion method under water (a) compressive strength (b) water absorption, and (c) volume change.

It is found from the results shown in Appendix : Table 15 and illustrated in Fig. 4.52 that the strength increases slightly and tends to be constant in the Na_2CO_3-activated specimens. At a period of 90 days under water, the $CaCl_2$-activated specimens exhibit higher strength than the Na_2CO_3-activated specimens. It may be caused by

the further pozzolanic reaction between the remaining hydrated lime in the specimens and the excess water in the system. The water absorption of both activated specimens is lower than those in the specimens without additive due to the filling of voids and pores in gypsums matrix with the hydration products, ettringite, C-S-H(I), Friedel's salt.

g.) Effect of wetting/drying cyclic storage on the physical properties of composite materials activated by thermally and chemically accelerating method.

Physical and mechanical properties at different cyclic storage of the 28-day composite materials, improved by thermally and chemically accelerating method, are shown in Appendix : Table 16 and illustrated in Fig. 4.53.

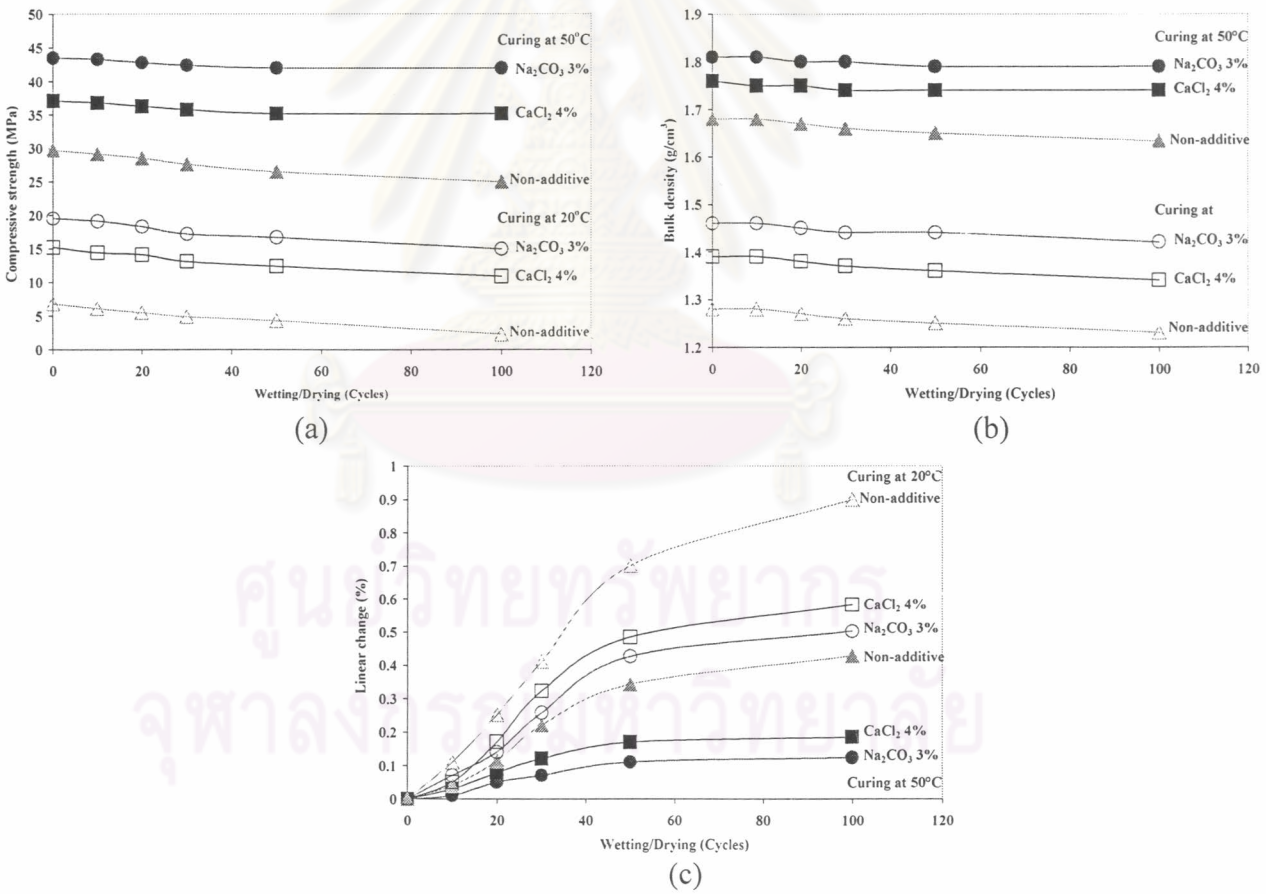

Fig. 4.53 Effect of wetting/drying cycles on the physical and mechanical properties of composite materials activated by thermally and chemically accelerating method (a) compressive strength, (b) bulk density, and (c) linear change.

The compressive strength of temperature and chemical accelerated composite materials measured after different cyclic storage shows the expected drop in strenght (Appendix : Table 16, Fig. 4.53). After 100 wetting/drying cycles, the strength of the non-additive specimens cured at high temperature, 50°C, drops 14.14% while those of the specimens activated with $CaCl_2$ and Na_2CO_3 decrease only 7.27% and 5.51%, repectively. The strength reduction in the specimens accelerated with additive is lower than those without additive due to their higher amount of hydrated products and lesser gypsum content in the system. This result is confirmed by the XRD results presented in Fig. 4.45. The hydration products, especially ettringite, increases the strength and densifies the structure. Therefore, The higher the content of hydrated products in the specimens, the lower the linear change is detected.

$CaCl_2$ 4 wt% activated paste cured at 50°C

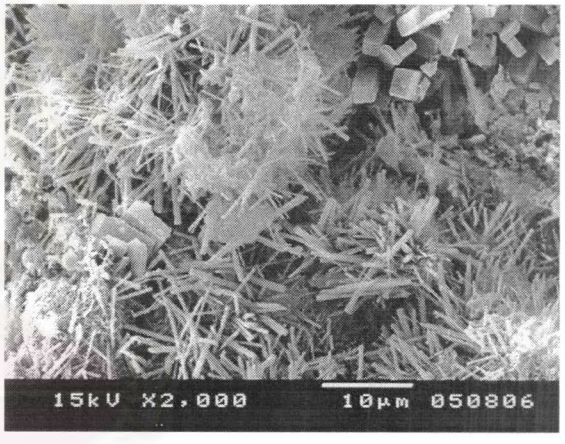

Na_2CO_3 3 wt% activated paste cured at 50°C

Fig. 4.54 SEM micrographs of composite materials activated by thermally and chemically accelerating method after 100 cycles of wetting/drying cyclic storage.

It is found from the SEM micrographs presented in Fig. 4.54 that the microstructures of composite materials after 100 cycles of wetting/drying cyclic storage are sound and in well-formed structure. However, it seems that there is a little part of some coagulation behavior showing in the micrographs. It might be caused by the dissolution of the remaining gypsum in the composition.

Rhombohedral crystals were investigated from the SEM micrograph of both $CaCl_2$- and Na_2CO_3-activated composite materials after 100 cycles of wetting/drying cyclic storage. The XRD results from Fig. 4.55 showed that those crystal are calcite. The occurance of calcite might be caused by the carbonation of the unreacted hydrated lime ($Ca(OH)_2$) remaining in the composition with carbon dioxide in the environment.

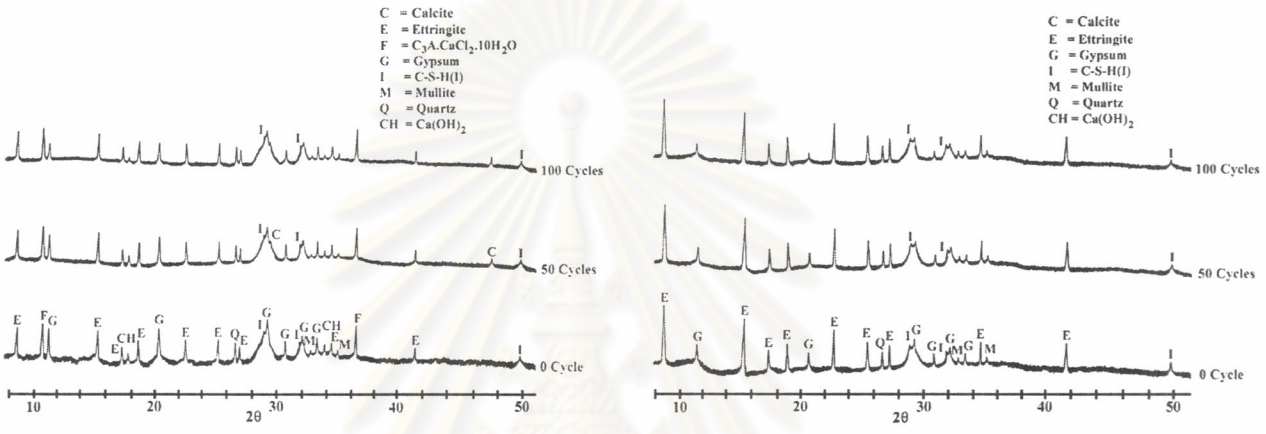

$CaCl_2$ 4 wt% activated paste cured at 50°C Na_2CO_3 3 wt% activated paste cured at 50°C

Fig. 4.55 XRD patterns of composite materials activated by thermally and chemically accelerating method after 100 cycles of wetting/drying cyclic storage.

4.4.5.2 Thermally, chemically, and mechanically accelerating method

a.) Phase analysis of composite materials improved by the combination of 3 accelerating methods

XRD results of the phase composition of composite materials acitvated with the above method, cured at scheduled age, are illustrated in Fig. 4.56.

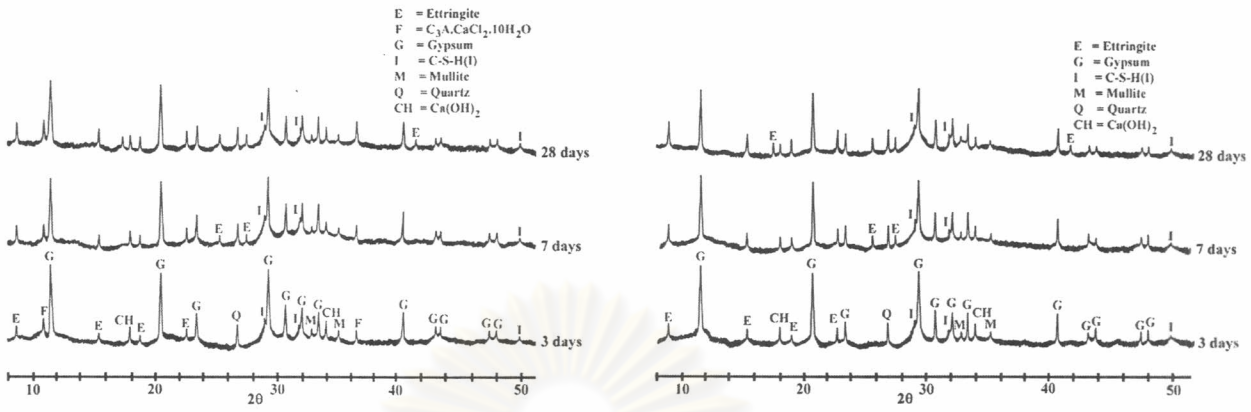

Activated with $CaCl_2$ 4 wt%, curing at 50°C

Activated with Na_2CO_3 3 wt%, curing at 50°C

Fig. 4.56 XRD patterns of thermally, chemically, and mechanically accelerating composite materials cured at various ages.

Fig. 4.56 shows the XRD patterns of composite materials activated by the combination of 3 methods, cured at 50°C for 3, 7, and 28 days, respectively. It is found that the poor ettringite and C-S-H(I) peaks begin to form in all the pastes cured for 3 days at high temperature and intensify with time. Sharp ettringite peaks are detected in both activated pastes and increase with time. Diffraction peaks of Friedel's salt are identified at 3 days in $CaCl_2$-activated pastes and intensify with curing time. Diffraction peaks of hydrated lime slightly decrease with time and weaker than those of the non-additive. However, the diffraction peaks of hydrated lime in the specimens from the combination of 3 methods are stronger than those from the combination of thermally and chemically accelerating methods. This may be due to the low content of absorbed water in the compacted composition to generate the reaction. Moreover, the humidity from the curing atmosphere is difficult to react with the remaining composition and carry on the reaction because of the high density of the specimens.

b.) Physical and mechanical properties of composite materials improved by the combination of 3 accelerating methods

Physical and mechanical properties of the composite materials activated by the combination of 3 accelerating methods, cured at scheduled age are presented in Appendix : Table 17 and illustrated in Fig. 4.57.

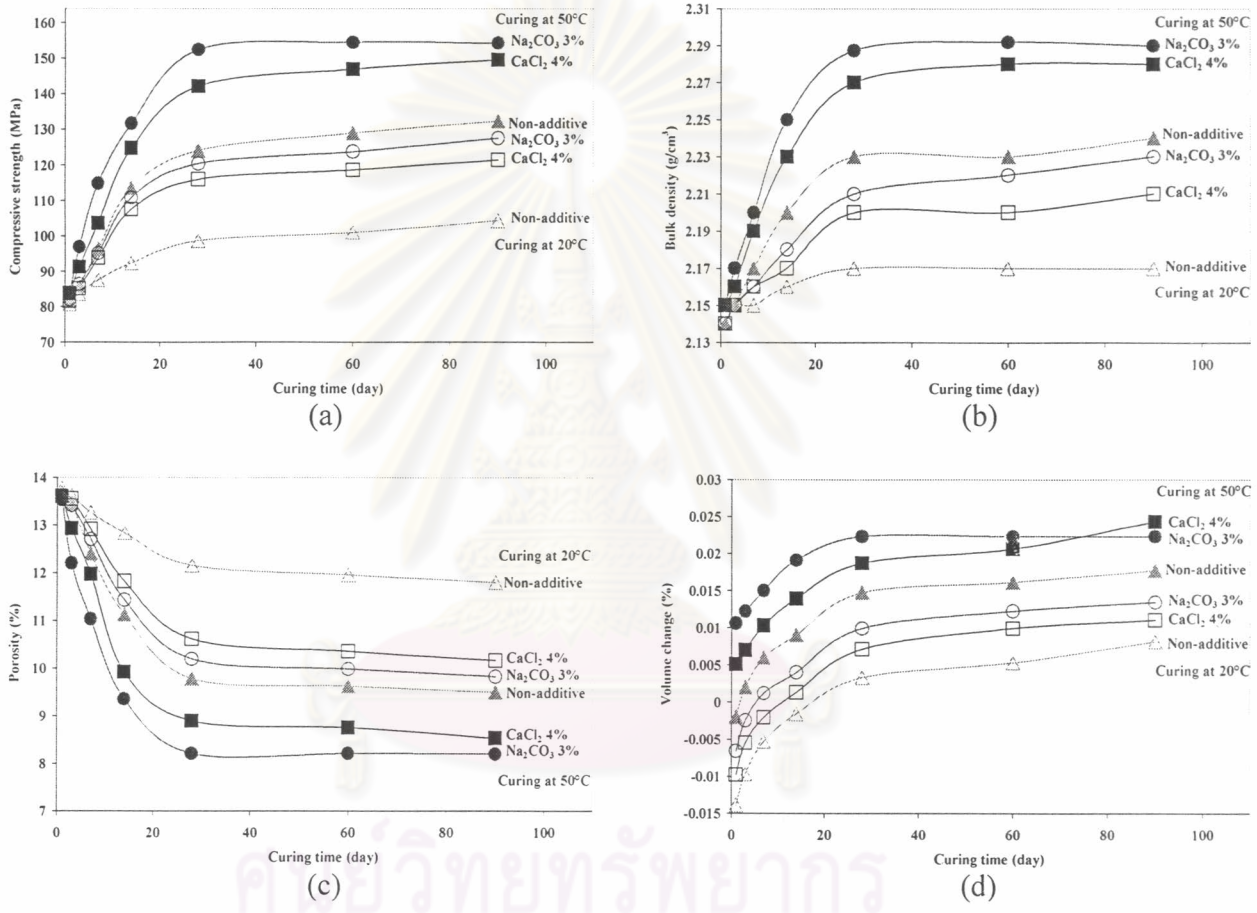

Fig. 4.57 Effect of the combination of 3 accelerating methods on the physical and mechanical properties of the composite materials (a) compressive strength, (b) bulk density, (c) porosity, and (d) volume change.

It is found from the results of physical and mechanical properties in Appendix : Table 17 and Fig. 4.57 that the increase in strength relates to the content of hydrated products which depend on curing temperature and chemical activator.

This result is also confirmed by the results of bulk density and porosity. It is found that the increase in hydrated phases increases the bulk density and reduces the porosity due to the filling of voids and pores with hydration products.

c.) Particle morphology of composite materials activated with the combination of 3 accelerating methods

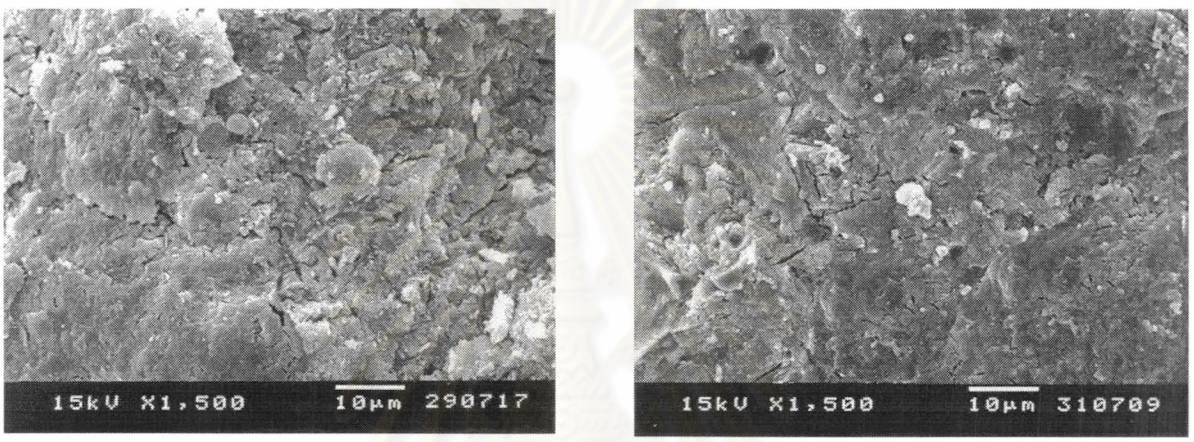

$CaCl_2$ 4 wt% activated paste cured at 50°C Na_2CO_3 3 wt% activated paste cured at 50°C

Fig. 4.58 SEM micrographs of composite materials activated by the combination of 3 accelerating methods cured for 28 days.

It is found from the SEM micrographs (Fig. 4.58) that the combination of 3 accelerating methods tremendously increases the formation of hydration products which later seal all the crystals or grains into a massive structure and no grain boundaries are visible. Therefore, the cementing action among grains creates the dense structure and causes of the high strength and density of specimens.

d.) Performance under water of composite materials activated by the combination of 3 accelerating methods

Performance under water of the composite materials improved by the combination of 3 accelerating methods, cured at 28 days and followed by immersion in water for different periods, are shown in Appendix : Table 18 and demonstrated in Fig. 4.59.

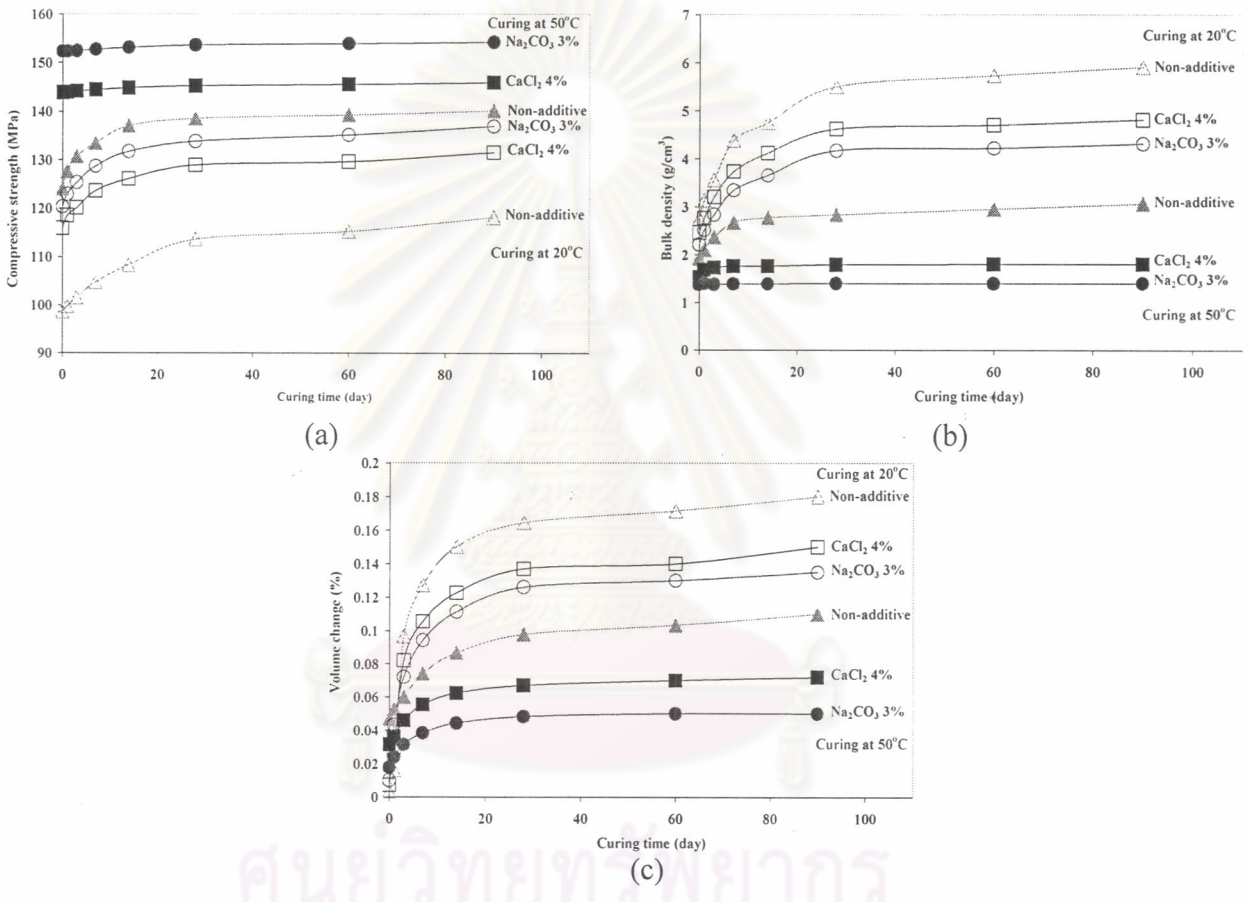

Fig. 4.59 Physical and mechanical properties under water of the 28-day specimens improved by the combination of 3 accelerating methods (a) compressive strength (b) water absorption, and (c) volume change.

It is found from Appendix : Table 18 and Fig. 4.59 that the strength and volume change increases slightly in the specimens activated with additive cured at 50°C due to the high density but clearly increases in the others. The increase in strength may be caused by the reaction of the remaining unreacted lime and pozzolan.

Pozzolanic reaction can proceed under the excess water system. The lower water absorption in the activated and high temperature curing specimens is also caused by the filling of hydration products in voids and pores.

e.) Effect of wetting/drying cyclic storage on the physical and mechanical properties of composite materials activated by the combination of 3 accelerating methods.

Physical and mechanical properties of the 28-day composite materials improved by the above method and followed by immersion in water for different periods are presented in Appendix : Table 19 and illustrated in Fig. 4.60.

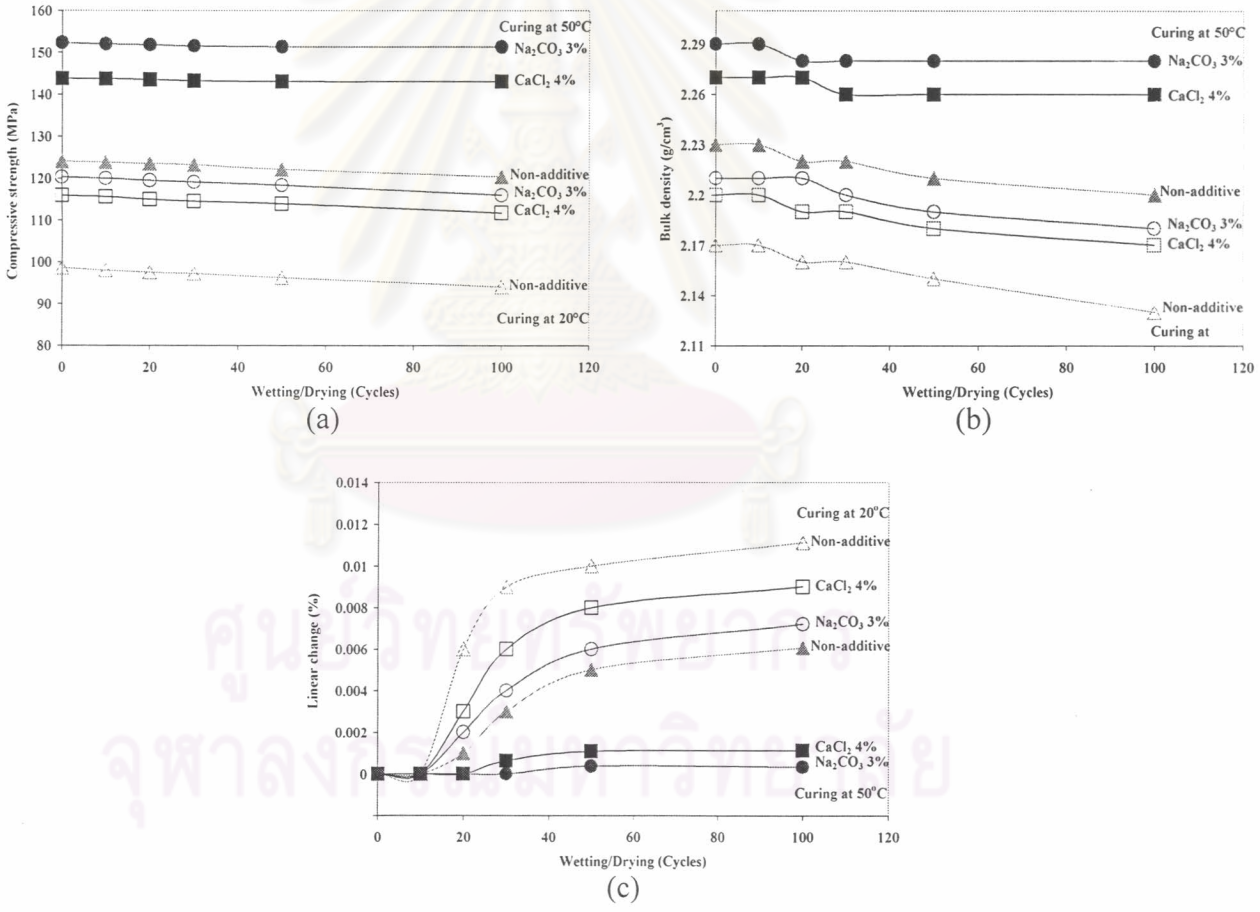

Fig. 4.60 Effect of wetting/drying cycles on the physical and mechanical properties of composite materials activated by the combination of 3 accelerating methods (a) compressive strength, (b) bulk density, and (c) linear change.

The physical and mechanical properties of the activated specimens after the cyclic storage are shown in Appendix : Table 19 and Fig. 4.60. The strength reduction in the specimens without additive cured at high temperature is 1.53% and only 0.56% and 0.45% in the $CaCl_2$- and Na_2CO_3-activated specimens, respectively. The superior properties of these accelerated specimens over those of thermally and chemically accelerating method are their higher strength and higher dimensional stability.

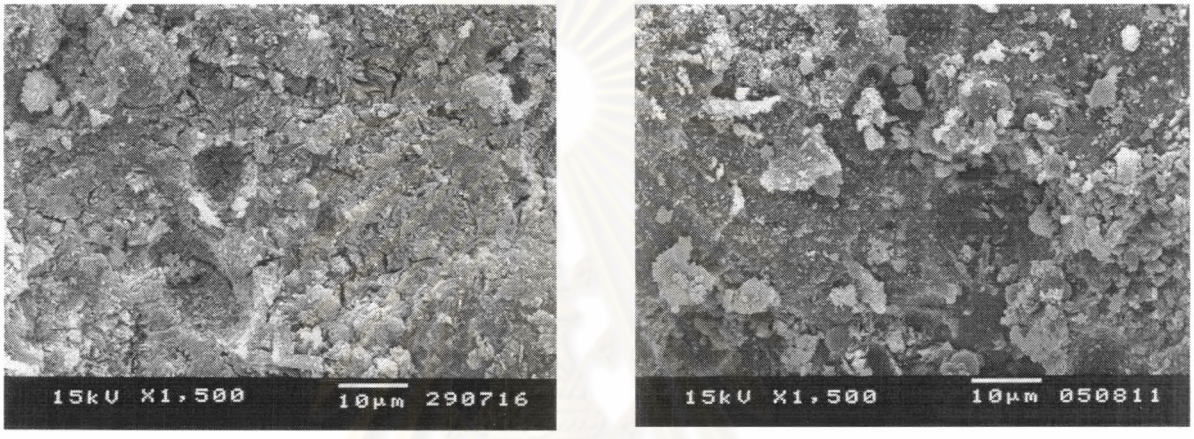

$CaCl_2$ 4 wt% activated paste cured at 50°C

Na_2CO_3 3 wt % activated paste cured at 50°C

Fig. 4.61 SEM micrographs of composite materials activated by the combination of 3 accelerating methods after 100 cycles of wetting/drying cyclic storage.

It is found from the SEM micrographs illustrated in Fig. 4.61 that microstructures of composite materials after 100 cycles of wetting/drying cyclic storage are still sound and in well-formed structure. Due to the lime remaining in the structure, the pozzolanic reaction proceeds in the excess water during cyclic storage. Moreover, rhombohedral crystals of $CaCO_3$ (Fig. 4.62) are also detected in both $CaCl_2$- and Na_2CO_3-activated composite materials.

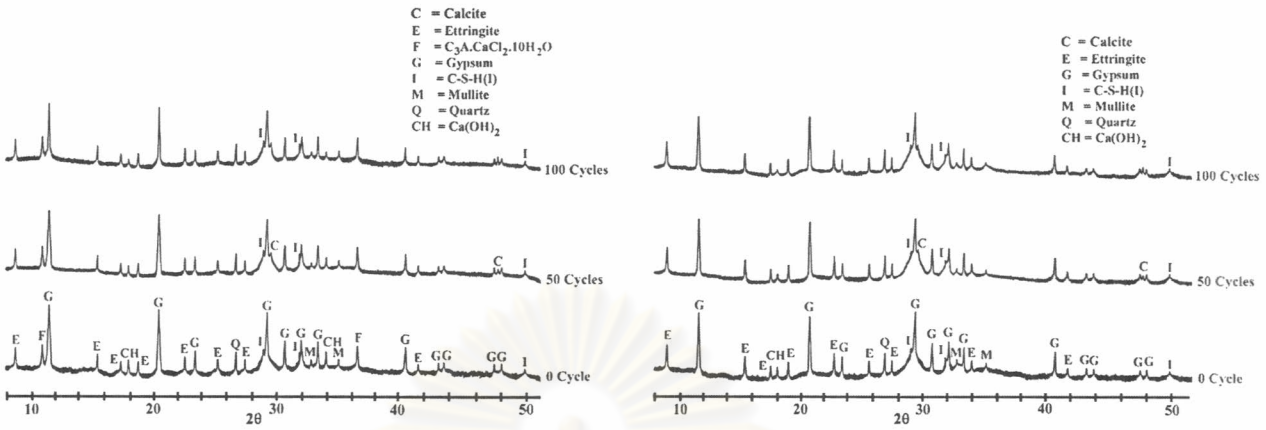

$CaCl_2$ 4 wt% activated paste cured at 50°C

Na_2CO_3 3 wt% activated paste cured at 50°C

Fig. 4.62 XRD patterns of composite materials activated by the combination of 3 accelerating methods after 100 cycles of wetting/drying cyclic storage.

4.5 Formulation of FGD gypsum-fly ash-lime containing materials

Results of physical and mechanical properties of composite materials with various contents of lime are tabulated in Appendix : Table 4.20 and presented in Fig. 4.63. Two lime-containing materials are employed : lime mud and sludge waste.

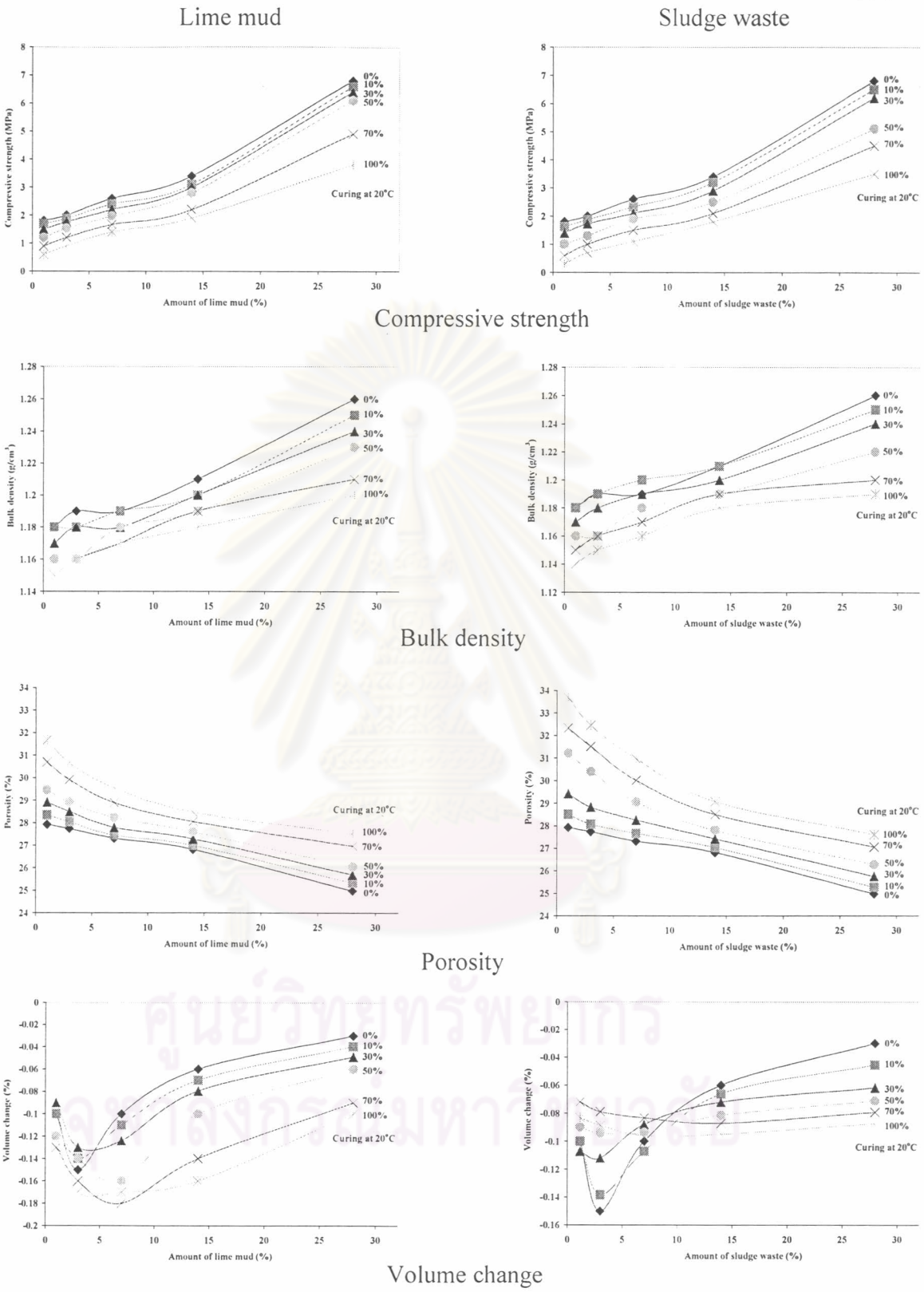

Fig. 4.63 Effect of the content of lime-containing material on the physical and mechanical properties of composite materials.

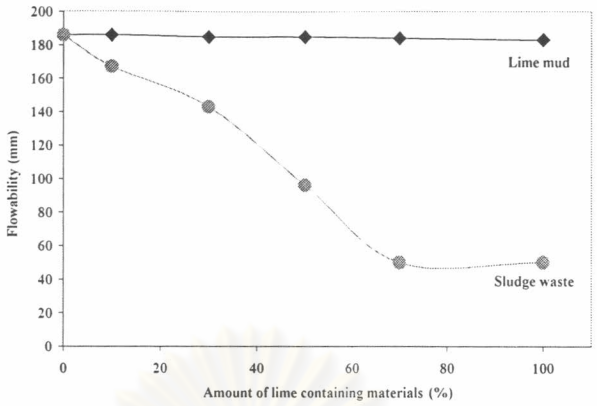

Fig. 4.64 Effect of the content of lime-containing material on the flowability of mixtures.

It is found from Appendix : Table 4.20 and Fig. 4.63 that the compressive strength of specimens decreases with increasing amount of lime containing materials in the composition. The composite materials containing either lime higher than 50 wt% or 30 wt% of lime mud and sludge waste show a significant drop in strength. The results of flowability of lime-containing mixtures are shown in Fig. 4.64. It is found that lime mud does not affect the flowability as much as sludge waste. The higher the content of sludge waste is used in the composition, the lower the flowability is resulted. Therefore, the highest content of lime-containing material in each system is lime mud 50 wt% and sludge waste 30 wt%.

4.6 Improvement of the physical and mechanical properties of FGD gypsum-fly ash-lime containing composite materials

4.6.1 Thermally and chemically accelerating method

a.) Phase analysis of FGD gypsum-fly ash-lime containing composite materials

XRD results of the phase composition of composite materials cured at different temperatures and scheduled age are presented in Fig. 4.65.

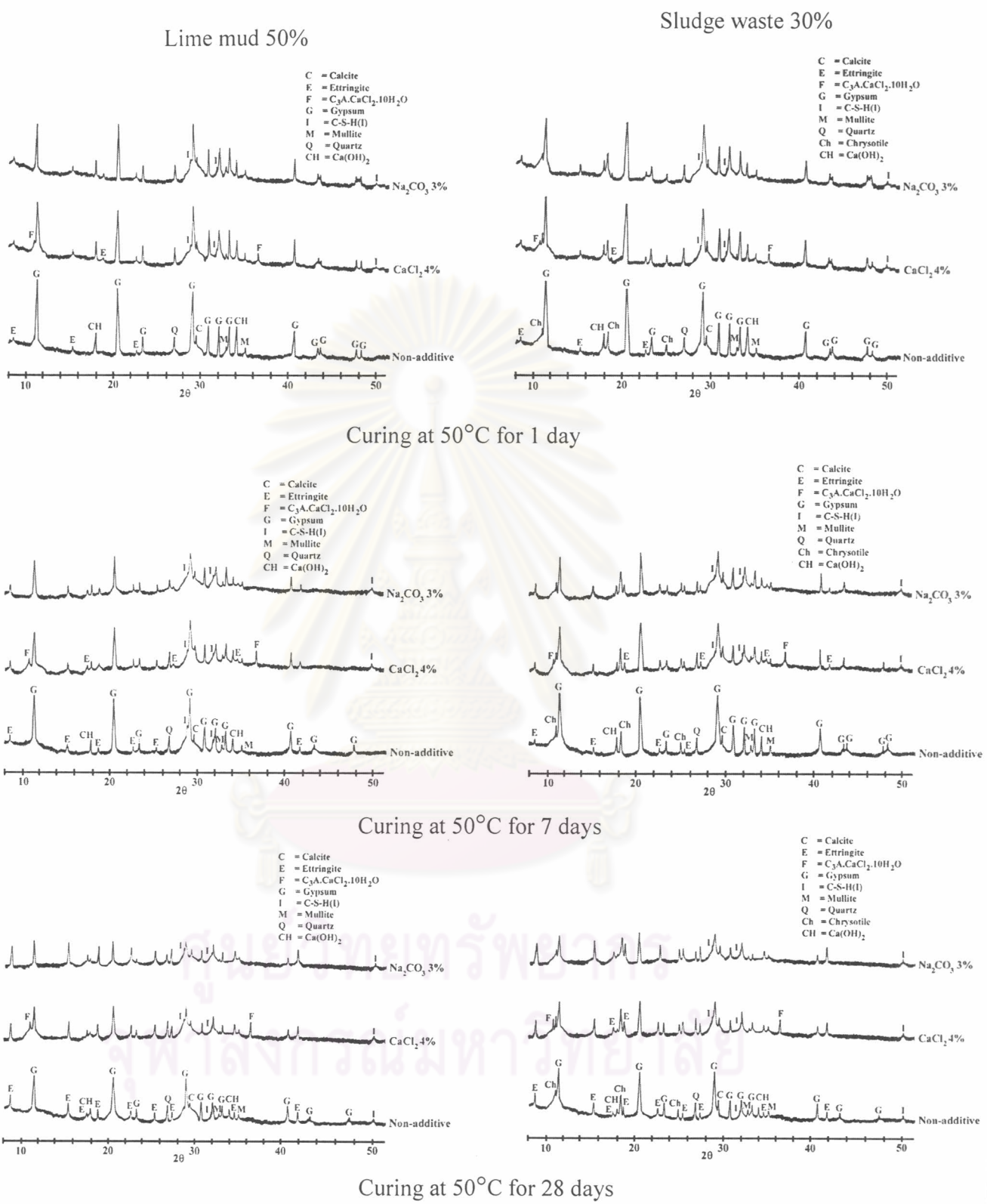

Fig. 4.65 XRD patterns of lime-containing composite materials improved by thermally and chemically accelerating method cured at different ages.

Fig. 4.65 shows the XRD patterns of lime-containing composite materials with and without additive cured at 50°C. It is found that hydrated product, ettringite, is detected from lime containing pastes without additive at 1 day. In the activated pastes, both ettringite and C-S-H(I) phases can be identified at 1 day and intensify with time. The diffraction peaks of hydrated lime in the activated lime containing pastes are weaker than those in the specimens without additive. The diffraction peaks of the unreacted hydrated lime from both pastes are detected from 1 to 7 days and disappear at 28 days.

b.) Physical and mechanical properties of lime containing composite materials improved by thermally and chemically accelerating method

Physical and mechanical properties of lime containing composite materials activated with $CaCl_2$ 4% and Na_2CO_3 3% cured at 50°C and scheduled age are presented Appendix : Table 21 and illustrated in Fig. 4.66.

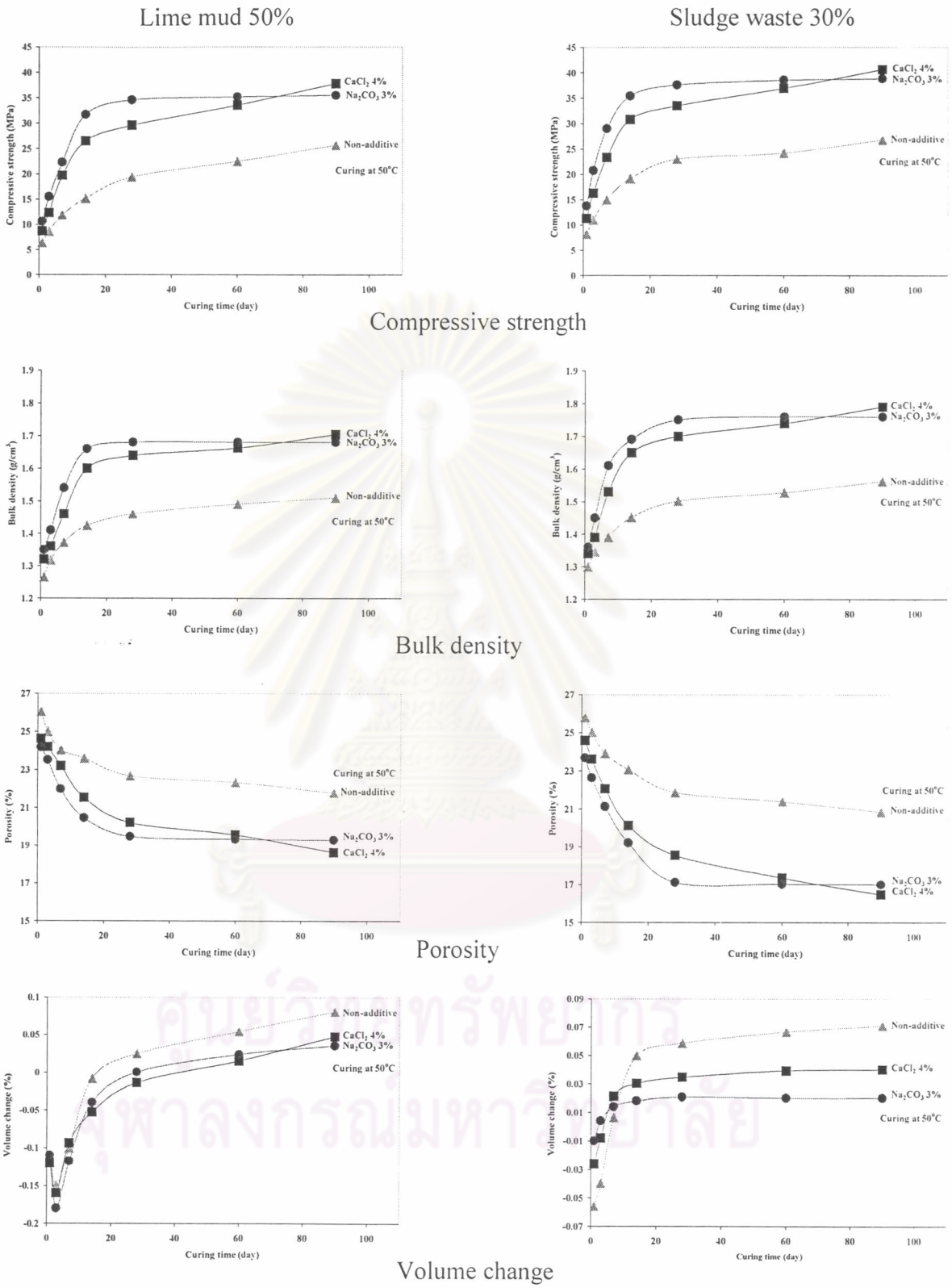

Fig. 4.66 Effect of thermally and chemically accelerating method on the physical and mechanical properties of lime-containing composite materials.

It is found from Appendix : Table 21 and Fig. 4.66 that both lime containing materials showed the same tendency in some properties, i.e. compressive strength increases with increasing curing time in all specimens due to the formation of more hydrated phases. This result is confirmed by the results of bulk density and porosity. It is found that the increase in hydrated phases increases the bulk density and decreases porosity because pores and voids in the structure are filled with hydrated products. However, the results of volume change are different. The volume change in the specimens with sludge waste tends to be constant at 14 days, but that of those with lime mud increases with time. Chrysotile fibers in the sludge waste assists in the reduction of expansion and because of their high surface area the bonding efficiency between hydrated products and matrix increases. Moreover, due to the high absorption, the hydrated products can be formed inside or on the surface of chrysoyile fibers (Fig. 4.74).

c.) Free lime content

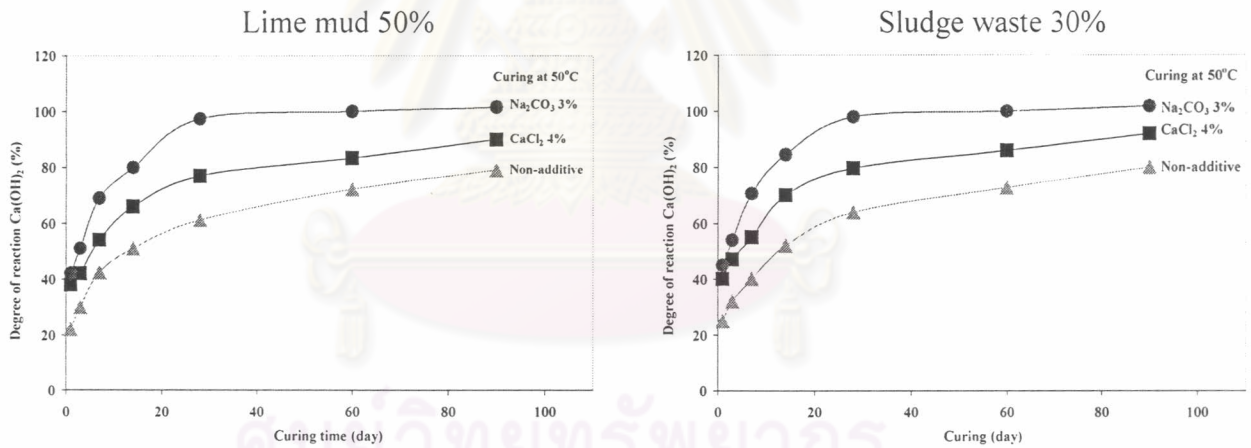

Fig. 4.67 The degree of $Ca(OH)_2$ reaction in the lime-containing composite materials improved by thermally and chemically accelerating method.

Fig. 4.67 shows the reacted percentage of $Ca(OH)_2$ in the lime containing composite materials activated with the combination of 2 methods. It can be concluded that Na_2CO_3 accelerates the early pozzolanic reaction since the $Ca(OH)_2$ is consumed very quickly and then much more slowly thereafter and completely consumed after 28 days. In the $CaCl_2$-activated pastes, the consumption of $Ca(OH)_2$ is similar to that in

the Na_2CO_3-activated pastes in the first 3 days and gradually differs in the later. It is also found from the results that the tendencies for the consumption of $Ca(OH)_2$ in Na_2CO_3- and $CaCl_2$-activated pastes are faster than that of the non-additive paste during the initial rapid reaction stage.

The results in Fig. 4.68 show that the slopes of the linear relationships are different. It is resulted from the formation of various hydration products with different mechanisms.

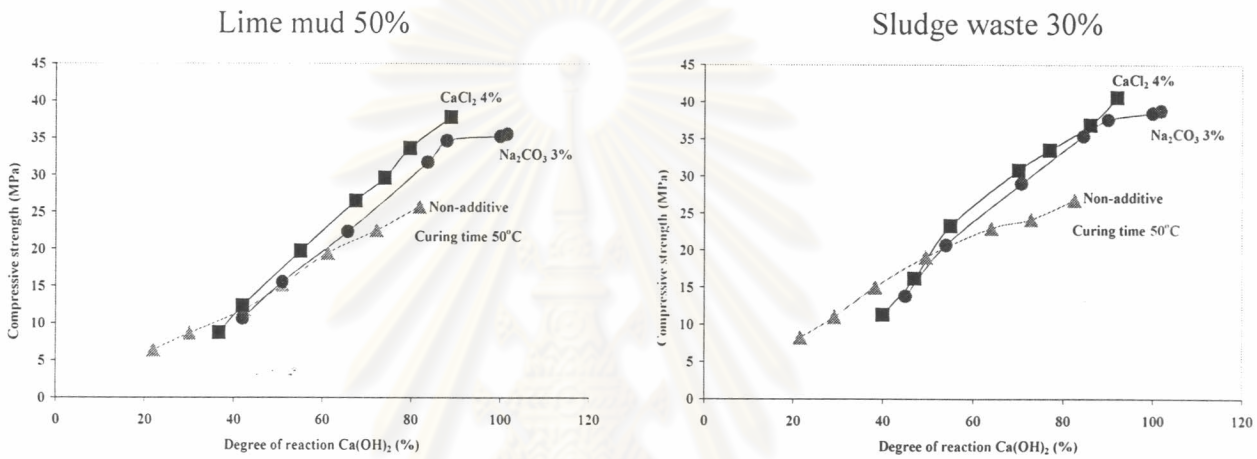

Fig. 4.68 Correlation between compressive strength and the degree of $Ca(OH)_2$ in the thermally and chemically accelerating lime-containing composite materials.

d.) Particle morphology of lime-containing composite materials activated by thermally and chemically accelerating method

Lime mud 50%

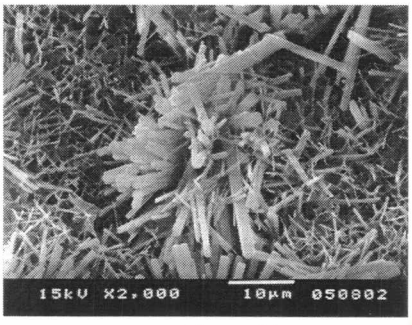

(a) Fracture surface of $CaCl_2$-activated specimen

Sludge waste 30%

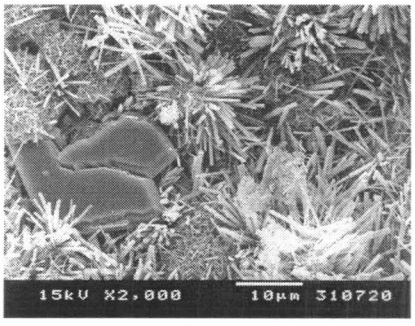

(b)

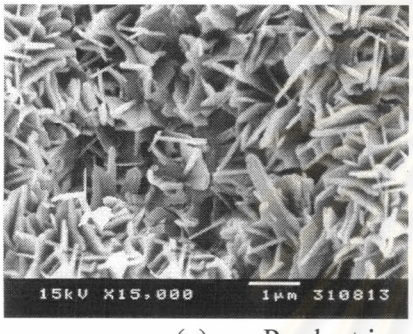

(c) Product in matrix of $CaCl_2$-activated specimen

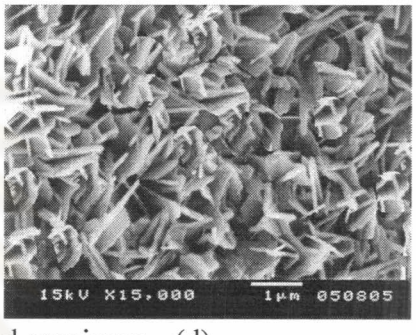

(d)

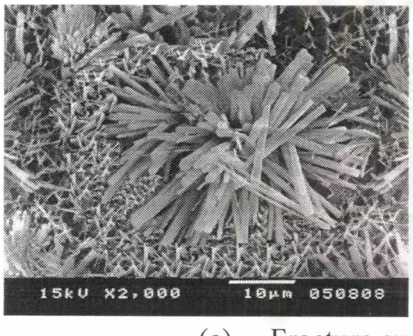

(e) Fracture surface of Na_2CO_3-activated specimen

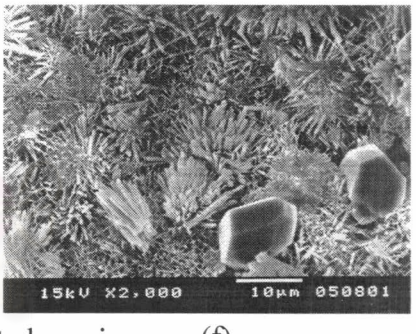

(f)

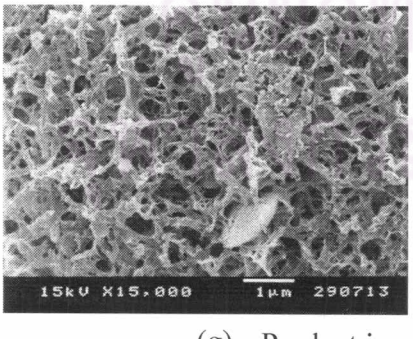

(g) Product in matrix of Na_2CO_3-activated specimen

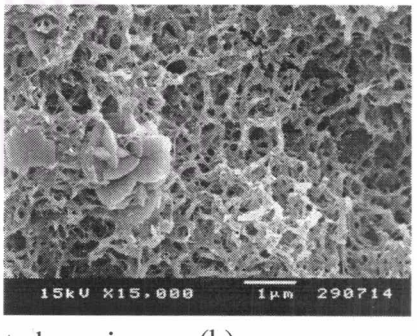

(h)

Fig. 4.69 SEM micrographs of thermally and chemically accelerating lime-containing composite materials cured at 28 days.

SEM micrographs illustrated in Fig. 4.69 show the effect of $CaCl_2$ and Na_2CO_3 on the microstructure of the 28-day hardened lime-containing composite materials. The fracture surfaces of lime-$CaCl_2$- or lime-Na_2CO_3-activated pastes clearly reveal hydration products. Moreover, some large foreign particles can be detected on the fracture surfaces of sludge waste composite materials. They might be the pieces of cement formerly included in the sludge waste.

The morphology of hydration products can be clearly detected on the fracture surface and in matrix of both lime-containing $CaCl_2$- and Na_2CO_3-activated pastes. According to the XRD analysis in Fig. 4.65, the large fibers showed in Fig. 4.69a, Fig. 4.69b, Fig. 4.69e, and Fig. 4.69f are ettrigite. These results have been confirmed by the results of EDS illustrated in Fig. 4.70a and Fig. 4.70b. The hexagonal plates detected in the matrix of both lime containing $CaCl_2$-activated pastes are Friedel's salt (Fig. 4.69c and Fig. 4.69d). These results have also been verified by the EDS presented in Fig. 4.70a and Fig. 4.70b. Honeycomb-liked structures can be investigated in the matrix of Na_2CO_3-activated pastes (Fig. 4.69g and Fig. 4.69h). Those structures are C-S-H(I) conformed with the results of XRD (Fig. 4.65) and EDS analysis (Fig. 4.70c and Fig. 4.70d).

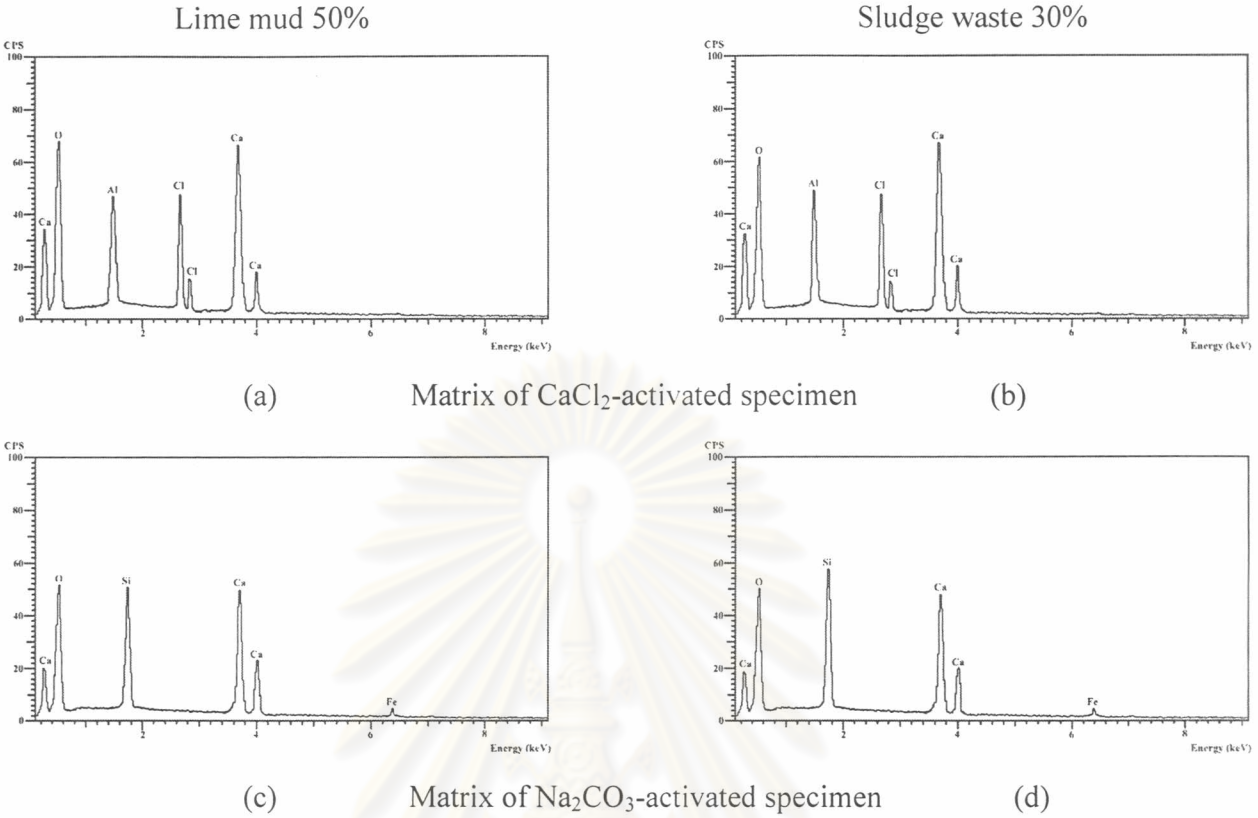

Fig. 4.70 EDS results of thermally and chemically accelerating lime containing composite materials analyzed on the different areas of the SEM micrographs illustrated in Fig. 4.69.

e.) Kinetic analysis

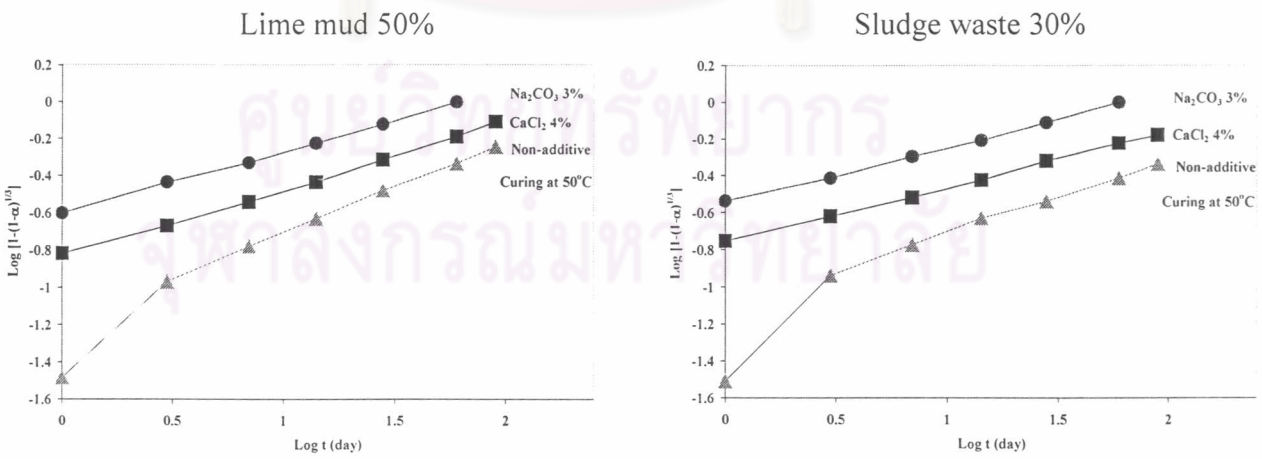

Fig. 4.71 Pozzolanic reaction kinetics in the thermally and chemically accelerating lime-containing composite materials.

Table 4.11 Reaction grade (N) and phase period of the lime-containing composite materials activated by thermally and chemically accelerating method.

Lime-containing material	Type of additive	Phase I ($N \leq 1$)		Phase II ($2 \geq N > 1$)		Phase III ($N > 2$)	
		N	Period	N	Period	N	Period
Lime mud	Non additive	N/A	N/A	1.10	3 days	2.66	> 3 days
	$CaCl_2$ 4 wt%	0.34	> 1 day	N/A	N/A	N/A	N/A
	Na_2CO_3 3 wt%	0.30	> 1 day	N/A	N/A	N/A	N/A
Sludge waste	Non additive	N/A	N/A	1.21	3 days	2.62	> 3 days
	$CaCl_2$ 4 wt%	0.37	> 1 day	N/A	N/A	N/A	N/A
	Na_2CO_3 3 wt%	0.33	> 1 day	N/A	N/A	N/A	N/A

N/A = not applicable.

The reaction kinetics illustrated in Fig. 4.71 and tabulated in Table 4.11 show that, regardless of curing age, only reaction grade (N) less than 1 in the lime-containing composite materials activated with the combination method is found. Therefore, the total pozzalanic reaction is controlled by the dissolution of reactants. Moreover, The pozzolanic reaction in Na_2CO_3-activated pastes should be faster than that of the $CaCl_2$-activated pastes due to its lower of reaction grade (N).

f.) Performance under water of lime-containing composite materials activated by thermally and chemically accelerating method.

Performance under water of the 28-day lime-containing composite materials improved by thermally and chemically accelerating method and followed by immersion in water for different periods are tabulated in Appendix : Table 22 and shown in Fig. 4.72.

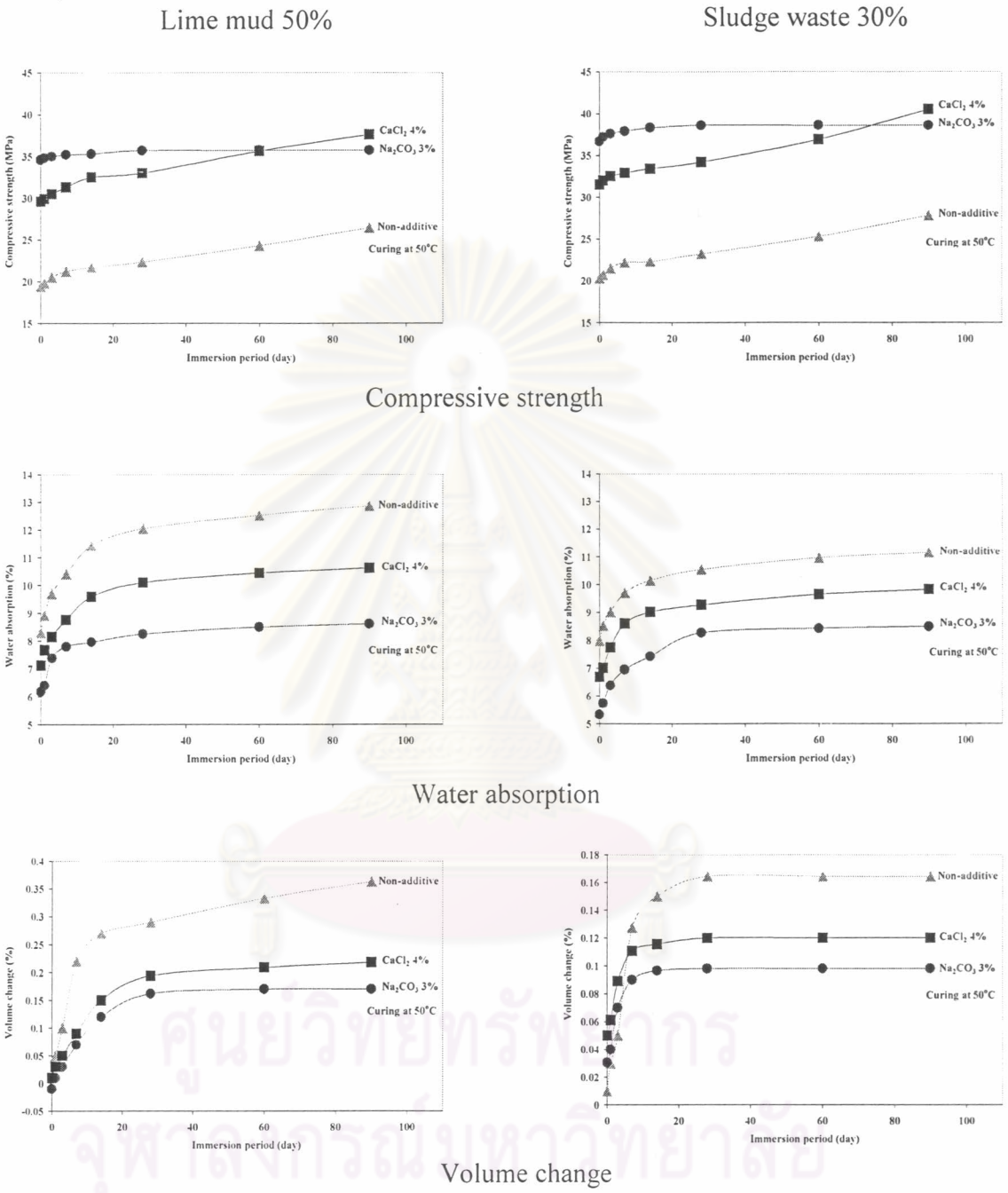

Fig. 4.72 Physical and mechanical properties of 28-day lime-containing composite materials improved by thermally and chemically accelerating method under water.

It is found from the results tabulated in Appendix : Table 22 and presented in Fig. 4.72 that the strength increases slightly and tends to be constant in lime and Na_2CO_3-activated specimens. It is also found that the lime and $CaCl_2$-activated specimens shows higher strength than that of the Na_2CO_3-activated specimens at 90 days under water. It might be caused by the pozzolanic reaction of the remaining hydrated lime in the composition and the excess water in the system. Both activated specimens show the same trend in water absorption, and it is found that the result of volume change of specimens containing sludge waste is lower and more stable under water than those containing of lime mud. It might be caused by the reinforcement of chrysotile fibers included in the sludge waste.

g.) Effect of wetting/drying cyclic storage on the physical and mechanical properties of lime-containing composite materials activated by thermally and chemically accelerating method.

Physical and mechanical properties of 28-day lime-containing composite materials improved by thermally and chemically accelerating method at various cyclic storage cycle are presented in Appendix : Table 23 and illustrated in Fig. 4.73.

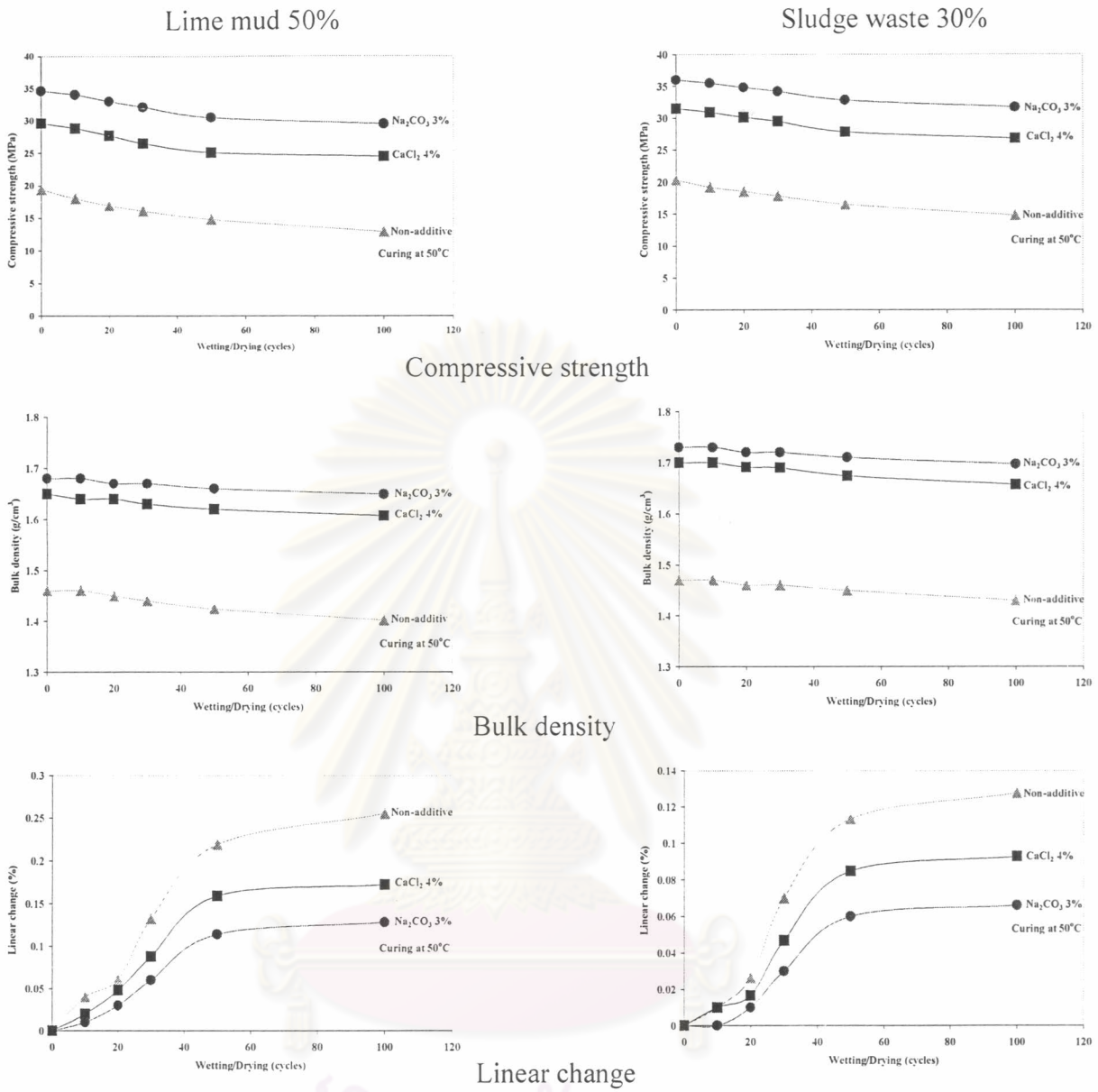

Fig. 4.73 Effect of wetting/drying cycles on the physical and mechanical properties of lime-containing composite materials activated by thermally and chemically accelerating method.

It is found from Appendix : Table 16 and Fig. 4.53 that compressive strength of lime containing composite materials activated by thermally and chemically accelerating method decreases with increasing cyclic storage. After 100 wetting/drying cycles, the strength of specimens reduces within the acceptable range[73] and the results are tabulated in Table 4.12.

Table 4.12 Strength reduction after cyclic storage (100 cycles) of lime-containing composite materials activated by thermally and chemically accelerating method.

Lime-containing composite materials	Strength reduction (%)		
	Non-additive	$CaCl_2$ 4 wt%	Na_2CO_3 3 wt%
Lime mud	30.35	15.33	12.76
Sludge waste	22.09	10.02	8.14

The strength reduction in lime-containing specimens accelerated by additive is lower than those of without additive due to their higher hydrated products and less gypsum content in the composition. It is verified by the XRD results shown in Fig. 4.65. The hydration products cause the increase in strength and densification of the structure. Both activated specimens also showed the same trend in compressive strength and bulk density but it is found that the results of linear change of specimens containing sludge waste is lower than those containing lime mud. The lower linear change of sludge waste composite materials might be caused by the chrysotile fibers. Becuase of the high surface area of chrysotile fibers (Fig. 4.74), the hydrated products can be formed on or inside of them and result in incraese of bonding between hydrated products and matrix.

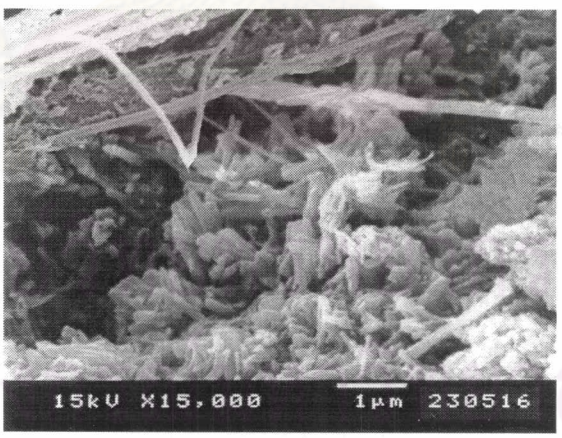

Fig. 4.74 SEM micrograph of chrysotile fibers in lime-containing, sludge waste, composite materials.

Lime mud 50%

Sludge waste 30%

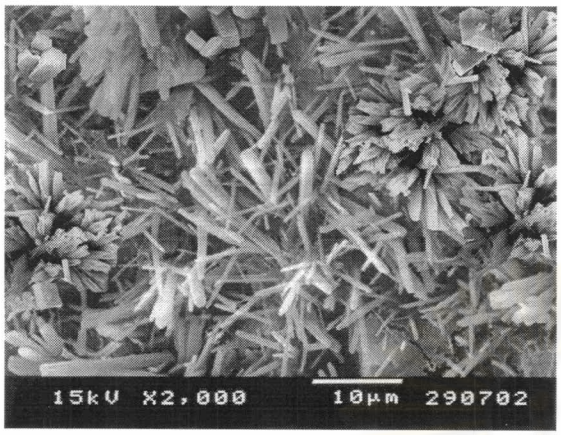

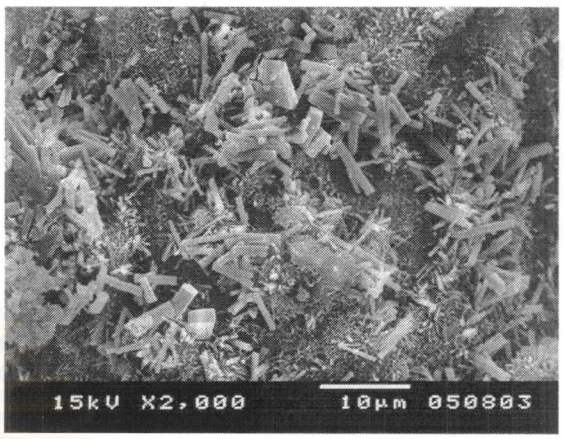

$CaCl_2$ 4 wt% activated paste cured at 50°C

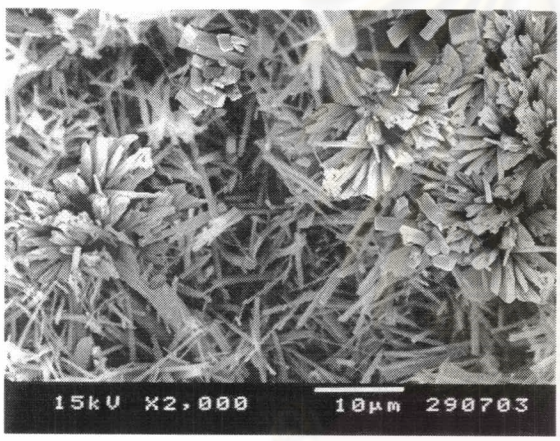

Na_2CO_3 3 wt% activated paste cured at 50°C

Fig. 4.75 SEM micrographs of lime-containing composite materials activated by thermally and chemically accelerating method after 100 cycles of wetting/drying cyclic storage.

It is found from the SEM micrographs in Fig. 4.75 that the microstructures of lime containing composite materials after 100 cycles of wetting/drying cyclic storage are still in sound and the well-formed structure. However, some parts of microstructure are coagulated together. It might be caused from the dissolution of the remaining gypsum in the system.

Moreover, rhombohedral crystals are also detected both $CaCl_2$- and Na_2CO_3-activated lime-containing composite materials after 100 cycles of wetting/drying cyclic storage. The XRD results from Fig. 4.76 reveal that those crystal are calcite, from the carbonation reaction of unreacted hydrated lime ($Ca(OH)_2$) remaining in the composition and carbon dioxide in the environment.

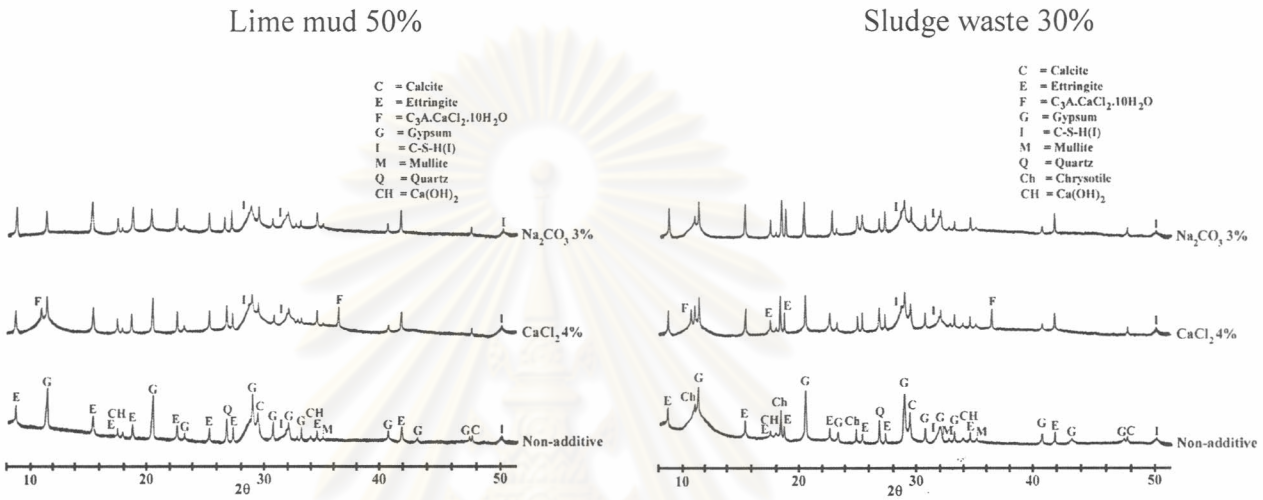

Fig. 4.76 XRD patterns of lime-containing composite materials activated by thermally and chemically accelerating method after 100 cycles of wetting/drying cyclic storage.

4.6.2 Thermally, chemically, and mechanically accelerating method

a.) Phase analysis of lime-containing composite materials improved by the combination of 3 accelerating methods

XRD results of the phase composition of composite materials activated by the combination of 3 methods, cured at scheduled age, are illustrated in Fig. 4.77.

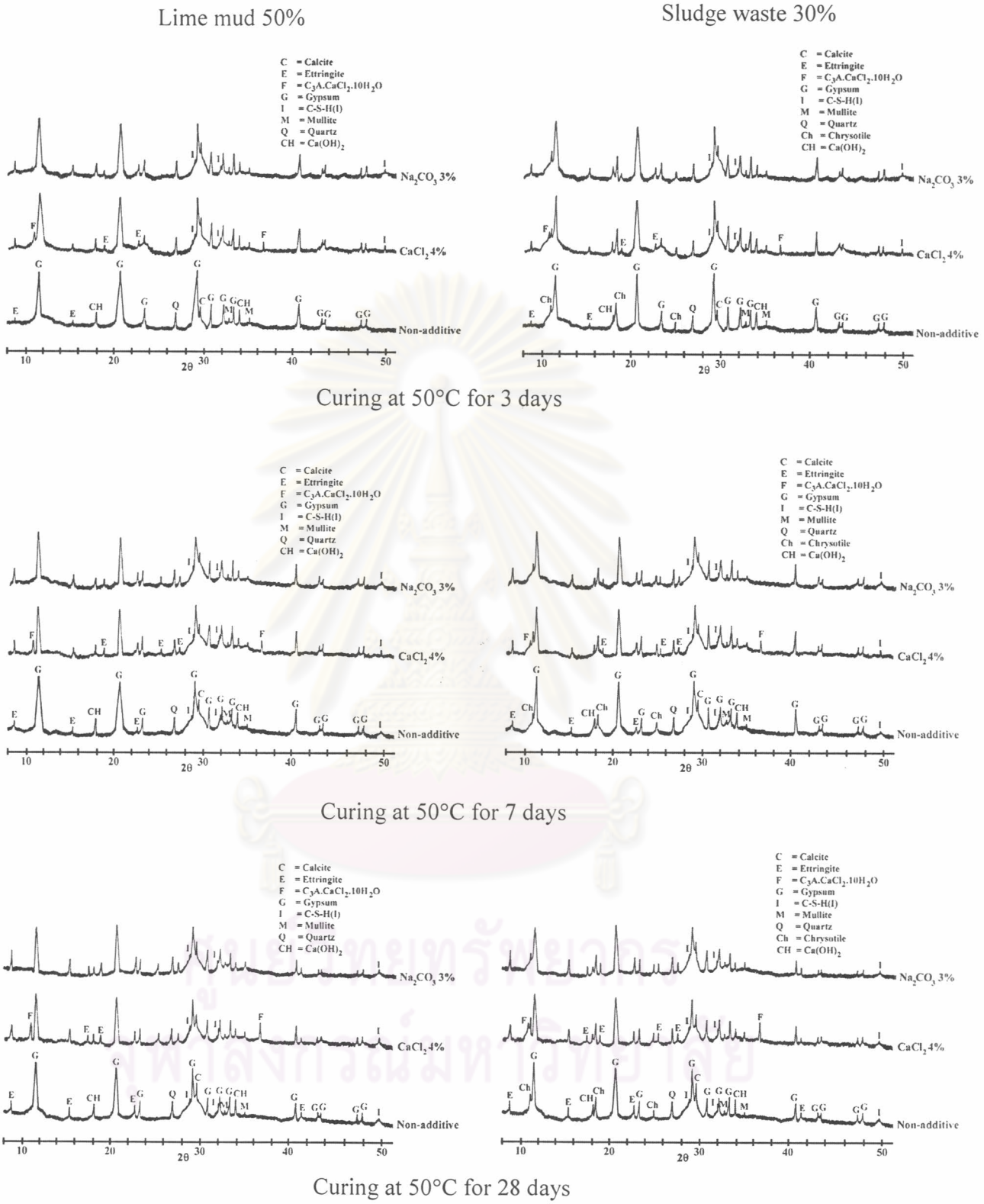

Fig. 4.77 XRD patterns of lime-containing composite materials activated by the combination of 3 accelerating methods, cured at various ages.

Fig. 4.77 shows the XRD patterns of lime containing composite materials activated by the combination of 3 methods cured at 50°C for 3, 7, and 28 days. It is found that the poor ettringite and C-S-H(I) peaks start to form in the pastes with additive at 3 days and increases with time. Diffraction peaks of Friedel's salt are detected at 3 days in $CaCl_2$-activated pastes and increase with time. The diffraction peaks of hydrated lime are weaker than those of thermally and chemically accelerating method. It is caused by the lesser water in the system to proceed the pozzolanic reaction due to the high density of specimens.

b.) Physical and mechanical properties of lime-containing composite materials improved by the combination of 3 accelerating methods

Physical and mechanical properties of lime-containing composite materials activated by the combination of 3 methods, cured at scheduled age, are tabulated in Appendix : Table 24 and presented in Fig. 4.78.

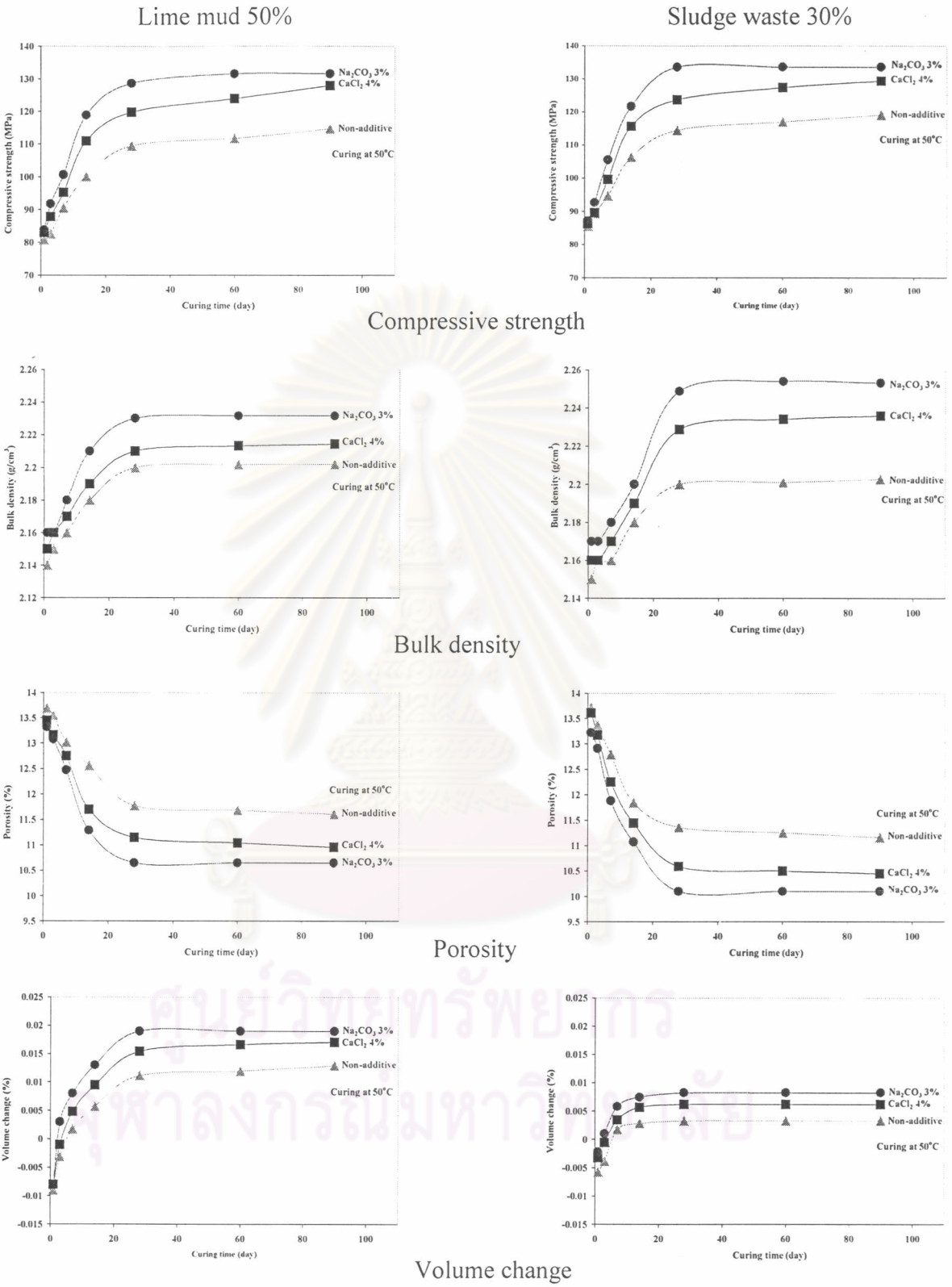

Fig. 4.78 Effect of the combination of 3 accelerating methods on the physical and mechanical properties of lime-containing composite materials.

It is found from Appendix : Table 24 and Fig. 4.78 that the increase in strength of the accelerated lime-containing composite materials relates to the content of hydrated products. This result is conformed with the results of bulk density and porosity. It is also found that the increase in hydrated phases increases bulk density and reduces porosity because of the filling of voids and pores with hydration products. The volume change of composite materials prepared from sludge waste is lower than those from lime mud. It might be caused by the chrysotile fibers in sludge waste composite specimens.

c.) Particle morphology of lime containing composite materials activated wby the combination of 3 accelerating methods

Lime mud 50%

Sludge waste 30%

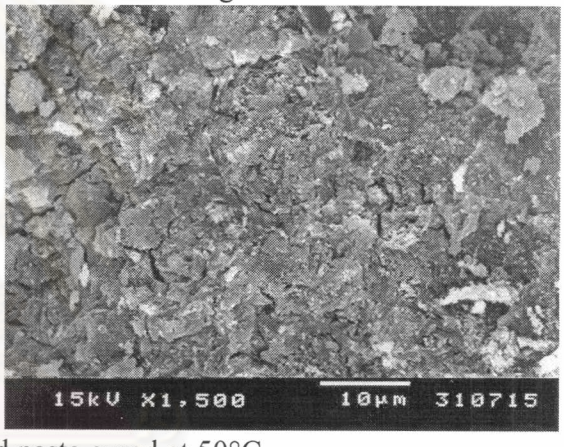

$CaCl_2$ 4 wt% activated paste cured at 50°C

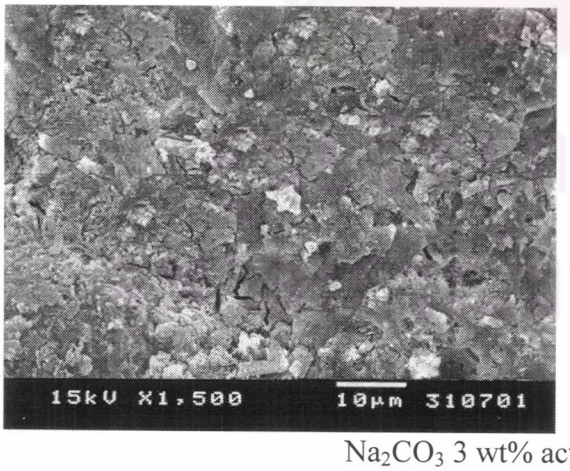

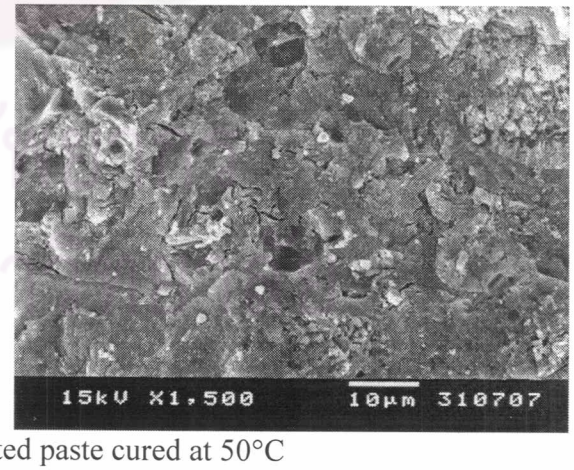

Na_2CO_3 3 wt% activated paste cured at 50°C

Fig. 4.79 SEM micrographs of lime-containing composite materials activated by the combination of 3 accelerating methods, cured at 28 days.

It is found from the SEM micrographs illustrated in Fig. 4.79 that the combined method increases the formation of hydration products. All of the materials in the specimens are bonded together by the hydrated products and yield high strength and high density of the hydrated specimens.

d.) Performance under water of lime-containing composite materials activated by the combination of 3 accelerating methods

Performance under water of the 28-day lime-containing composite materials improved by combination of 3 methods and followed by immersion in water for different periods are shown in Appendix : Table 25 and presented in Fig. 4.80.

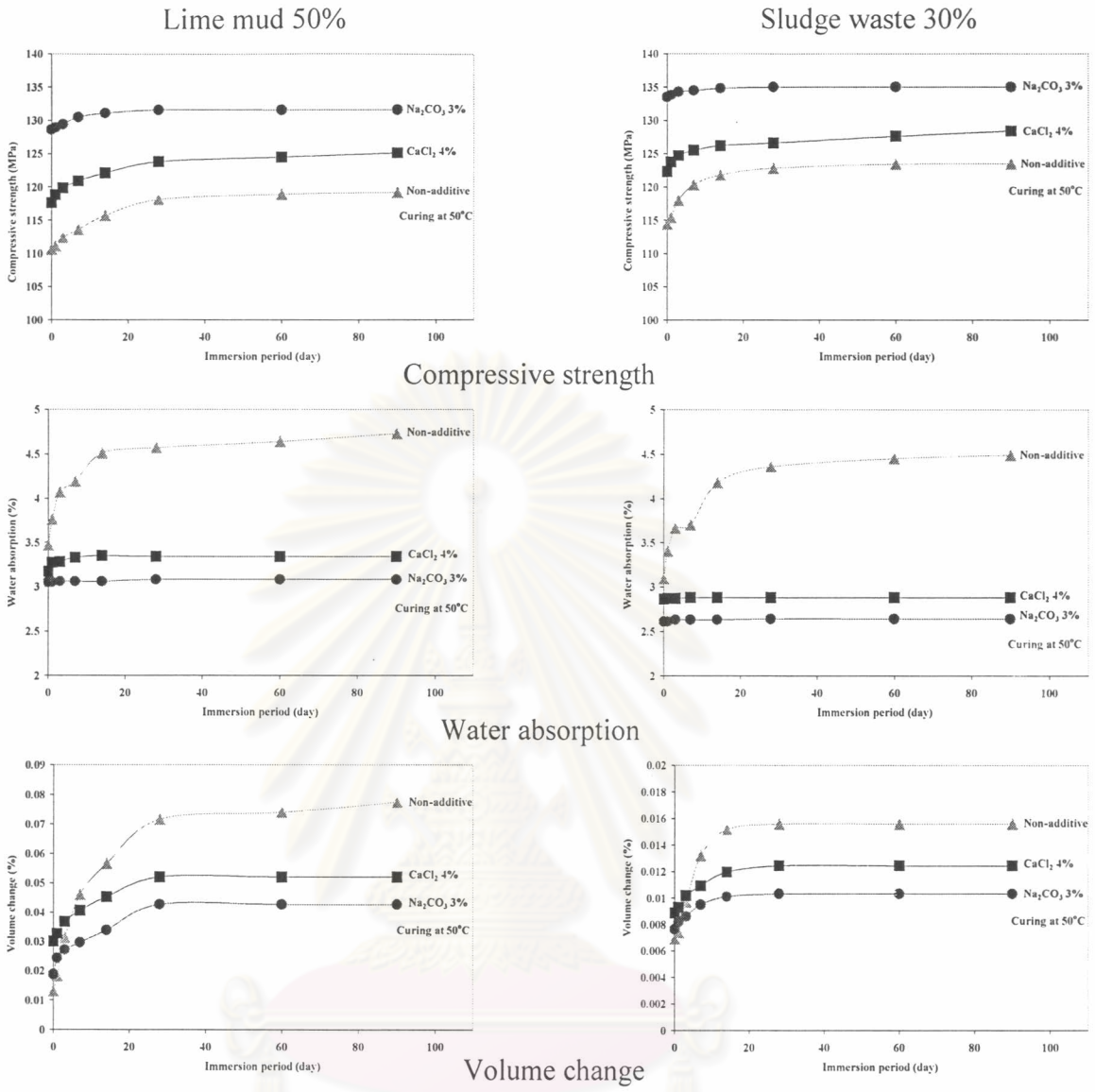

Fig. 4.80 Physical and mechanical properties under water of 28-day lime-containing specimens improved by the combination of 3 accelerating methods.

It is found from Appendix : Table 25 and Fig. 4.80 that the strength increases slightly in both lime-containing specimens activated with additive due to their high density. The increase in strength might be caused by the reaction between the remaining unreacted products. The pozzolanic reaction can continue under the excess water system. The water absorption of the lime-containing specimens by this method is quite stable due to the filling of all voids and pores with hydration products. The composite materials prepared from sludge waste show more dimensional stability under water than those from lime mud. It is, again, caused by the chrysotile fibers containing in sludge waste.

e.) Effect of wetting/drying cyclic storage on the physical and mechanical properties of lime-containing composite materials activated by the combination of 3 accelerating methods.

Physical and mechanical properties of the 28-day composite materials improved by the combined method, and followed by immersion in water for different periods, are shown in Appendix : Table 25 and illustrated in Fig. 4.81.

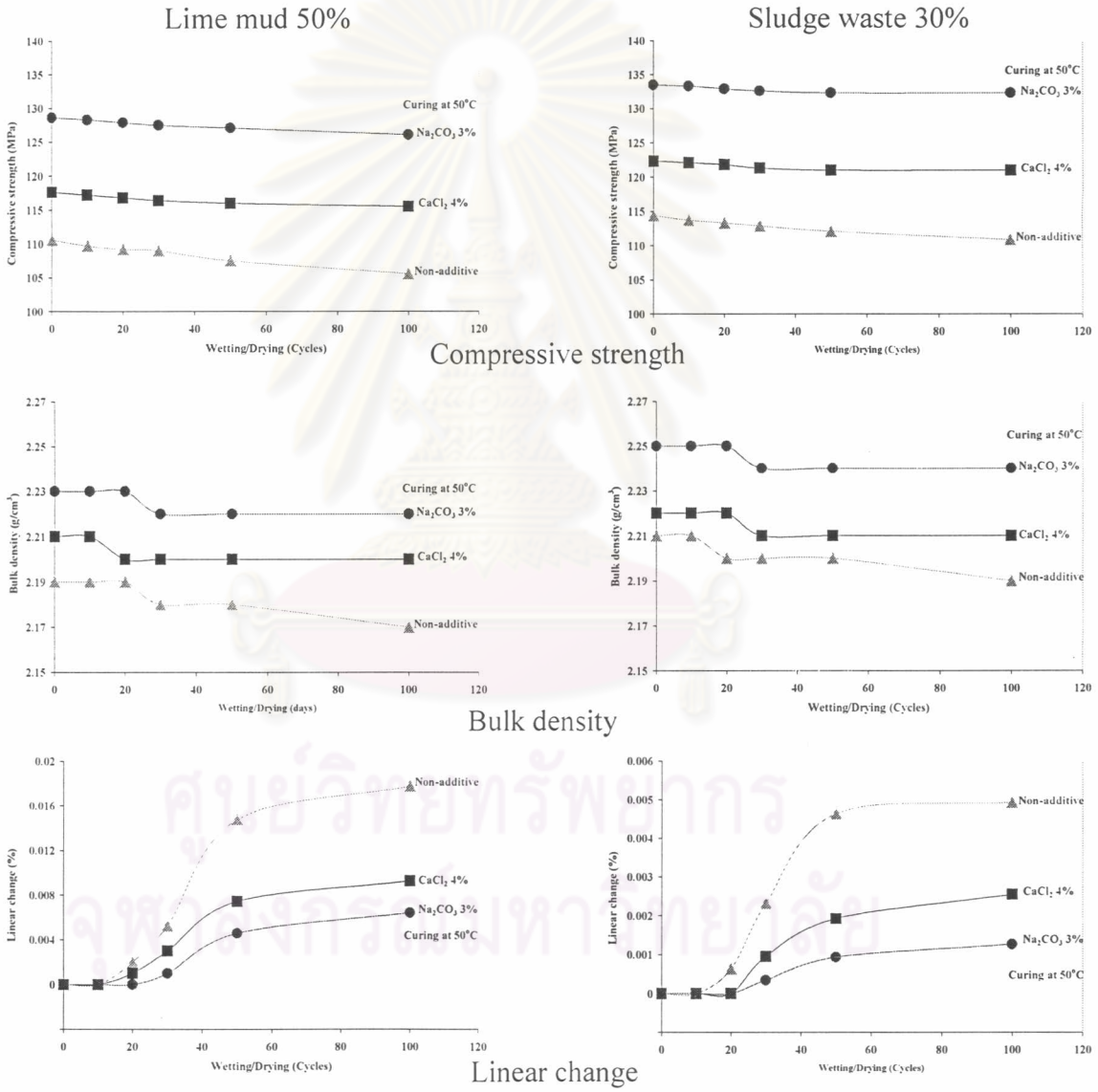

Fig. 4.81 Effect of wetting/drying cycles on the physical and mechanical properties of lime-containing composite materials activated by the combination of 3 accelerating methods.

The physical and mechanical properties of the activated specimens after cyclic storage are presented in Appendix : Table 25 and Fig. 4.81. It is found that compressive strength of lime-containing composite materials decreases slightly with increasing cyclic storage. However, the reduction of strength of specimens is within the acceptable range after 100 wetting/drying cycles and the results are tabulated in Table 4.13. The superior properties of the specimens from this method over those from the thermally and chemically accelerating method are the higher strength and higher dimensional stability.

Table 4.13 Strength reduction after cyclic storage (100 cycles) of lime-containing composite materials activated by the combination of 3 accelerating methods.

Lime-containing composite materials	Strength reduction (%)		
	Non-additive	$CaCl_2$ 4 wt%	Na_2CO_3 3 wt%
Lime mud	30.35	1.88	1.54
Sludge waste	22.09	1.06	0.69

Lime mud 50%

Sludge waste 30%

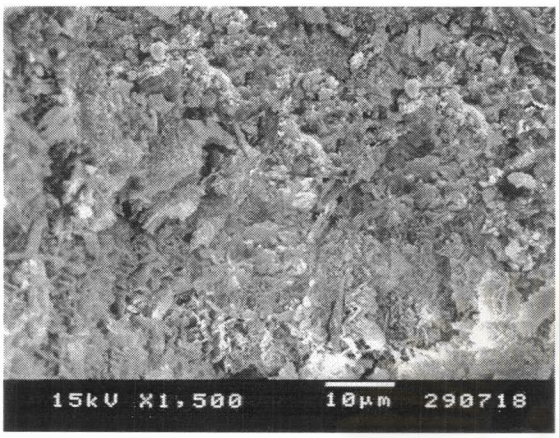

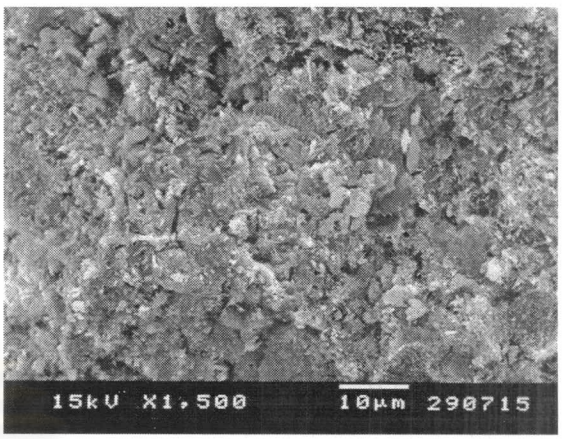

$CaCl_2$ 4 wt% activated paste cured at 50°C

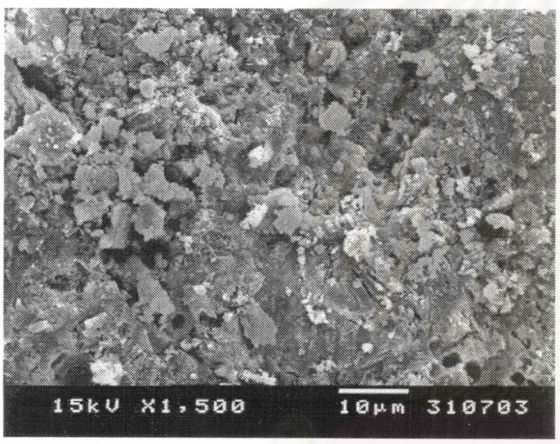

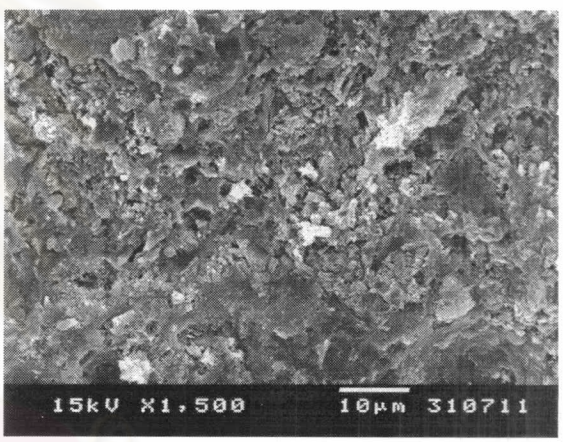

Na_2CO_3 3 wt% activated paste cured at 50°C

Fig. 4.82 SEM micrographs of lime-containing composite materials activated by the combination of 3 accelerating methods after 100 cycles of wetting/drying cyclic storage.

The SEM micrographs shown in Fig. 4.82 revealed that the microstructures of lime containing composite materials after 100 cycles of wetting/drying cyclic storage are still sound and in the well-formed structure. The pozzolanic reaction can be further proceed due to the reaction between lime and pozzolan remaining in the structure. Rhombohedral crystals can be detected in both $CaCl_2$- and Na_2CO_3-activated lime-containing composite materials. The results from XRD analysis are shown in Fig. 4.83 confirm the presence of calcite from the carbonation reaction.

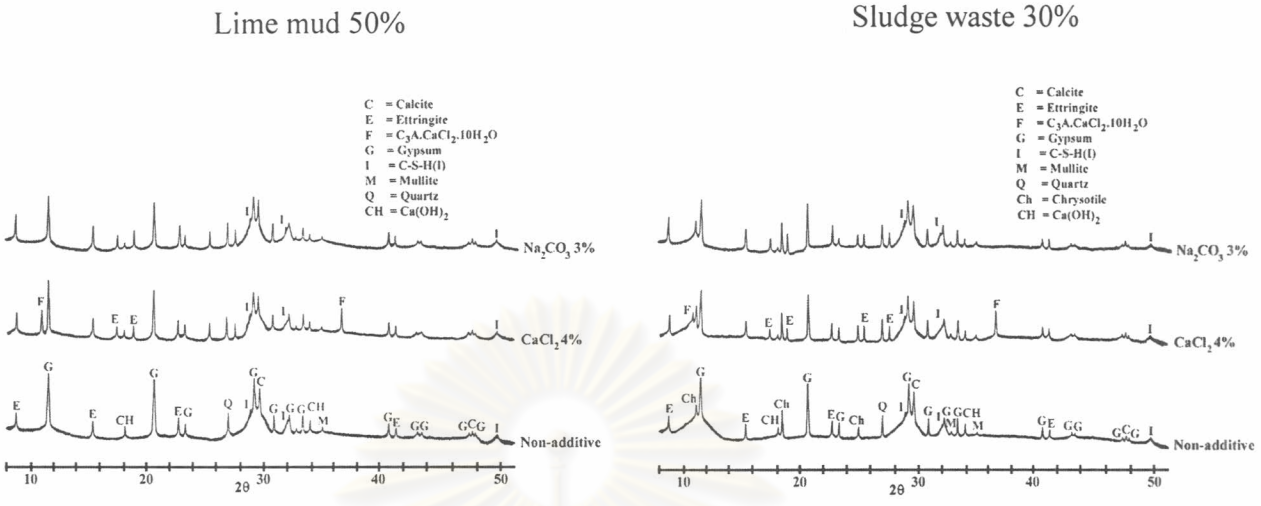

Fig. 4.83 XRD patterns of lime-containing composite materials activated by the combination of 3 accelerating methods after 100 cycles of wetting/drying cyclic storage.